Aus dem

Institut für Schlaganfall- und Demenzforschung (ISD)

Klinikum der Ludwig-Maximilians-Universität München

Acute and chronic brain damage after experimental traumatic brain injury: temporal profile of neuroinflammatory, vascular and neurodegenerative changes

Dissertation

zum Erwerb des Doktorgrades der Medizin

an der Medizinischen Fakultät

der Ludwig-Maximilians-Universität München

vorgelegt von

Chiara Anina Braun

aus

Erlangen

Jahr

2025

Mit Genehmigung der Medizinischen Fakultät der
Ludwig-Maximilians-Universität München

Erstes Gutachten : Prof. Dr. Nikolaus Plesnila

Zweites Gutachten: Prof. Dr. Nicole Terpolilli

Drittes Gutachten: Prof. Dr. Pfefferkorn

Dekan: Prof. Dr. med. Thomas Gudermann

Tag der mündlichen Prüfung: 18. November 2025

Table of Contents

Summary (English):

Traumatic brain injury (TBI) is a leading cause of death and long-term neurological deficits worldwide. It causes primary brain damage, which develops immediately and is irreversible, and secondary brain damage, which develops over the following hours to years and should therefore in principle be amenable to treatment. Current purely symptomatic therapeutic options are unable to treat the chronic consequences of TBI due to limited knowledge of the underlying pathophysiology. This study investigates the complex acute, subacute and chronic pathophysiology of TBI, focusing on the chronic progression of neuroinflammatory, microvascular, and neurodegenerative responses following the injury.

Following a controlled cortical impact (CCI) or a sham operation, male C57BL/6N mice were investigated alongside naive animals for 15 minutes, 24 hours, seven days, one month, three months, six months, and 12 months after TBI. Immunohistochemistry was used to evaluate histopathological alterations. The findings reveal persistent activation of astrocytes up to 12 months and microglia up to six months post TBI, characterized by elevated GFAP and Iba-1 levels, indicating ongoing neuroinflammation. Notably, astrocyte and microglial activation peaked at seven days post-injury. Moreover, the Aqp4 fluorescence intensity in the ipsilateral hemisphere increased significantly at 24 hours post-TBI, followed by a decline at seven days and normalization by six months, indicating an early but transient astrocytic response to trauma. CD31 intensity showed acute microvascular damage with a decrease at 24 hours and recovery by seven days, while transient reductions in astrocytic end feet coverage of endothelial surfaces peaked at seven days, highlighting a period of vulnerability in neurovascular unit integrity and potential susceptibility to secondary injury. BBB disruption was evidenced by transient albumin extravasation, peaking at 24 hours, followed by a progressive decline over the next six months without reaching control levels, suggesting early vascular instability. Chronic neurodegeneration was also observed, as indicated by sustained amyloid-beta accumulation up to 12 months and acute neuronal loss within the initial week, analyzed by the NeuN cell count, raising concerns about long-term cognitive impacts of TBI, including increased risks for neurodegenerative diseases.

The study emphasizes the importance of the chronic sequel of TBI pathophysiology in understanding TBI outcomes, suggesting that interventions targeting chronic neuroinflammation, neurovascular integrity and neurodegeneration may improve long-term recovery post TBI. These insights present critical implications for developing therapeutic strategies to mitigate TBI-related long-term consequences and enhance rehabilitation efforts.

Zusammenfassung (Deutsch):

Das Schädelhirntrauma (SHT) ist weltweit eine der häufigsten Ursachen für Todesfälle und langfristige neurologische Defizite. In der Pathophysiologie des SHT unterscheidet man den primären Hirnschaden, der sich sofort entwickelt und daher irreversibel ist, und den sekundäre Hirnschäden, der sich in den folgenden Stunden bis Jahren entwickelt und daher prinzipiell einer Therapie zugänglich sein müsste. Die derzeitigen, rein symptomatischen therapeutischen Möglichkeiten sind aufgrund der begrenzten Kenntnis der zugrunde liegenden Pathophysiologie nicht in der Lage, die chronischen Folgen eines SHTs zu behandeln. In dieser Studie wird die komplexe akute, subakute und chronische Pathophysiologie des SHT untersucht, wobei der Schwerpunkt auf dem chronischen Verlauf der neuroinflammatorischen, mikrovaskulären und neurodegenerativen Reaktionen nach der Verletzung liegt.

Nach einem controlled cortical impact (CCI) oder einer Scheinoperation wurden männliche C57BL/6N-Mäuse neben naiven Tieren 15 Minuten, 24 Stunden, ein Monat, drei Monate, sechs Monate und 12 Monate nach SHT untersucht. Zur Bewertung der histopathologischen Veränderungen wurde die Immunhistochemie eingesetzt. Die Ergebnisse zeigen eine anhaltende Aktivierung von Astrozyten bis zu 12 Monaten und von Mikroglia bis zu sechs Monaten nach SHT, gekennzeichnet durch erhöhte GFAP- und Iba-1-Werte, was auf eine anhaltende Neuroinflammation hinweist. Bemerkenswert ist, dass die Aktivierung von Astrozyten und Mikroglia sieben Tage nach der Verletzung ihren Höhepunkt erreichte. Darüber hinaus stieg die Aqp4-Fluoreszenzintensität in der ipsilateralen Hemisphäre 24 Stunden nach SHT signifikant an, gefolgt von einem Rückgang nach sieben Tagen und einer Normalisierung nach sechs Monaten, was auf eine frühe, aber vorübergehende astrozytäre Reaktion auf das Trauma hinweist. Die CD31-Intensität zeigte eine akute mikrovaskuläre Schädigung mit einer Abnahme der Intensität nach 24 Stunden und einer Erholung nach sieben Tagen, während die vorübergehende Verringerung der astrozytären Endfußbedeckung der Endotheloberflächen nach sieben Tagen ihren Höhepunkt erreichte, was auf eine Periode der Anfälligkeit der neurovaskulären Einheit und eine potenzielle Anfälligkeit für sekundäre Verletzungen hinweist. Die Unterbrechung der Bluthirnschranke wurde durch eine vorübergehende Albumin-Extravasation nachgewiesen, die nach 24 Stunden ihren Höhepunkt erreichte, gefolgt von einem progressiven Rückgang über die nächsten sechs Monate, ohne die Kontrollwerte zu erreichen, was auf eine frühe vaskuläre Instabilität hindeutet. Es wurde auch eine chronische Neurodegeneration beobachtet, die sich in einer bis zu 12 Monate andauernden Amyloid-Beta-Akkumulation und einem akuten neuronalen Verlust innerhalb der ersten Woche zeigte, der anhand der NeuN-Zellzahl analysiert wurde. Dies deutet auf eine langfristige kognitiven Auswirkung eines SHT hin, einschließlich eines erhöhten Risikos für neurodegenerative Erkrankungen.

Die Studie unterstreicht die Bedeutung der chronischen Folgen eines SHTs und legt nahe, dass Maßnahmen, die auf chronische Neuroinflammation, neurovaskuläre Integrität und Neurodegeneration abzielen, die langfristigen Folgen eines SHTs modulieren könnten.

List of Figures

List of Abbreviations

AD	Alzheimer's Disease
Aqp4	Aquaporin-4
BBB	Blood Brain Barrier
BDNF	Brain-Derived Neurotrophic Factor
CCI	Controlled Cortical Impact
CCL2	C-C Motif Chemokine Ligand 2
CD68	Cluster of Differentiation 68
CNS	Central Nervous System
CSPGs	Chondroitin Sulfate Proteoglycans
CT	Computed Tomography
CTE	Chronic Traumatic Encephalopathy
CXCL1	C-X-C Motif Chemokine Ligand 1
DAI	Diffuse Axonal Injury
DC	Decompressive Craniectomy
ECM	Extracellular Matrix
GCS	Glasgow Coma Scale
GDNF	Glial Cell-Derived Neurotrophic Factor
GFAP	Glial Fibrillary Acidic Protein
ICP	Intracranial Pressure
Iba-1	Ionized Calcium-binding Adapter Molecule 1
IL-1β	Interleukin-1 beta
IL-6	Interleukin-6
MRI	Magnetic Resonance Imaging
NADPH	Nicotinamide Adenine Dinucleotide Phosphate Hydrogen
ROI	Region of Interest
TBI	Traumatic Brain Injury
TNF-α	Tumor Necrosis Factor-alpha
VEGF	Vascular Endothelial Growth Factor
WHO	World Health Organization

1. Introduction

1.1 Traumatic Brain Injury

Traumatic brain injury (TBI) is defined by the World Health Organization (WHO) as “an acute brain injury resulting from mechanical energy to the head from external physical forces” [1]. It is a very common event, with an average of one in two people suffering a TBI in their lifetime [2], and it is one of the leading causes of death and disability worldwide [3], making it one of the biggest challenges for medical care, public health, and the economy [4, 5, 6, 7, 8]. In 2017, the first *Lancet Neurology* Commission on TBI advocated for a coordinated approach to address the global health problem posed by TBI [9]. Years after TBI, many serious and permanent neurological disorders such as dementia and chronic traumatic encephalopathy (CTE) can occur [10], reducing patients' life expectancy and quality of life and frequently making it impossible for them to return to work [9, 10, 11, 12]. Recent evidence shows that TBI is not only an acute event, but also as a complex chronic illness with many long-term effects [9, 10]. The lack of targeted therapeutic options, including for long-term sequelae, results from the fact that the exact pathomechanisms of post-traumatic brain injury are still not fully understood [10, 13, 14].

1.2 Epidemiology and Etiology

With a steady rise in incidence of 3.6% over almost three decades, traumatic brain injury presents a significant global public health concern [15]. Globally, approximately 70 million new cases of TBI occur annually with an incidence rate of 369 per 100 000 population worldwide [15, 16]. In Europe, 2.5 million people suffer from TBI each year, with around 1.5 million hospitalizations, including 75,000 fatalities [17, 18]. However, these numbers do not reflect patients who have not received medical care; especially after mild TBI, patients often do not seek medical help or treatment, therefore these cases are often left untreated and, thus, not reported. The WHO estimates the global incidence and burden of TBI to be much higher than assumed [19]. All age groups are affected by TBI, but TBI is more likely to result in hospitalization and death in people over the age of 65 [20, 21]. Most TBI patients are men, who are two to three times more likely to suffer from TBI than women, and they are mostly under 25 or over 75 years of age [17]. This is due to differences in etiology related to age and geography. In low-income and middle-income countries and in early to middle adulthood, road traffic accidents are the most common cause [9]. In high-income countries and in young children and elderly, the occurrence of TBI is mainly caused by falls [9]. In 2018, the WHO predicted that the incidence, morbidity, and mortality of TBI will rise sharply due to increasing motorization in emerging and developing countries and increasing age in industrialized countries, making TBI the third most common cause of death worldwide [22, 23]. Globally, the estimated yearly financial expenses of TBI are over $400 billion [24]. Tragically, the overall mortality of patients with severe TBI remains high, at 30–40% [24, 25]. Within 14 days, 18% of patients with severe TBI pass away, even after receiving emergency neurosurgery [26]. Up to 30% of survivors—including those with mild to moderate TBI—develop a substantial disability that can persist long-term [15, 24].

1.3 Classification of Traumatic Brain Injury

TBI is a very heterogeneous disease and can be categorized by injury mechanism, severity, etiology, and injury pattern. Based on the mechanism of injury, TBI can be classified as a closed (non-penetrating) or open (penetrating), diffuse or focal, and acceleration or deceleration injury [27]. If the dura mater is open, it is referred to as an open craniocerebral trauma; if it remains intact, it is referred to as a closed injury [28]. This distinction is relevant for the initial treatment of the patient, as a dural injury is associated with an increased risk of infection [29]. Focal injuries are characterized by neurological deficits that depend on the region affected, whereas closed head injuries are usually more diffuse in nature and can also affect distant regions of the central nervous system (CNS) such as the spinal cord [30]. Acceleration-deceleration trauma may be associated with vascular injury and shear lesions [30]. However, most TBIs have a combination of different injury mechanisms, resulting in a very heterogeneous clinical presentation.

In the clinical assessment, the Glasgow Coma Scale (GCS) is the most common clinical tool used to assess TBI severity. It was introduced by Teasdale and Jennett in 1974 and is characterized by high interobserver reproducibility and good prognostic value [31]. It assesses loss of consciousness, which is one of the strongest predictors of unfavorable outcome and a common symptom in TBI and therefore very important for the classification of its severity [32]. The GCS evaluates three functions: eye opening, verbal response, and motor response. An awake, oriented patient has a maximum score of 15, while a deeply comatose patient has a minimum score of 3 (**Table 1**).

Behavior	**Response**	**Score**
Eye Opening Response	Spontaneous	4
	To verbal prompt	3
	To pain	2
	None	1
Verbal Response	Oriented to time, place, person	5
	Confused, but able to answer questions	4
	Inappropriate words	3
	Incomprehensible	2
	None	1
Motor Response	Obeys commands	6
	Purposeful movement to painful stimulus	5
	Flexion withdrawal from pain	4
	Abnormal flexion	3
	Abnormal extension	2
	None	1
Total score	Mild Brain Injury	13–15

	Moderate Brain Injury	9–12
	Severe Brain Injury	3–8

Table 1: Assessment of the state of consciousness using the Glasgow Coma Scale.

TBI severity is most commonly assessed using the GCS score on admission to the hospital. Approximately 90% of TBIs are classified as mild, which is associated with a score of 13–15 [27]. In mild TBI, loss of consciousness (if present) usually recovers within seconds (< 30 min) and most patients are asymptomatic with no radiological evidence of morphological damage [27]. Most fully recover within the first weeks after trauma, however in the acute stage, patients often suffer from headaches, memory loss, slower reaction times, emotional instability, and irritability and 30% suffer from long-term symptoms [33] such as long-lasting neurocognitive disorders [34, 35, 36].

Moderate trauma with a GCS of 9–12, indicates a loss of consciousness lasting 20 minutes to 6 hours, whereas a severe TBI with a GCS of ≤ 8 indicates a profound coma or a loss of consciousness lasting more than 6 hours [27]. Here, imaging can identify structural damage to the brain parenchyma, including contusions, intra- and extracerebral hemorrhages, edema, and ischemia [30, 37]. When it comes to moderate and severe traumatic brain injury, 60% of patients are predicted to have an unfavorable functional prognosis that includes severe neurocognitive deficits, a vegetative state, or death [38]. In addition to mental illnesses like depression, these neurodegenerative diseases include post-traumatic epilepsy, chronic traumatic encephalopathy (CTE), Alzheimer's disease (AD), or dementia, and amyotrophic lateral sclerosis [39].

1.4 Pathophysiology

TBI is not a singular occurrence, but rather a highly dynamic process that is initiated by the primary mechanical impact, i.e. the primary injury, followed by subsequent secondary injury cascades (**Figure 1**) [40]. In the first stage, primary damage occurs within a few milliseconds after the trauma due to irreversible cell death, which is not amenable to therapy [39, 41, 42]. The second phase leads to the development of secondary brain damage, which can evolve over hours to years and affects brain areas not initially injured. It can exceed the volume of the primary damage several times [43]. The secondary injury refers to a cascade of cellular and molecular events triggered by damaging mechanisms such as brain edema, ischemia, programmed cell death, and inflammatory reactions [44]. These processes lead to chronic inflammation and vascular changes, which may represent targets for specific therapeutic interventions to improve patient outcomes. Secondary posttraumatic brain damage can be separated into three phases: acute (24 hours after the injury), subacute (1 day to 3 weeks after the injury), and chronic (more than 3 weeks after the injury). These time frames, however, are merely estimates and vary depending on a number of variables, including age, the nature of the injury, and the location [45, 46].

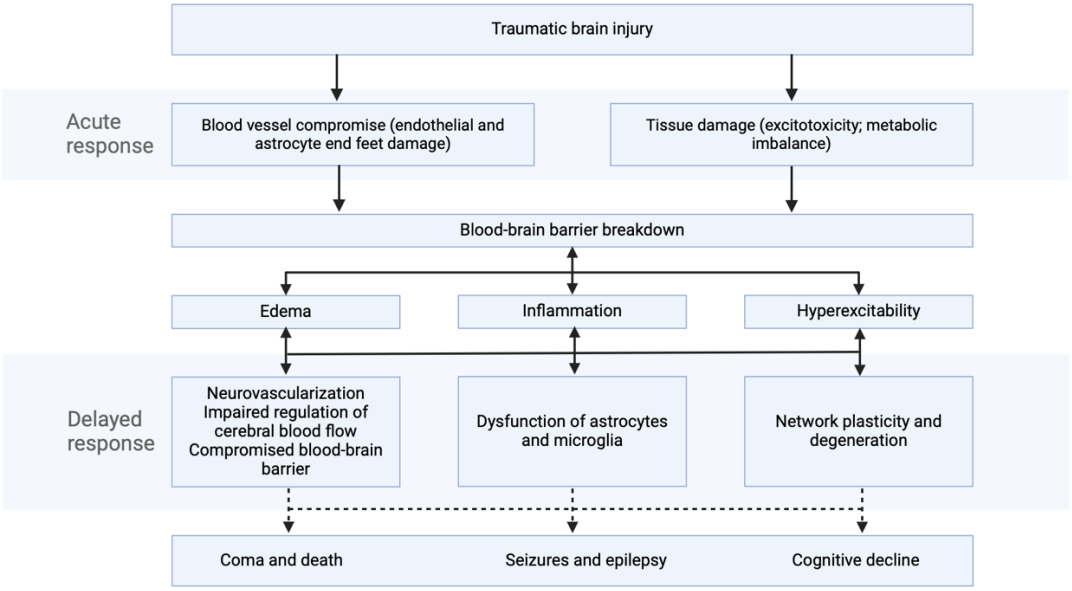

Figure 1: Pathophysiological events in traumatic brain injury. Adapted from [47].

1.4.1 Primary Brain Injury

The primary brain injury is defined as parenchymal damage to the brain within a few hundred milliseconds caused by direct external mechanical forces [48]. It is irreversible and cannot be influenced therapeutically. The initial impact can result in two types of damage: focal and diffuse [49]. The focal injury can include cerebral hemorrhage due to ruptured vessels, contusion, coup-contrecoup injuries and is characterized by necrosis of neurons and glial cells [50]. Brain contusion, which is a bruising of the brain tissue, occurs in around 20–30% of severe TBI patients [37]. This kind of damage may eventually lead to a reduction in psychological function and can cause cerebral herniation, a potentially fatal condition associated with brain edema [51]. Due to tissue compression and rebound against the skull or bone protrusions, a second contusion known as a "contre-coup" may develop opposite to this so-called "coup" [52]. Cerebral hemorrhage is a frequent complication of TBI [53], occurring in 13–35% of cases [54, 55], with hemorrhagic volume progression observed in 38–59% of patients [56, 57, 58]. Various types of hemorrhages, such as delayed traumatic intracerebral hematoma [59] and progressive hemorrhage [60, 61], often contribute to worsening outcomes, with secondary hemorrhagic lesions expanding over time in both epidural and subdural brain regions following injury [60, 62, 63, 64].

Diffuse brain injury occurs when the brain experiences rapid acceleration and deceleration, leading to shearing, stretching, and tearing of brain tissue in specific axons, that may globally affect the brain function [65, 66]. This non-contact force damages the cytoskeleton of neurons, astrocytes, blood vessels, and oligodendrocytes, causing disruption of the blood-brain barrier (BBB), ionic imbalances, and axonal damage [67]. The damage primarily affects subcortical and deep white matter, including the brainstem and corpus callosum, resulting in impaired axonal transport and neuron connectivity through myelin sheath disruption and degradation but can also affect many different parts of the brain [68]. Diffuse axonal injury (DAI) is present in nearly all severe TBI cases and more than half of moderate TBI cases [69, 70]. Histopathologically, it can be divided into three grades: grade 1 involves axonal injury in the parasagittal white matter of the cerebral hemispheres, grade 2 includes additional lesions in the corpus callosum, and grade 3 involves further damage extending to the cerebral peduncles [71]. The severity and location of the injury lead to a wide range of symptoms and neurological deficits, often bilateral, reflecting

the diffuse nature of the damage [72]. For example, the diffuse loss of white matter has been associated with the development of post-traumatic dementia symptoms [73]. In summary, primary brain injury encompasses a range of irreversible focal and diffuse damages, each with distinct pathological mechanisms and clinical implications, contributing to the complex and heterogeneous outcomes observed in TBI patients.

1.4.2 Secondary Brain Injury

Secondary brain damage after TBI refers to a cascade of events that occur hours to days and years following the initial injury, representing a longitudinal disease process rather than a single event. Various disease processes exacerbate the brain's condition and lead to enlargement of the primary lesion and neurological impairment; however, the underlying pathophysiology is still not completely understood. Several delayed but progressive processes that follow the initial injury, such as inflammation, ischemia, oxidative stress, disturbances of the BBB, and neurodegeneration have been identified as contributors [39, 74]. These mechanisms result in swelling, axonal damage, and neuronal cell death which can increase intracranial pressure and reduce cerebral blood flow, further worsening brain function [39, 41]. Due to its delayed development, secondary brain injury presents a time-window for therapeutic intervention, with the goal of halting or slowing down these processes, hence reducing secondary brain damage, thereby improving the long-term outcomes for TBI patients.

Acute secondary brain injury, which may progress into chronic secondary brain injury, refers to delayed tissue damage that develops over a period of several days and is triggered by the original trauma and primary damage [75]. Biochemical factors, including excitatory amino acids [76], such as glutamate toxicity [76], endogenous opioid peptides [77, 78], extracellular potassium [79], intracellular magnesium [80, 81, 82], oxidative stress [83], cytokine release [84, 85, 86] and mitochondrial dysfunction, drive neuroinflammation, cell death, and the formation of cerebral edema [79, 83, 87]. Cerebral edema, a defining feature of secondary brain injury, manifests in two forms: vasogenic and cytotoxic [43, 83, 88]. These two forms develop at different time points after trauma but may also occur simultaneously [89]. Vasogenic edema results from BBB disruption, leading to plasma protein and fluid leakage into the interstitial space, predominantly affecting white matter in the first few hours after TBI [90, 91]. In contrast, cytotoxic edema arises from cellular swelling due to oxidative damage and inflammatory processes, predominantly impacting gray matter and persisting for up to two weeks [91, 92, 93, 94, 95]. The progression of cerebral edema elevates intracranial pressure (ICP), as the rigid skull limits compensatory mechanisms like cerebrospinal fluid and venous blood displacement [96, 97]. This increase in ICP reduces cerebral perfusion pressure (CPP) [98], impairing blood flow to the penumbra—vulnerable tissue surrounding the primary injury [99, 100]. Ischemia and hypoxia within the penumbra exacerbate metabolic stress, further fueling tissue damage and edema [101]. Severe ICP elevation can cause life-threatening herniation syndromes, while even moderate increases can critically restrict oxygen and nutrient delivery, amplifying neuronal death and inflammation [88, 102, 103]. The interplay of factors such as the activation of the kallikrein-kinin system [83, 87, 104, 105, 106, 107], oxidative stress, aquaporin-4 (Aqp4) dysregulation [108, 109, 110], and damage to the BBB further aggravates edema. Despite advances in understanding, the complex temporal and spatial progression of these mechanisms, including the role of conditions like hydrocephalus and ischemia [111], remains incompletely understood. Continued research into these processes is essential for developing strategies to mitigate secondary brain damage and improve patient outcomes.

Despite advances in understanding and treating acute brain injury, relatively little is known about long-term mechanisms underlying chronic secondary brain damage, i. e. processes that develop months and years after the initial trauma.

A growing body of evidence shows that the development of posttraumatic brain damage after a single TBI can evolve over many years and may lead to progressive neurological decline over time [112, 113]. For example, TBI has been linked to an elevated risk of developing neurodegenerative disorders, such as Parkinson's disease, cognitive decline, and dementia [10]. To effectively address these long-term consequences, it is crucial to deepen our understanding of the pathophysiological temporal and spatial cellular post-traumatic changes over time. This knowledge will be essential for developing new therapeutic strategies aimed at mitigating these delayed, yet devastating, effects of brain injury.

Using histological methods and repetitive small animal magnetic resonance imaging (MRI) in a mouse model, our research group was recently able to show that experimental TBI leads to a progressive expansion of secondary brain tissue loss in the long term, i.e. up to one year after trauma (**Figure 2**) [64]. This is accompanied by a progressive impairment of learning and memory performance, depressive behavior, and persistent fine motor skill disorders. These findings from the study conducted in our lab by Dr. Xiang Mao not only highlight the phenomenon of continued lesion expansion but also form the foundation for the research question addressed in this thesis. Observations of lesion volume growth, hippocampal atrophy, and neurocognitive impairments emphasized the need to identify the cellular processes underlying these histopathological and MRI findings. We hypothesized that cellular mechanisms such as neuroinflammation, vascular disruption, and chronic neurodegeneration might be key drivers of the observed pathology. Therefore, this study was specifically designed to investigate the cellular correlates responsible for progressive tissue loss and the associated long-term impairments. The major pathophysiological mechanisms of secondary brain damage that are pertinent to this thesis are covered in the paragraphs that follow.

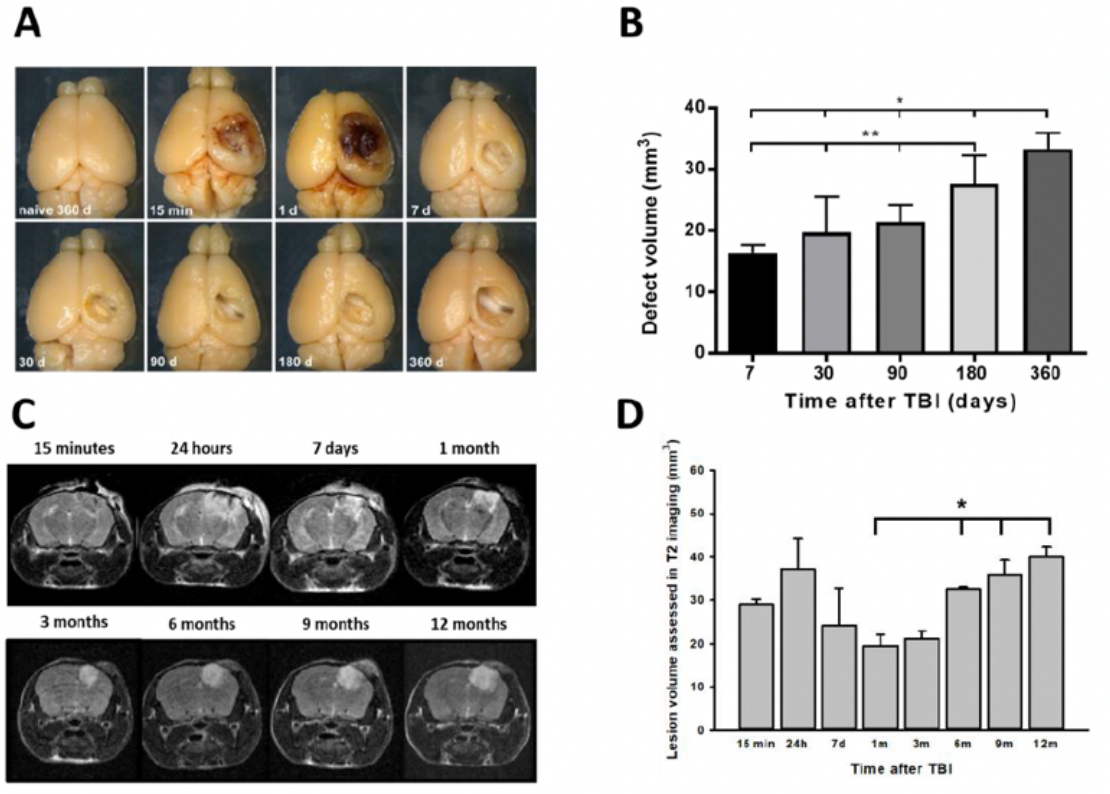

Figure 2: Progressive post traumatic brain damage after CCI. (A) Overview pictures of mice brains of naïve and 15 minutes to 12 months after CCI. (B) Histologically determined lesion volume which increases almost linearly over time. (C) MRI example coronal brain images 15 minutes to 12 months after CCI. (D) MRI quantification analysis of the brain damage with progression of lesion volume over time. Adapted from [64].

1.4.2.1 Neuroinflammation

Neuroinflammation plays a crucial role in secondary injury following TBI and can have both harmful and beneficial effects [114, 115]. Animal and human studies suggest that immune modulation may have a major impact on TBI patients' clinical outcomes [116, 117]. However, before developing immunomodulatory therapies, it is important to fully understand the timing and complexity of the immune response triggered by TBI.

Neuroinflammation after TBI involves a dynamic interplay between central nervous system (CNS) cells and peripheral immune cells, occurring primarily at the site of the injury and in the surrounding penumbra. Microglia and astrocytes are key players, with microglia initiating inflammation and astrocytes contributing through cytokine release and glial scar formation [118, 119, 120]. Peripheral neutrophils, monocytes, and macrophages infiltrate the CNS, clearing debris but potentially exacerbating damage [121]. T and B lymphocytes add adaptive immune responses, while endothelial cells and the BBB modulate immune cell infiltration [122, 123]. Notably, neuroinflammation can also extend to areas further away from the primary injury site, including remote regions of the brain, through mechanisms such as the spread of inflammatory mediators, altered neural connectivity, and systemic immune activation [124, 125, 126, 127]. This complex cellular response, affecting both localized and distant brain regions, evolves over time, contributing to acute and chronic inflammatory processes.

Immune cell activation and a process known as astrogliosis are key players in the inflammatory response, brain function, and recovery after TBI [128, 129, 130]. If dysregulated or prolonged, these processes may contribute to secondary injury and long-term neurological abnormalities

[119, 131, 132]. Astrogliosis is the growth of astrocytes, that aims to create a glial scar, isolate injured tissue, and release chemicals such as cytokines, chemokines, reactive oxygen species, neurotrophic factors, extracellular matrix molecules, glutamate and lipid mediators, which collectively regulate neuroinflammation, tissue repair, and neuronal survival [133, 134, 135]. Microglia, the brain's resident immune cells, become activated in response to injury, undergoing morphological changes and proliferating as they engage in phagocytosis and release pro-inflammatory cytokines. Although microglia are generally thought of as acute injury's short-term responders, recent studies indicate that their activation may continue for months or even years following the original trauma [136, 137, 138].

Clinical studies using positron emission tomography (PET) with translocator protein (TSPO) ligands, which likely bind activated microglia, show chronic neuroinflammation occurring up to 17 years in moderate to severe TBI survivors, particularly in areas remote to the trauma including the thalamus, putamen, and occipital cortex [136]. These findings are supported by an analysis of autopsy specimens from individuals who survived a TBI for one year or more, and in some cases for up to 18 years. This analysis showed a notable increase in amoeboid microglia (which represent the activated, immune-responsive state of microglia) in subcortical white matter pathways when compared to control tissue, lasting up to 18 years. Moreover, thinning of the corpus callosum was also linked to activated microglia, which was seen in 28% of the autopsies [137].

The clinical evidence of a chronic inflammatory state following TBI is supported by experimental studies. In a controlled cortical impact (CCI) model, microglial activation, analyzed via immunohistochemistry of cell surface markers; Major Histocompatibility Complex (MHC) II, Cluster of Differentiation 68 (CD68), and Nicotinamide Adenine Dinucleotide Phosphate Hydrogen **(**NADPH) oxidase, is sustained one year following a moderate to severe TBI [41]. Another closed-head mouse model of TBI revealed a contralateral and large ipsilateral increase in microglia density one week after the damage, which stayed elevated at intermediate levels in brain regions distant from the lesion after two to five months and one and a half years [114]. Moreover, these microglia showed an amoeboid (retracted processes) morphology at chronic stages (one week and one and a half years) in high-magnification confocal images that was similar to the activated microglia/macrophages observed in the acute stage of TBI. In the same study, it was discovered that astrogliosis, as measured by the Glial Fibrillary Acidic Protein (GFAP) astrocyte density, was highly elevated in the ipsilateral and contralateral hemisphere at one week, two to five months and one and a half years after TBI compared to the naive mice. On the other hand, another experimental study of a mild-moderate CCI, showed that astrogliosis was first apparent and peaked at three days post injury in the peri-contusional region and glial scar formation began at seven days post injury and persisted up until 60 days, without changes in the contralateral hemisphere [139].

The prolonged microglia activation is a defining feature of the chronic phase of TBI, and it can have both detrimental and protective effects on brain recovery process. The chronic activation of microglia is characterized by changes in their morphology (for example: a more amoeboid shape), and continued secretion of pro-inflammatory cytokines, such as Tumor Necrosis Factor-alpha (TNF-α), Interleukin-1 beta (IL-1β), and Interleukin-6 (IL-6) [120]. Although these cytokines together with other neurotrophic factors are essential for neuronal survival and repair [140] and for removing debris and combating infections during the acute stage, prolonged production of these cytokines can induce a toxic environment that promotes oxidative stress, impairs synaptic function, and ultimately leads to the death of neurons [120] and promotes neurodegenerative diseases like Alzheimer’s and Parkinson’s [127, 136, 141]. The balance between the pro-inflammatory and

anti-inflammatory actions of microglia is critical for determining long-term outcomes after TBI. Furthermore, it is thought that this persistent neuroinflammatory state also plays a role in the long-term cognitive and functional deficits frequently seen in TBI survivors [142, 143]. Additionally, microglia are involved in synaptic pruning, which is the process of eliminating excess synapses [144]. Aberrant microglial activity can lead to excessive or inappropriate pruning of synapses, disrupting neural circuits, and impairing cognitive functions such as learning and memory. Moreover, microglia can interact with astrocytes to form glial scars around the site of injury [144]. Microglia also influence neuroplasticity by modulating the extracellular matrix, secreting growth factors, and interacting with other glial cells and neurons which makes them key players in brain recovery and its adaptation to injury [144]. Furthermore, chronically activated microglia have the potential to transition into dystrophic states, characterized by fragmented processes and reduced functionality [145]. This makes them less effective at responding to new injuries or infections and may also contribute to an environment that fosters ongoing neurodegeneration, as this state is associated with neurodegenerative diseases like Alzheimer's disease [145]. Many studies showed that long-lasting neuroinflammation is increasingly recognized as a chronic feature of neurodegenerative disease [114, 141, 146, 147, 148, 149]. However it remains unclear if neuroinflammation is the trigger for neurodegenerative disease or if the accumulation of abnormal proteins such as Aβ initiates the inflammatory response [150]. Understanding the chronic role of microglia and their role after TBI is crucial for developing interventions that could ameliorate the chronic effects of TBI.

Astrocytes, a type of glial cell abundant in the central nervous system, also undergo significant changes after TBI that influence brain recovery. They are vital for maintaining metabolic homeostasis, supporting neuronal function, responding to injury, and become activated through a process known as astrogliosis [151]. This involves their proliferation, migration towards lesional or damaged tissue, hypertrophy, and expression of certain proteins, such as GFAP, leading to the formation of glial scars [120]. Glial scars isolate the damaged tissue, prevent the spread of inflammation and thereby protect healthy tissue from further damage [120]. Nonetheless, they also create a chemical and physical barrier that prevents neuronal circuit reconnection and axonal regeneration, which may restrict the brain's capacity to fully recuperate function. Moreover, astrocytes can modify the extracellular matrix (ECM), a network of molecules that supports cells structurally and affects their behavior, by producing ECM components like chondroitin sulfate proteoglycans, which are known to inhibit axonal growth and thus regeneration. Additionally, they are also essential for preserving the brain's metabolic homeostasis and synaptic plasticity, which includes controlling neurotransmitter and glucose levels [151]. Astrocytes may suffer from metabolic dysfunction in the chronic phase following TBI, which contributes to excitotoxicity and further neuronal damage by altering glucose uptake, decreasing the synthesis of lactate, which neurons use as fuel, and impairing the recycling of neurotransmitters like glutamate [152] which further impairs neuronal survival and recovery [120, 128]. Astrocytes are also key regulators of the CNS immune response and can modulate microglia activity [153]. They can act in a pro-inflammatory manner, producing cytokines such as TNF-α, IL-1β, and IL-6, and chemokines like C-C motif chemokine ligand 2 (CCL2) and C-X-C motif chemokine ligand 1 (CXCL1), which contribute to ongoing neurodegeneration; or in an anti-inflammatory manner, producing neurotrophic factors such as brain-derived neurotrophic factor (BDNF), glial cell-derived neurotrophic factor (GDNF), and vascular endothelial growth factor (VEGF), which support neuronal survival and repair—highlighting their dual role in chronic TBI [120, 154, 155].

GFAP-positive astrocytes in a mouse CCI model were seen to proliferate at one, three, and seven days after injury, with the number of proliferating astrocytes peaking three days after injury [124].

These astrocytes were hypertrophic with long processes and were seen close to the lesion, showing that astrocytes have a proliferative response that is most prominent during the acute period following experimental TBI. Another stab wound model of injury revealed that, seven days after injury, GFAP-labeled astrocytes had enlarged cell bodies, elongated processes and up-regulated GFAP expression, which were signs of hypertrophy [156]. Expanding our knowledge of astrocytes in both acute and subacute phases of TBI as well as the chronic stages is crucial, considering their pivotal role in TBI pathophysiology.

Despite the recognized importance of these glial cells in TBI, there remains a significant gap in our understanding of the temporal dynamics of neuroinflammation, particularly concerning the chronic phases of microglial and astrocytic responses post-injury. Most research has focused on the acute to subacute phases of TBI, leaving the long-term changes over months and years and their implications underexplored. Further elucidation of the precise temporal response following brain injury may reveal potentially critical time points for intervention.

1.4.2.2 Cerebral Microvasculature

After TBI, disruption of the cerebral microvasculature can occur [157, 158]. The neurovascular unit (NVU) is a structural and functional component of the central nervous system that describes the close interaction between neurons, glial cells (astrocytes and microglia) and blood vessels (including endothelial cells and pericytes) [159, 160]. Explicitly, cerebral microvessels adequately surrounded by astrocyte end-feet are an important part of NVU which have been specifically analyzed in this study [160]. TBI leads to acute and chronic damage of the cerebral microvasculature, which presents a determining factor in the development of secondary brain injury, including impaired blood flow and oxygen delivery, breakdown of the BBB, edema formation, neuroinflammation and impaired waste clearance [161, 162, 163]. In the early phase after trauma, this cerebrovascular dysfunction contributes to reduced cerebral perfusion [164], the extent of which significantly affects the patient's prognosis [165, 166]. Patients may experience this period of decreased or inadequate perfusion for several months [167].

A further indication of damage to cerebral (micro)vessels caused by TBI is the impairment of cerebral autoregulation. The ability to continuously adapt cerebral blood flow to the current demand (neuronal activation, CO_2 concentration) and blood pressure through vasodilation and constriction is an important protective mechanism of the brain under physiological conditions [168]. Autoregulation is often disturbed or even cancelled shortly after TBI, which worsens the patient's prognosis [169, 170, 171, 172, 173]. To date, the long-term development of cerebrovascular injury and neurovascular coupling following trauma is mostly unknown. However, indirect evidence suggests that it contributes to the long-term persistence of neurocognitive deficits and epilepsy after trauma [174, 175, 176].

Furthermore, the BBB, a physical barrier that divides the brain parenchyma from the body's circulation, is additionally damaged by brain injury [47, 177]. The BBB is comprised by astrocytes, pericytes, microglia, neurons, the extracellular matrix, and the cerebral microvascular endothelium, which makes up a NVU that interacts closely to build a functioning CNS [47]. Following damage, the BBB becomes more permeable, allowing both small (286-10,000 Da) and large (like albumin - 66.5 kDa) molecules to enter the brain parenchyma [178] and permits infiltration of blood borne, i. e. peripheral, immune cells, which complicates the neuroinflammatory response [125, 179]. Chronic neuroinflammation through infiltration of peripheral immune cells contributes

to secondary injuries, including oxidative stress, neuronal death, and glial scarring, impairing long-term recovery [127, 174].

Astrocytes contribute to the integrity of the BBB by encircling endothelial cells with astrocytic end feet [180, 181]. Development and maintenance of the BBB depend heavily on astrocyte interactions with endothelial cells, which include intracellular and intercellular communication [181]. Aquaporin-4 (Aqp4) is a key water channel protein in the brain, predominantly expressed in astrocyte end feet around blood vessels. It facilitates the passage of water and other small solutes across membranes and through cells, thus playing a central role in brain edema formation by regulating water balance. Under physiological conditions, Aqp4 on astrocytic end feet is found covering 98% of the vascular endothelium and the reduced coverage of astrocytic end feet is associated with BBB dysfunction after TBI [182]. A rat CCI study demonstrated that Aqp4 is upregulated close to the TBI lesion and that a downregulation of this molecule occurs adjacent and contralateral to the site of injury in the acute phase of TBI (up to 24 hours) [183]. Another human study revealed that while Aqp4 expression at the damage site rose from 15 hours and even more after eight days, it did not change 6–14 hours after brain injury [184]. However, the long-term time dependence of Aqp4 expression following TBI is still unclear.

Based on controlled cortical impact (CCI) and closed head injury models, it is hypothesized that BBB breakdown occurs in two stages after damage: an early rise in permeability hours after TBI, which then declines, and a secondary delayed phase that occurs three to seven days after injury [120, 185, 186]. Despite this, there are a significant number of discrepancies between the research regarding the second opening's timing [187]. A study on barrier permeability in a mouse TBI model found that large molecules regain restricted entry within hours, while smaller molecules can penetrate the brain for up to four days post-injury [178]. Many other results from both extensive clinical data and animal model research indicate that BBB disruption can continue for days, weeks, or even years following the acute incident [175, 187, 188]. However, there is insufficient data to determine whether these persistent disruptions are primary processes due to shear injury, impairments in the regulation of the BBB, cerebral blood flow and metabolic processes or secondary pathological events after TBI due to aberrant brain activity, metabolic abnormalities, inflammation-related mechanisms, and astrocytic dysfunction [47, 177]. Ultimately, the temporal sequence of the post-traumatic vascular dysfunction underlying pathophysiological mechanisms is not fully understood and remains the basis of controversial discussions.

1.4.2.3 Neurodegenerative changes after TBI

TBI is a longitudinal disease process that involves ongoing cellular damage, neuronal cell death, and an increased long-term risk of neurodegenerative diseases, including Alzheimer's disease (AD), Parkinson’s disease and chronic traumatic encephalopathy (CTE) [42, 127, 189]. Among the chronic neurodegenerative disorders that may follow TBI, the association with Alzheimer’s disease has the strongest support [190]. The biological mechanisms that relate TBI to the development of AD are supported by emerging research that suggests a major overlap in the pathophysiological processes of TBI and AD. Acutely in TBI, axonal injury and disturbed transport impact molecular systems essential for the production of pathogenic proteins such hyperphosphorylated tau and amyloid-β peptide [191]. In the context of TBI, posttraumatic changes trigger the activation of delta-secretase, which cleaves tau and amyloid precursor proteins, which leads to changes known from AD, ultimately inducing an AD like pathophysiology [192]. These abnormal protein deposits have the potential to transform into hyperphosphorylated tau-positive neurofibrillary tangles and amyloid-β plaques, leading to the progressive degeneration and loss of neurons,

particularly in brain areas responsible for memory and cognitive function [191]. This can result in the classic symptoms of Alzheimer's disease, the most prevalent form of dementia [193].

Reduced levels of amyloid-beta (Aβ) are the most well-characterized cerebrospinal fluid (CSF) indicators for AD [194], as amyloid-beta peptides improperly accumulate in the brain and form plaques that are linked to the pathogenesis of AD [195]. Although extensive research has established TBI as a risk factor for Alzheimer's disease (AD), there is still inconsistency in the findings on the pathogenic mechanisms and the relationship between these two disorders. This variability may stem from differences in study designs [196], populations [197], and methodologies [198]. Additionally, cognitive recovery after TBI is influenced by a complex interplay of factors, including injury severity, time elapsed since the injury, age, gender, genetic predisposition, lifestyle, and coping mechanisms [199, 200].

The mechanisms of chronic posttraumatic neurodegeneration are poorly understood [201, 202]. In TBI, a necrotic focus rapidly forms at the site of impact due to compromised membrane integrity in vascular and parenchymal cells [47]. This process is further aggravated by reduced metabolic supply relative to increasing demand and by excitotoxicity. Later, a delayed wave of apoptosis, closely linked to inflammation and edema, has been observed in both animal models and humans [13, 203, 204]. TBI also triggers cell cycle re-entry in both mitotic (astroglia and microglia) and non-mitotic (neurons) cells, contributing to glial scar formation, amplified neuroinflammation, and apoptotic signaling pathways leading to cell death [205]. Moreover, according to the limited number of human post-mortem studies that are currently available, brain atrophy is a hallmark of chronic traumatic brain injury [206, 207], and it may be linked to neuroinflammation (active microglia) [136, 137]. Cell debris released by dying or injured cells in the brain's peri-lesional and lesional zones primes local microglia and astrocytes [120]. For example, a study found persistent inflammation (examined through microglial density and morphology) together with ongoing white matter degeneration in the corpus callosum and adjacent parasagittal cortex up to 18 years post-trauma [137]. Experimental investigations in mice and rats that demonstrate long-term progressive brain atrophy [208, 209] as well as a sustained monocyte invasion and microglia activation for up to one and a half years following TBI, support these findings [138]. It is yet unknown if this is the pathophysiological correlate of progressive neurodegeneration and progressive neurocognitive deterioration. There is an urgent need for more thorough and integrative research to elucidate the connection between TBI and neurodegenerative diseases such as AD.

1.5 Clinical Management of Traumatic Brain Injury

TBI presents a significant challenge in clinical management due to its complexity, heterogeneity and our incomplete understanding of its underlying pathophysiology. As a result, current treatment strategies are primarily symptomatic and not neuroprotective, focusing on mitigating secondary damage rather than addressing specific pathways. Despite advances in medical research, there are still no causal treatment options available for TBI, making the management of patients with this condition complex and reliant on carefully monitored supportive care.

Current therapy for TBI focuses on treating symptoms and stabilizing the patient to prevent secondary brain damage. This is achieved by maintaining optimal blood pressure, ventilation, intracranial pressure, and body temperature to ensure adequate oxygenation and perfusion of the brain, as hypotension and hypoxemia are known risk factors for poor outcomes [16, 210, 211, 212]. The primary goal of the early (emergency and ICU) management of TBI is to achieve cardi-

opulmonary stabilization of the patient and acquire baseline neurological and radiological examination to plan further therapy and estimate the outcome [213]. The spine and cranio-cervical junction are immobilized until definitive radiological exclusion of an injury. Additionally, the head is raised to promote venous outflow in patients, which lowers intracranial pressure (ICP), ensures sufficient brain perfusion, and prevents brain herniation [214]. The German Guidelines for the Treatment of TBI state that computed tomography should be performed as soon as a patient is admitted to the hospital and is stable in order to determine the degree and severity of the TBI and to identify any possible extracranial injuries [215]. The imaging findings can then prompt surgical intervention in case of localized pathologies such as epidural or subdural hematomas. ICP monitoring should be taken into consideration for individuals who are unconscious and exhibit diffuse lesion patterns. In the event of increased ICP, staged treatment strategies are recommended by the Brain Trauma Foundation [213]. These include permissive hypocapnia (pCO_2 between 30 and 35 mmHg) attained by hyperventilation, which causes vasoconstriction and subsequently lowers ICP [216], and hyperosmolar therapy utilizing osmo-diuretics, such as mannitol or hypertonic saline, to reduce brain edema formation [217]. Additionally, benzodiazepines and barbiturates that cause a medically induced comatose state or therapeutic cooling can be utilized to reduce brain metabolism/energy demand and protect tissue [97, 218].

Surgical therapy is recommended if intracranial hypertension becomes unmanageable. Secondary decompressive craniectomy (DC) performed for late but not for early refractory ICP elevation is recommended to improve mortality and favorable outcomes [219]. Primary DC occurs when an intracranial mass lesion is removed early following a head trauma and the bone flap is not replaced. When a patient's elevated ICP is unresponsive to previous treatments, secondary DC is indicated [219]. The effectiveness of decompressive craniectomy in lowering intracranial pressure in TBI patients is well-documented, but its impact on long-term neurological outcomes is less clear. The DECRA study, a large randomized controlled trial, found that while DC effectively reduced ICP, it did not significantly improve mortality or functional outcomes after 12 months as compared to standard medical care [220]. In fact, patients in the DECRA study had more unfavorable outcomes six months post-injury [221]. In contrast, the RESCUE ICP study showed that although DC reduced mortality in patients with refractory intracranial hypertension, it was also linked to higher rates of adverse outcomes, such as a vegetative state or severe disability compared to conservative treatment [222]. These mixed results suggest that the decision to use DC in TBI cases must be carefully considered, with attention to the timing and individual patient circumstances. In the later stages of TBI treatment, patients undergo neurorehabilitation including physical, occupational, and speech therapies as well as psychological, vocational, and cognitive counseling [223].

As of yet, no causal treatment strategy has been discovered to stop TBI's long-term effects, resulting in neuroprotection. Comprehending the enduring consequences of TBI is essential for formulating effective therapy alternatives. Researchers can identify specific molecular and cellular targets involved in the injury and recovery processes by gaining deeper insights into how traumatic brain injury affects the brain over time. With this information, medications that target the fundamental causes of brain damage as well as its symptoms may be developed, potentially improving patient outcomes and reducing the risk of chronic complications such as neurodegeneration and chronic neurological impairment. Although numerous experimental studies have demonstrated promising approaches, implementation in the clinical domain has not yet proven successful [224, 225, 226].

1.6 Significance and Long-Term Symptoms of Traumatic Brain Injury

1.6.1 Neuroinflammation

The long-term symptoms of neuroinflammation following TBI extend far beyond the acute recovery phase. Chronic neuroinflammation contributes to structural, functional, and cognitive deficits that can persist for years, impacting survivors' quality of life [12] and increasing their risk of developing neurodegenerative conditions [12, 127, 227].

The ongoing inflammatory response through chronic microglia and astrocyte activation creates a toxic microenvironment, damaging neuronal structures and impairing synaptic function which is critical for learning and memory. This exacerbates neurodegeneration, promoting neurodegenerative diseases like Alzheimer's and Parkinson's, as it perpetuates a cycle of inflammation and neuronal loss [127, 136, 141]. Survivors of TBI often experience problems with attention, executive functioning, and memory, along with increased susceptibility to anxiety, depression, and impulsivity [191, 228]. Disrupted neural circuitry, caused by prolonged microglial and astrocytic activation, plays a central role in these impairments. Chronic neuroinflammation can also result in visible structural alterations in the brain. Imaging and autopsy studies reveal thinning of critical structures like the corpus callosum and persistent microglial clusters in subcortical white matter pathways up to 18 years post-TBI [127, 137, 229, 230]. These changes correlate with functional impairments, including motor deficits, reduced cognitive flexibility, and memory loss.

1.6.2 Cerebral Microvasculature

The role of cerebral microvascular dysfunction in persistent neuroinflammation, impaired cerebral blood flow, its effects on the NVU and BBB breakdown makes it a critical focus for understanding the long-term challenges and consequences of TBI survivors.

After TBI, the cerebral microvasculature remains compromised for extended periods of time, affecting the brain in several ways. The ability to adjust cerebral blood flow (CBF) to neuronal activity is impaired, reducing the brain's capacity to meet metabolic demands during cognitive or physical activities. This mismatch contributes to persistent cognitive deficits, including difficulties with memory, attention, and executive function and increases the vulnerability to secondary insults such as stroke due to impaired hypo- or hyperperfusion [174, 231, 232, 233, 234]. Chronic disruption of the cerebral microvasculature, including impaired neurovascular coupling and ongoing inflammation, has been linked to post-traumatic dementia and epilepsy [10, 208, 235, 236, 237, 238]. Abnormal vascular activity can exacerbate neuronal hyperexcitability, creating conditions conducive to seizures.

The BBB dysfunction leads to prolonged permeability that allows harmful substances, such as neurotoxic proteins and peripheral immune cells, to enter the brain [185, 187]. This disruption has several significant consequences. Ongoing BBB dysfunction has been associated with progressive neuronal damage and may accelerate the onset of neurodegenerative conditions like Alzheimer's disease [42, 191, 196, 231]. Moreover, the dysregulation of components of the BBB such as water channels like aquaporin-4 in astrocytes leads to abnormal fluid accumulation and edema [160, 181].

Long-term damage to the cerebral microvasculature contributes to observable structural changes, such as white matter degradation and cortical thinning, as well as functional deficits [68]. Chronic hypoperfusion and inflammation disrupt axonal integrity and myelination, leading to long-term connectivity issues between brain regions [68, 127, 161, 233]. This contributes to impairments in motor coordination, sensory processing, and higher-order cognitive functions, limiting recovery of function and the effectiveness of rehabilitation therapies [119].

1.6.3 Neurodegeneration

Neurodegeneration following TBI represents a critical and long-lasting consequence of brain injury, with significant implications for cognitive health and quality of life. For example, chronic TBI-induced brain atrophy, linked to ongoing neuroinflammation, contributes to long-term neurocognitive deterioration [64]. Survivors often face challenges in memory, executive function, and emotional regulation.

Previous studies have demonstrated that a history of a single TBI with loss of consciousness increases the likelihood of developing later-life dementia [44, 239]. Additionally, it has been observed that decades after the initial injury, tau and amyloid pathology can be detected in the brains of TBI survivors [240, 241, 242]. A recent experimental TBI study demonstrated accumulation of AD-related protein variant pathology (including Aβ and tau) in multiple brain regions as well as sensorimotor, cognitive and affective deficits (elevated plus maze, forced swim task) up to 28 days post fluid percussion injury. These studies establish a mechanistic link between TBI-induced protein pathology and early AD hallmarks, highlighting the potential for TBI to contribute to neurodegenerative disease progression.

Though primarily associated with repetitive brain injuries, CTE highlights the broader link between head trauma and progressive neurodegeneration. CTE is a progressive degenerative brain disease that affects people who have experienced repeated brain trauma, symptomatic concussions, or asymptomatic sub-concussive head injuries. CTE is marked by mood disturbances, behavioral changes, and cognitive impairments, demonstrating the multifaceted consequences of traumatic brain injuries [243]. First identified by Dr. Harrison Martland in 1928 as "punch-drunk" syndrome, it was primarily noted in athletes who were frequently subjected to repetitive brain damage, such as boxers, American football players, and ice hockey players [244, 245]. A study found that its incidence among National Football League (NFL) players reached 99% [246]. Despite the similarities between AD and CTE, there are still notable differences on an etiological, biochemical and histopathological level and since it involves repetitive brain damage, it is not further addressed in this study [247, 248].

Since the precise etiology of chronic posttraumatic neurodegeneration is unknown, there is no targeted or specialized therapeutic approach to treat or prevent it. To develop effective preventative strategies for TBI-related neurodegeneration, it is crucial to determine when these processes begin, how they evolve over time, and the duration of their impact on the brain.

1.7 TBI Models

To study the pathophysiology of TBI in an experimental context, the use of animal models is essential for examining the physiological, biomechanical, and molecular processes involved, as well as for identifying potential therapeutic targets. Because of their manageable size, easier care, and access to genetically modified versions, rodent models have taken center stage in TBI research, despite the fact that larger animals—like primates and pigs—share more physiological parallels with humans. The complexity and heterogeneity of TBI in humans have led to the development of numerous experimental models, each of which has its own advantages and disadvantages. The most common models for traumatic brain injury are the controlled cortical impact (CCI) [249], blast injury [250], fluid percussion injury [251] and weight-drop injury [252, 253]. The mouse CCI model was chosen for this study, whereby a craniotomy is carried out above the right parietal cortex, and trauma is induced using a pneumatic bolt under constant, predetermined parameters [249]. Typical features of this injury model include cerebral contusion, intraparenchymal bleeding, axonal damage, and consequent tissue loss. This model's primary benefit is its high reproducibility since the highly controlled parameters create a consistently sized lesion in all animals, which can also be adjusted, depending on experimental requirements [254].

1.8 Aim of the Study

As described above, despite the high prevalence of traumatic brain injury and the large number of patients with long-term consequences, there are still no targeted therapeutic options for this disease and its consequences. Therefore, it is extremely important to identify pathomechanisms contributing to chronic post-traumatic brain injury that could aid in the development of therapeutic strategies. Previous scientific studies have often focused on the acute consequences of TBI, but little is known about the pathomechanism of the chronic sequelae of TBI. Therefore, the aim of this study is to analyze the course and role of primary and secondary damage after TBI. Specifically, this study aims to characterize the temporal sequences of histomorphological inflammatory, cerebrovascular, and neurodegenerative changes that lead to secondary chronic brain damage up to 12 months in a mouse model of TBI.

2. Materials and Methods

2.1 Experimental Animals and Husbandry

The experiments were performed on C57Bl/6N mice obtained from Charles River Laboratories in Kisslegg, Germany. These mice were 8—10 weeks old males, weighing between 18—22 g. They had free access to water and food and were kept on a 12 hour day-night cycle. Before surgery, mice were placed in groups of up to five per cage (dimensions: 207 x 140 x 265 mm, Macrolon II, Ehret Life Science Solutions, Emmendingen, Germany). After surgery, the animals were kept individually for up to one week and then reunited. Health examinations and hygiene checks were carried out in accordance with FELASA guidelines and recommendations [255]. All surgical procedures were performed in accordance with the regulations of the animal welfare facilities of the University of Munich and were approved by the appropriate authority, the Government of Upper Bavaria (ROB-55.2-2532.Vet_02-17-44 and ROB-55.2-2532.Vet_02-21-112)

2.2 Experimental Groups

Animals were randomly selected for the experiment and assigned, in a blinded manner, to either the control group or TBI group with different survival time points after trauma. The control group included naïve non-traumatized animals (young and 12 months old) and sham-operated animals 24 hours and 12 months post-sham operation. The TBI group included the following experimental cohorts: animals that were sacrificed after 15 minutes, 24 hours, 7, 30, 90, 180 and 360 days after CCI. Five mice were operated/analyzed per group/time point, unless otherwise stated. For standardization purposes, either the control group was used to standardize the TBI animals to each other, or the ipsilateral hemisphere was standardized to the contralateral hemisphere. **Figure 3** shows a schematic overview of the experimental groups. Surgical preparation and all immunohistochemical analyses were performed in a blinded manner. Surgeries were performed by two researchers, Dr. Xiang Mao and me, in a blinded fashion.

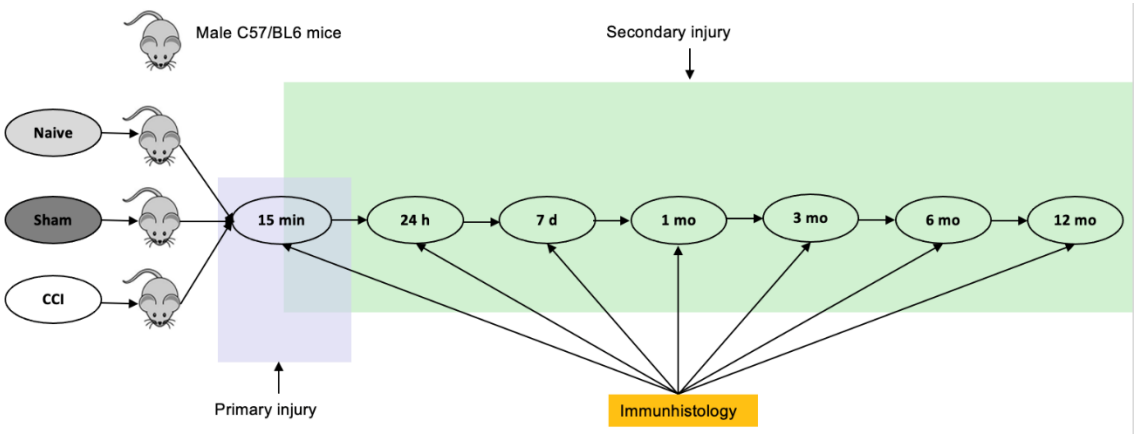

Figure 3: Schematic overview of the experimental design and experimental groups.

2.3 Anesthesia and Analgesia

The mice were given an intraperitoneal injection of buprenorphine (Temgesic®, Reckitt Benckiser, Berkshire, UK; 0.1 mg/kg body weight) 30 minutes prior to surgery. Anesthesia was then induced by 45 seconds of 5% isoflurane (1 ml/ml, 250 ml, CP-Pharma®, Burgdorf, Germany) in a specially

prepared anesthesia chamber, then continued with 1.5—2% isoflurane in an air/oxygen mixture (70% / 30%), using a mask in spontaneously breathing mice. To avoid drying of the cornea, the eyes were protected with dexpanthenol ointment (Bepanthen®, Bayer, Leverkusen, Germany) during the procedure. During the first three days, buprenorphine was injected every 8 hours to relieve pain.

2.4 Experimental Traumatic Brain Injury - the Controlled Cortical Impact Model (CCI)

Traumatic brain injury was induced by the Controlled Cortical Impact model (CCI). James W. Lighthall first described this model in ferrets in 1988 [249] and it was later modified to different animal species [256]. Our group has more than 20 years of experience with this technique in mice, CCI is characterized by high reproducibility through highly controlled parameters that create consistently sized lesions in all mice [257, 258].

A custom-built, pressure-operated CCI device was used to perform the TBI (Mouse-Katjuscha 2000, L. Kopacz, University of Mainz, Germany, **Figure 4A**). It has a micrometer tip that allows precise adjustment of the impact depth and a velocity microsensor at the tip of the instrument to accurately determine the impact velocity and contact time.

Animals were positioned in prone position after induction of anesthesia and their heads were fixed with a palate plate clamp in a stereotaxic frame (Model 900 Small Animal Stereotaxic Instrument, David KOPF Instruments®, Tujunga, California, USA). To maintain core body temperature at 37°C, mice were placed on a temperature-controlled heating mat and body temperature was monitored via a rectal temperature probe. A longitudinal skin incision was made along the sagittal suture (approximately 2 centimeters long), followed by removal of the galea aponeurotica with a cotton swab. With the aid of a surgical microscope (Leica M80, Leica, Germany), a 5x5 mm craniotomy was performed above the right parietal cortex using a diamond-coated high-speed drill (Rewatronik® products, Wald-Michelbach GmbH, Germany; drill head GD890R, diameter 0.6 mm, Aesculap, Tuttlingen, Germany), leaving the bone undissected along the sagittal suture (see **Figure 4B** for a schematic drawing). The bone flap was then opened towards the sagittal suture, exposing the intact dura mater. Drilling was done very carefully so as not to damage the dura mater. The skull cap was also cooled continuously with physiological saline solution during drilling to avoid heat damage. After partial removal of the skull bone, the mouse was placed under the CCI device. The tip of the impact ram was lowered under the microscope to allow accurate vertical placement of the impact pin on the dura mater in the center of the craniotomy. Trauma induction was then performed with a penetration depth of 1 mm, an impact duration of 150 ms and an impact velocity of 8 m/s. Immediately after the impact, the initially displaced bone flap was repositioned and fixed with tissue glue (No. 1469SB, 3M VetbondTM, USA) and the scalp was sutured with monofilament sutures (6/0, SERAFIT®, SERAG-WIESSNER GmbH, Naila, Germany). In the sham group, only a craniotomy was performed, the pressure stamp was placed, but no trauma was applied. After the wound was closed, the isoflurane supply was stopped, and the animal was allowed to wake up. The operated mice were given 100% oxygen until they regained consciousness and placed in a heating chamber (MediHEAT TM, Peco Services, United Kingdom) at 34°C and 55% humidity to avoid postoperative hypothermia.

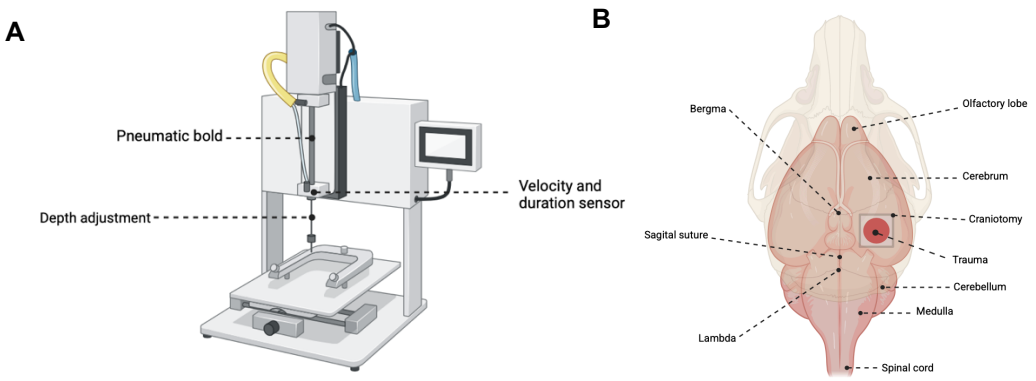

Figure 4: (A) Image of the CCI device used in this study. (B) Position of the craniotomy and trauma. Created with BioRender.com.

2.5 Histology for Assessment of Lesion Volume

After surgery and the respective post-trauma survival time points, the animals were euthanized under deep Isofluran anesthesia by cervical dislocation. Subsequently, the brains were carefully removed, immediately frozen in powdered dry ice, and stored at -20 °C until further processing. The brains were then embedded in Tissue-Tek® (Sakura Finetek Europe, Zoeterwoude, NL). Subsequently, using a cryostat (Cryostar MH 560, Microm, Walldorf), 14 sequential frozen brain sections (50 µm thickness) were cut at intervals of 500 µm, with the first section positioned 1000 µm distal to the bulbus olfactorius and then mounted on glass slides (ELKA, Glaswarenfabrik Karl Hecht GmbH & Co KG, Sondheim, Germany). Next, sections were stained according to Nissl using cresyl violet (see **Figure 5** for a detailed protocol), fixed and covered with a coverslip (Eukitt®, O. Kindler GmbH & Co, Freiburg, Germany). This staining allows distinction of viable/non-viable neuronal bodies and thus a differentiation of the lesioned versus the healthy brain tissue [64].

2 min	Fix sections with 70% Ethanol
10-15 min	Cresyl violet solution Rinse shortly with water (2 x)
2 min	Ethanol 70%
2 min	Ethanol 96%
2 min	Ethanol 100%
2 min	Isopropanol
5 min	Rotihistol I
5 min	Rotihistol II

Figure 5: Protocol for Nissl staining.

The stained brain sections were placed under a microscope (Zeiss Axio Imager M2, Carl Zeiss Microscopy GmbH, Munich, Germany) and photographed at 12.5 X magnification with a digital camera connected to the computer (Zeiss Axio Imager M2, Carl Zeiss Microscopy GmbH, Munich, Germany, see **Figure 6**). The area of the ipsilateral hemisphere, contralateral hemisphere and lesion, which is the Nissl negative area, was measured with the help of an imaging software (AxioVision LE 4.8, Carl Zeiss Microscopy GmbH, Munich, Germany). The defect volume was

then determined using the following formula: V = d*(E1/2 + E2 + E3...+ En/2) with d = 0.5 (0.5 for 500 µm, distance between two sections) and E being the lesion area.

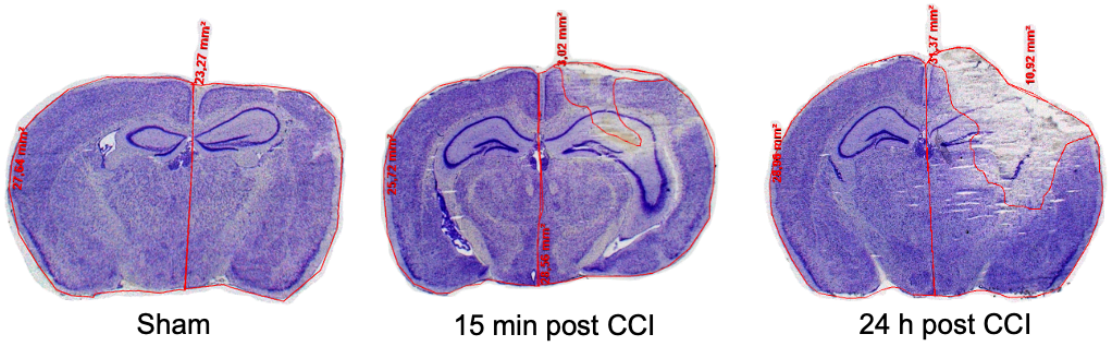

Figure 6: Histomorphological determination of the lesion volume for sham, 15 min and 24 h post CCI using the Nissl staining to depict the Nissl$^+$ and Nissl$^-$ area.

2.6 Body Weight

Body weight, as a parameter for normal feeding behavior and, thus, overall health of the mice, was measured directly before induction of anesthesia. In the first 7 days after CCI, weight was measured daily and thereafter once a month, until the end of the observation period, using a precision scale with movement correction (OHAUS®, Waagendienst Winkler GmbH, Munich, Germany).

2.7 Immunohistochemical Assessment of the Parameters for Traumatic Brain Injury

2.7.1 Tissue Harvesting

Following the induction of deep anesthesia by intraperitoneal injection of medetomidine (0.5 mg/kg body weight; Domitor®, Pfizer, Karlsruhe, Germany), midazolam (5 mg/kg, ratiopharm, Ulm, Germany), and fentanyl (0.05 mg/kg body weight, Jannsen Cilag, Neuss, Germany), the animals were sacrificed by transcardial perfusion at the end of each respective observation period. After opening the costal arch, a cannula (21G, Safety-Multifly® needle, Sarstedt, Nümbrecht, Germany) was placed in the left ventricle of the heart and the animal was perfused with 30 ml physiological saline solution (NaCl 0.9%, B.Braun AG, Melsungen, Germany) for 1 minute, followed by 50 ml of 4% paraformaldehyde (PFA) (Morphisto GmbH, Frankfurt am Main, Germany) for 2 minutes, using a pressure-controlled perfusion system (Perfusion One, Lecia Biosystems, Richmond, VA, USA). The brain was then carefully removed by cutting the cranial calvaria along the sagittal sutura (Aesculap AG & Co KG, Tuttlingen, Germany) and severing the nasal bone. The ossa parietalia were opened laterally with a metal spatula and the brain was removed from the cranial calvaria by cutting through the medulla oblongata and taking the bulbi olfactorii with it. The brain was post-fixed in 4% PFA at 4°C over night and then stored in phosphate-buffered saline (PBS) until it was further processed.

2.7.2 Preparation and Staining of Brain Sections

Brains were embedded in 4% agarose (PEQLAB, VWR International GmbH, Erlangen, Germany) and coronal sections were prepared using a vibratome (Leica VT1200S, Nussloch, Germany) set to the following parameters: 0.8 vibration speed (amplitude) and 0.8 m/s feed speed. Starting 1000 µm behind the olfactory bulb, 12 sequential 50 µm thick coronal sections were collected every 600 µm and stored in PBS or cryoprotection solution (0.1 M PBS, glycerin, ethylenglycol) at -20°C until staining.

For each experimental group, three sections per animal were selected which were located as close as possible to each other in the center of the contusion. The continuous principle of immunohistochemical staining consisted of antigen detection, which was achieved in three steps. First, the specimen was incubated with an unconjugated primary antibody that binds the specific antigen to be analyzed. Sequentially, the secondary antibody was used, which is directed against the Fc/Fab fragment of the primary antibody and contains a fluorescent marker which can be visualized with a microscope.

All staining's were performed according to the same scheme, except that the optimum incubation time and concentration of the antibodies varied, which was individually determined in preliminary tests. First, blocking was performed for two hours with 0.5% Triton X-100 in 0.01 M PBS. Sections were then incubated with a primary antibody buffer (consisting of 1% bovine serum albumin, 0.1% gelatin from cold water fish skin, 0.5% Triton X-100 in 0.01 M PBS) and the primary antibodies of choice at pH 7.2—7.4, 4°C, and individual incubation times (see Table 2). The sections were then washed three times for 15 minutes in PBS and incubated with the secondary antibodies of choice in 0.01 M PBS at pH 7.2—7.4 containing 0.05% Tween 20. Nuclei were stained with 4',6-diamidin-2-phenylindole (DAPI, Invitrogen, #D1306) 1:10,000 in 0.01 M PBS. Finally, the sections were washed three times for 15 min in PBS and fixed on glass slides with aqueous mounting medium.

While the majority of these antibodies were validated by our lab members [13, 64, 259, 260] and others, specificity and validity of new antibodies was confirmed using the appropriate negative controls. Negative controls serve to check the specificity of the antigen-antibody binding. For this purpose, a tissue section was stained which certainly did not contain the primary antibody and incubated only with the secondary antibody. If this preparation showed a positive color reaction, unspecific protein binding by the secondary antibody reagents could be inferred.

A ZEISS LSM 980 confocal microscope (Carl Zeiss Microscopy GmbH, Jena, Germany) was then used for imaging.

Name	Description	Concentration	Incubation time	Provider
Anti-rabbit Iba-1	019-19,741	1:200	48 hours	Wako
Anti-rat CD68	Mca1957	1:200	48 hours	Biorad
Anti-mouse GFAP CY3	2905	1:500	2 hours	Sigma aldrich

Anti-goat CD31/ PECAM-1	Af3628	1:100	7 days	R&d systems
Anti-rabbit Aqp4	Ab2218	1:200	48 hours	Merck millipore
Anti-guinea pig NeuN	266 004	1:200 or 1:100	48 hours or 24 hours	Synaptic systems
Anti-rabbit laminin	L9393	1:100	24 hours	Sigma
Anti-goat albumin	Af3329	1:100	24 hours	Novus
Anti-rabbit Tau K9JA	A0024	1:1000	24 hours	Dako

Table 2: Primary antibodies.

2.7.2.1 Astrogliosis and Microglia

As previously mentioned, dysregulated astrogliosis and the inflammatory/immune response that follow traumatic brain damage have serious long-term effects. For this reason, these processes were examined using a variety of antibodies both during the acute and chronic phases of the injury. Microglia, the resident immune cells of the central nervous system [261], were investigated to visualize the immune response following traumatic brain injury. For this purpose, the primary antibody Iba-1 (Ionized Calcium-binding adapter molecule 1) was utilized. It is thought to be the superior antibody for evaluating microglia in the brain because of its high specificity and accurate visualization, which enable analysis of microglial morphology and distribution within the brain [262]. Secondly, we sought to identify the microglia that are actively involved in immune defense, tissue regeneration, and restoring homeostasis following brain injury. Since the antibody CD68 is an effective marker for identifying and characterizing active microglia and macrophages [263], it was chosen to address this question. In addition, research was done on astrogliosis. The specific astrogliosis marker GFAP (glial fibrillary acidic protein), which is strongly expressed in activated astrocytes [264] and is a commonly used antibody by our lab team [13] and others, was utilized for this purpose.

Thus, the first staining set, which assessed the immune response and the development of scars following TBI, contained the following primary antibodies: Iba-1 which stains microglia (rabbit, Wako, #019-19,741, 1:200) and CD68 which stains activated microglia (rat, BioRad, #MCA1957, 1:200). The primary antibodies were incubated for 48 hours. The secondary antibodies: anti-rabbit coupled to Alexa-fluor 488 (donkey anti-rabbit, Jackson, #711-546-152, 1:150), anti-rat coupled to Alexa-fluor 647 (donkey anti-rat, Jackson, #712-606-150, 1:150) and GFAP Cy3 594 (mouse, Sigma Aldrich, #2905, 1:500) which stains for astrogliosis and scarring were incubated for two hours.

2.7.2.2 Staining of the Cerebral Microvasculature

After TBI, disruption of the neurovascular unit (NVU) can occur [158] which results in a series of pathological processes that exacerbate brain injury [161]. Thus, the cerebral microvasculature integrity was investigated as it provides insights into the complex structural and functional relationship between neurons, glial cells, and blood vessels that play a crucial role in maintaining the integrity and function of the brain [160].

Therefore, to visualize the blood vessels, the following antibodies were used: CD31 (also known as platelet endothelial cell adhesion molecule-1 or PECAM-1) which specifically stains for endothelial cells, lining blood vessels [265] and laminin which stains the basement membrane surrounding blood vessels [266] and thus provides further information about the structural integrity of blood vessels and their surrounding extracellular matrix. Moreover, the BBB dysfunction is associated with reduced coverage of the vascular endothelium with astrocytic end feet [182]. Thus, glial cells and their relationship with blood vessels were assessed using the astrocyte end foot marker Aquaporin-4 (Aqp4) [267]. Additionally, the presence of albumin, a plasma protein, in the interstitial space was assessed as an indication for BBB permeability to larger molecules [74].

The second staining included the primary antibodies: CD31/PECAM-1 which stains endothelial cells (goat, R&D Systems, #AF3628, 1:100), Aqp4 which stains astrocyte end feet (rabbit, Merck-Millipore, #AB2218, 1:200) and NeuN, a neuronal marker (guinea pig, Synaptic Systems, #266 004, 1:200). The primary antibody CD31/PECAM-1 was incubated first for 5 days. After 5 days, the other two primary antibodies (Aqp4 and NeuN) were added and incubated for further 48 hours. Subsequently, the following secondary antibodies were used at a concentration of 1:200 for 24 hours: anti-goat coupled to Alexa-fluor 647 (donkey anti-goat, Jackson, #705-606-147), anti-rabbit coupled to Alexa-fluor 488 (donkey anti-rabbit, Jackson, #711-546-152), and anti-guinea pig coupled to Alexa-fluor 594 (donkey anti-guinea pig, Jackson, #706-586-148).

The third staining combination analyzed the presence of blood components in the extravascular space, thus assessing BBB leakage. The following primary antibodies were incubated at a concentration of 1:100 for 24 hours: laminin, a marker of the vascular basement membrane (rabbit, Sigma, #L9393) and albumin, the largest molecular intravascular component (goat, Novus, #AF3329). Secondary antibodies incubated at a concentration of 1:100 for two hours included: anti-rabbit coupled to Alexa-fluor 488 (donkey anti-rabbit, Jackson, #711-546-152) and anti-goat coupled to Alexa-fluor 647 (donkey anti-goat, Jackson, #705-606-147).

2.7.2.3 Neurodegeneration Staining

TBI represents a risk factor for neurodegenerative disease such as dementia and chronic traumatic encephalopathy that have been found in post-mortem studies [10, 191]. Hence, to investigate the impact of TBI on neurodegenerative processes, this study utilized the antibody NeuN (neuronal-nuclei) to quantify neuronal cell populations affected by TBI-induced neurodegeneration, alongside Aβ 6E10 to target amyloid-β peptide deposits [268], key factors implicated in the pathogenesis of AD.

Hence, the fourth staining combination included the primary antibodies: Tau K9JA (rabbit, DAKO #A0024, 1:1000) and NeuN (guinea pig, Synaptic Systems, #266 004, 1:100) which were incubated for 24 hours. The secondary antibodies: anti-rabbit coupled to Alexa-fluor 647 (donkey anti-rabbit, Jackson, #711-606-152, 1:500) and anti-guinea pig coupled to Alexa-fluor 488 (donkey anti-guinea pig, Jackson, #706-546-148, 1:100) were incubated for two hours.

The fifth staining combination included the following primary antibodies for 24 hours: Aβ 6E10, which stains amyloid plaques in Alzheimer's development (mouse, BioLegend, #SIG-39320, 1:100) and NeuN (rabbit, Abcam, #ab177487, 1:100). The sections were incubated with the following secondary antibodies for two hours: anti-mouse coupled to Alexa-fluor 647 (donkey anti-mouse, Jackson, # 715-606-150, 1:100) and anti-rabbit coupled to Alexa-fluor 488 (donkey anti-rabbit, Jackson, #711-546-152, 1:100).

2.7.3 Analysis of the Immunohistochemical Stainings

2.7.3.1 Astrogliosis Analysis

Analysis of astrogliosis and astrocyte coverage was performed using GFAP stained sections. GFAP staining was recorded with a 10x objective (EC Plan-Neofluar 10x/0.30 Pol M27), an image matrix of 1024 × 1024 pixels, a speed of 8, bit depth 16, zoom 0.6, interval 21 µm, range of 63 µm, 10% overlap and bi-directional scanning using a confocal microscope (Zeiss etc.). Whole brain images were acquired in Z-stacks as tile scans, with a z-step distance of 10 µm and a total range of 63 µm.

The Z-stacks were imported into Fiji ImageJ2 (open-source image processing software, version 2.3.0/1.53q, date 2021-09-13) and assessed as maximum intensity projections. GFAP intensity was then measured using the mean grey value and normalized to the contralateral hemisphere to assess potential differences in staining intensity. The measured GFAP fluorescence therefore represents the sum of the grey values of all pixels divided by the number of pixels.

Two different analyses were performed. Firstly, the GFAP fluorescence of the complete ipsilateral and contralateral hemisphere was measured (see **Figure 7A** for a schematic representation). Secondly, seven different regions of interest (ROIs) were selected, four of them close to the contusion margin and three further away to analyze the spread of astrogliosis. Each individual ROI is 300 µm x 300 µm. ROI 1 is located ipsilaterally in the center of the striatum directly at the lesion margin and ROIs 2 and 3 are located 300 µm laterally and medially from ROI 1 along the lesion margin. ROIs 4, 5 and 6 are each located 1000 µm vertically downwards from ROIs 1, 2 and 3 and ROI 7 is located in the center of the cortex at the lesion margin (see **Figure 7B** for a schematic representation). Three slices per animal were selected in the center of the trauma for the timepoints 15 minutes, 24 hours, 7 days, 1-, 3-, 6- and 12-months post TBI, as well as three slices per animal for the control group with the same approximate location in the brain as the TBI animals and their GFAP fluorescence intensity was averaged.

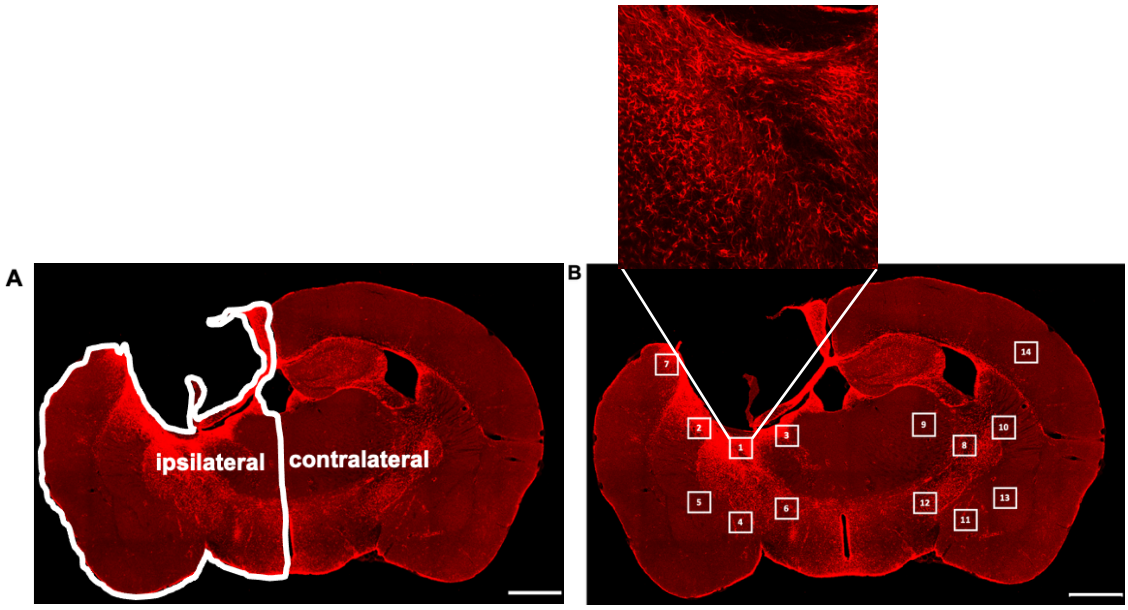

Figure 7: (A) GFAP fluorescence analysis 1 of a coronal brain section. (B) GFAP fluorescence analysis 2 of a coronal brain section. Scale bar = 1 mm.

2.7.3.2 Microglia Density Analysis

Microglia coverage was assessed in sections stained with Iba-1 – a canonical marker for microglia within the brain parenchyma which may stain perivascular macrophages too [262]. The same confocal microscope settings were used as in the GFAP analysis described above. After creating a maximum intensity projection in ImageJ, the intensity of the Iba-1 fluorescence was measured. The mean grey values for five ROIs (300 µm x 300 µm each) in the ipsilateral hemisphere were measured and normalized to the respective ROIs in the contralateral hemisphere. ROI 1 is located in the center of the striatum directly at the lesion margin, ROIs 2 and 3 are each located 600 µm laterally and medially from ROI 1 along the lesion margin, ROI 4 is located 600 µm vertically downwards from ROI 1 and ROI 5 is located in the center of the cortex at the lesion margin (see **Figure 8**).

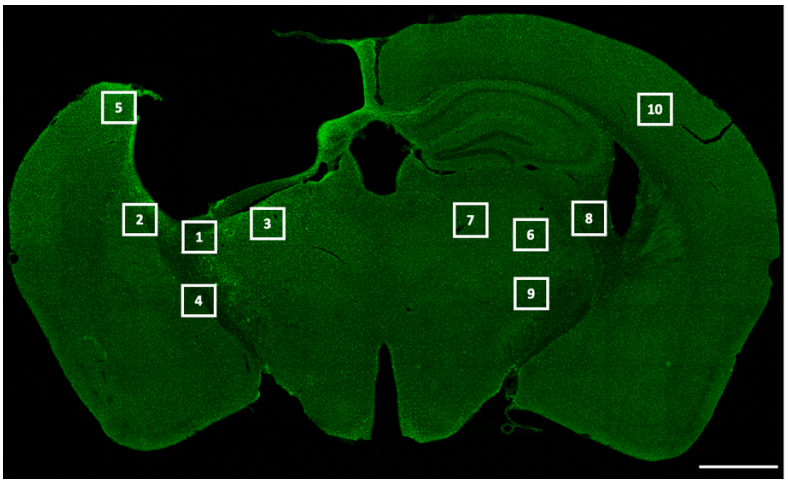

Figure 8: Microglia density analysis of Iba-1 fluorescence staining's within the 5 ROIs in the ipsilateral hemisphere and the corresponding ROIs in the contralateral hemisphere of a coronal brain section. Scale bar = 1 mm.

2.7.3.3 Microglia Morphology Analysis

Microglial morphology was manually assessed in maximum intensity projections of Iba-1 stained sections using Sholl and Fractal analyses and measured at three different ROIs: ROI 1 ipsilateral in the center of the striatum directly at the lesion margin, ROI 2 ipsilateral in the center of the cortex adjacent to the lesion margin and ROI 4 as a mirror-image to ROI 2, contralateral in the center of the cortex (see **Figure 9**). The striatum in the contralateral side was not assessed as the staining was not clear enough/non-uniform. A control group with sham 24 hours after surgery and TBI animals at seven days and six months after trauma were assessed. The confocal microscope images were acquired with a 40× objective (EC Plan-Neofluar 40x/1.30 Oil DIC M27), an image matrix of 1024 × 1024 pixels, a pixel size of 0.2 × 0.2 µm and a color depth of 8 bits. The ROIs were collected in Z-stacks to include the entire slice thickness with a z-step distance of 0.4 µm.

Using a modified protocol from Young and Morrison [269], the total cell size/area, ramifications, span across hull, and circularity of brain immune cells were analyzed. Z-stack images were converted to a maximum intensity projection, and the microglia that were fully captured in the Z-stack were individually cut out using the polygon selection tool in ImageJ. After background subtraction and using the paintbrush tool to trace any disconnected processes and fill gaps, the images were binarized and resized to 600 × 600 pixels, maintaining the original scale. The paintbrush tool was also used to remove speckles or debris around the microglia. Sholl analysis was performed using the Sholl analysis plugin in ImageJ. Concentric circles centered around the soma with an increasing radius of 1 µm were drawn, and the number of intersections at each radius were measured.

The fractal analysis was then carried out after converting binary images into outline images using the FracLac plugin for ImageJ. The total number of pixels in the cell image of the filled or outlined binary image was measured and later converted to µm² (pixel area = 0.208 µm²). The cell circularity was calculated as circularity = 4 π area/perimeter². The maximum span across the convex hull represents the maximum distance between two points in the convex hull.

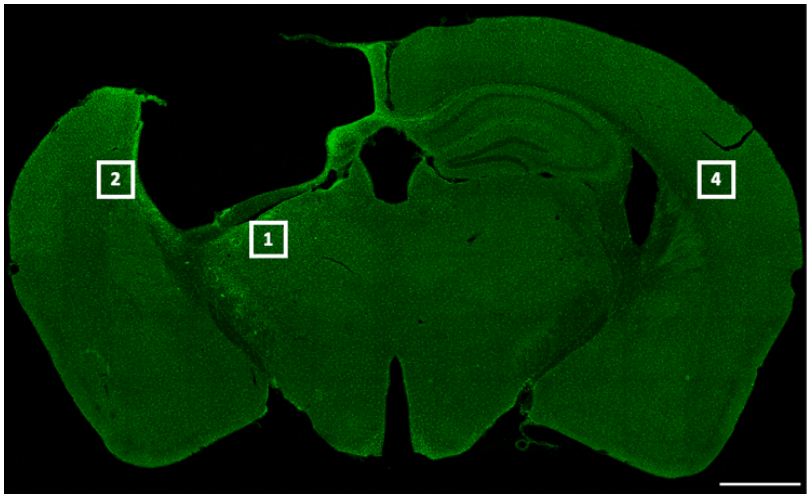

Figure 9: Microglia morphology analysis within ROI 1, 2 and 4 of a coronal brain section. Scale bar = 1 mm.

2.7.3.4 Microglia Activation Analysis

Activation of microglia was assessed using Iba-1 and CD68-stained sections. CD68 is expressed in the intracellular lysosomes of microglia and its intensity correlates with activation state and phagocytic activity of activated microglia [74]. The same confocal microscope settings were used

for the study as in the GFAP analysis described above. After creating a maximum intensity projection of the Z-stacks, the images were imported into ImageJ to measure the intensity of CD68. The mean grey values of the same five ROIs were measured as in the microglia density analysis, also normalized to the contralateral side (see **Figure 10**). In addition, the CD68 fluorescence divided by the Iba-1 fluorescence of the previously determined microglia density analysis was measured.

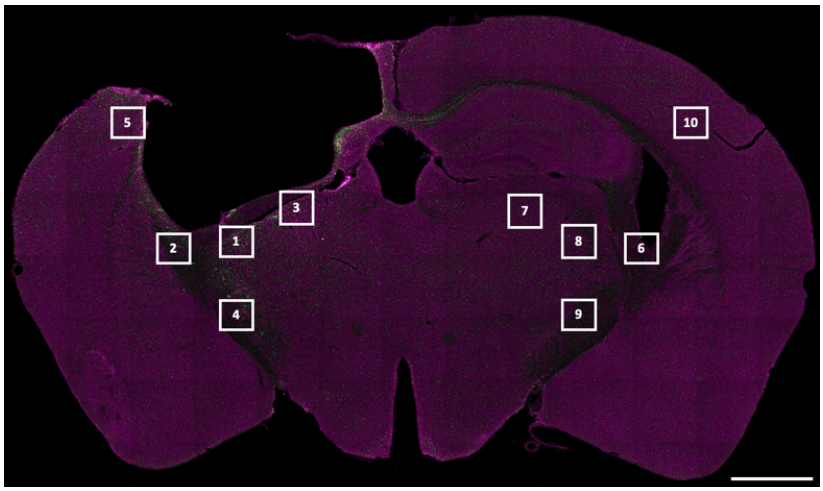

Figure 10: Microglia activation analysis at ROI 1-5 in the ipsilateral and ROI 6-10 in the contralateral hemisphere of a coronal brain section. Scale bar = 1 mm.

2.7.3.5 Colocalization of CD68 with Activated Microglia Analysis

A three-dimensional model was used to determine more precisely how many microglia were activated, as the two-dimensional measurement of the microglial activation analysis described above could not indicate which CD68 signal was associated with which individual microglia. The colocalization of the CD68 signal within the Iba-1 signal was determined in two ROIs (300 µm x 300 µm each). ROI 1 was located ipsilateral in the center of the striatum adjacent to the lesion margin, and ROI 2 ipsilateral in the center of the cortex adjacent to the lesion margin (**see Figure 11)**. Both were normalized to the corresponding ROIs in the contralateral hemisphere. The same confocal settings as in the microglia morphology analysis were used.

The colocalization analysis was carried out using the Imaris x64 software (Oxford Instruments, version 9.5.1). Using three-dimensional image analysis, the CD68 was masked within the Iba-1 surface and assigned its own surface. The sum of the volume of the CD68 signal masked within the Iba-1 surface was then divided by the sum of the volume of the Iba-1 surface and normalized to the contralateral side.

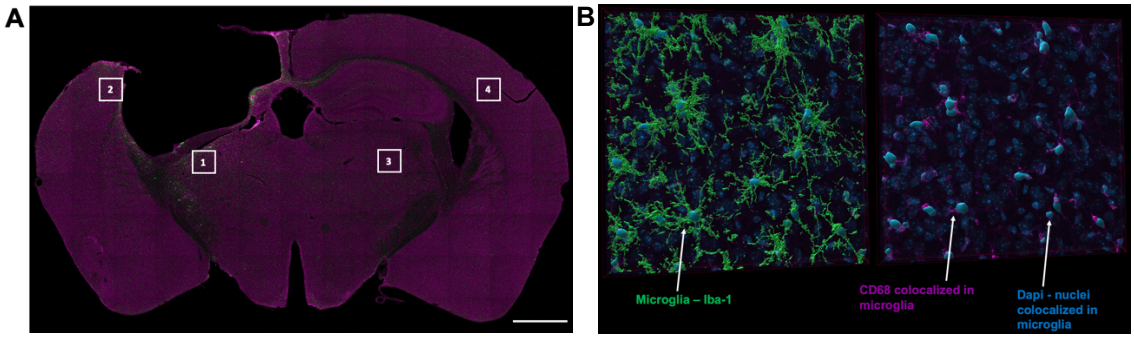

Figure 11: Colocalization of CD68 with activated microglia analysis at ROI 1 and 2 in the ipsilateral and ROI 3 and 4 in the contralateral hemisphere. (A) Exemplary Iba-1 (green) and CD68 (magenta) staining with ROI 1 in the striatum and ROI 2 in the cortex of the ipsilateral hemisphere. (B) Exemplary 3D volume analysis with the Imaris software of Iba-1 (green), CD68 (magenta) and Dapi (blue).

2.7.3.6 Cerebral Microvessel and Blood Brain Barrier Analysis

Mature endothelial cells with CD31 and aquaporin-4 (Aqp4) on astrocytic end-feet enwrapping them, along with pericytes are essential for a fully functioning NVU and BBB. We assessed cerebral microvessels using CD31 and Aqp4 as vascular and astrocyte endfeet markers. Furthermore, the BBB disruption was investigated by the appearance of parenchymal albumin. Albumin is a plasma protein that is not normally present in the tissue and its extravascular presence indicates that that the BBB is disrupted [74].

The images were acquired with a 40× objective (EC Plan-Neofluar 40x/1.30 Oil DIC M27), an image matrix of 1024 × 1024 pixels, a pixel size of 0.2 × 0.2 µm and a color depth of 8 bits. The ROIs were acquired in Z-stacks with a slice distance of 1 µm.

2.7.3.6.1 Cerebral Microvessel Integrity

To investigate cerebral microvessels, the staining of Aqp4, which stains the astrocyte end feet, with CD31, which stains the vascular endothelium, was imported into ImageJ as a maximum intensity projection. The CD31 fluorescence and the thresholded Aqp4 fluorescence in terms of the mean grey value was measured. Furthermore, the CD31 fluorescence was thresholded and set as a mask on top of the Aqp4 signal. Within this vascular endothelial mask, the Aqp4 fluorescence was measured to determine the percentage of the endothelial surface covered by astrocyte end feet (see **Figure 12**). Only one ROI (300 µm x 300 µm) was analyzed ipsilaterally in the middle of the cortex 300 µm away from the lesion margin (ROI 2), which was normalized to the contralateral side (ROI 4) (see **Figure 13**). No analysis could be performed in the striatum as the staining here was indistinct and there was too much unspecific background staining. We analyzed the control group, including sham 24 hours after surgery and naive animals, and the following time points after TBI: 24 hours, 7 days and 6 months.

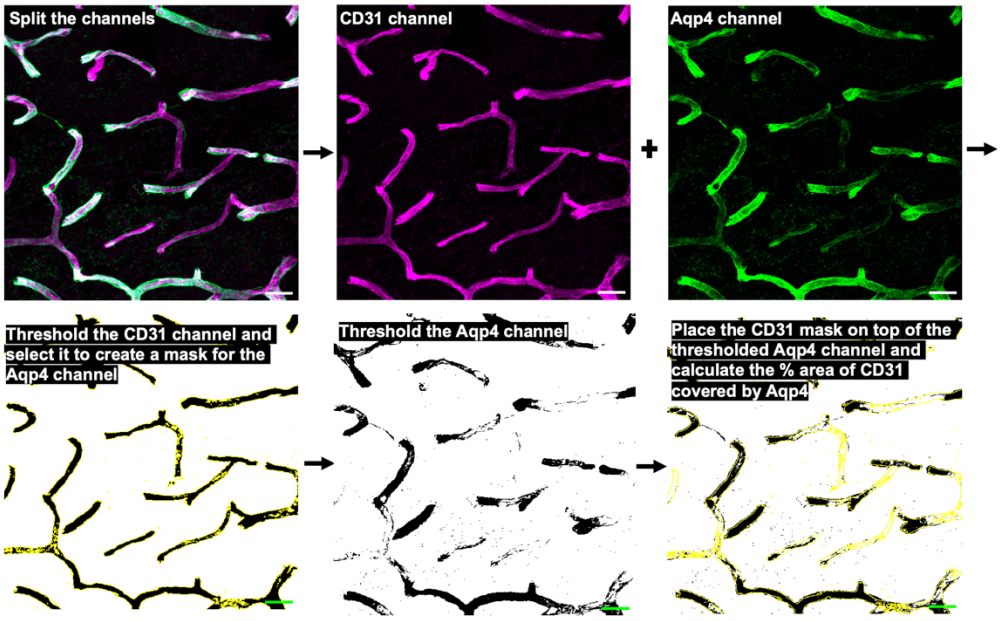

Figure 12: Step by step flow diagram of the astrocyte coverage analysis with the CD31 (magenta) and Aqp4 (green) staining at ROI 1 of a Sham 24 h mouse. Scale bar = 20 µm.

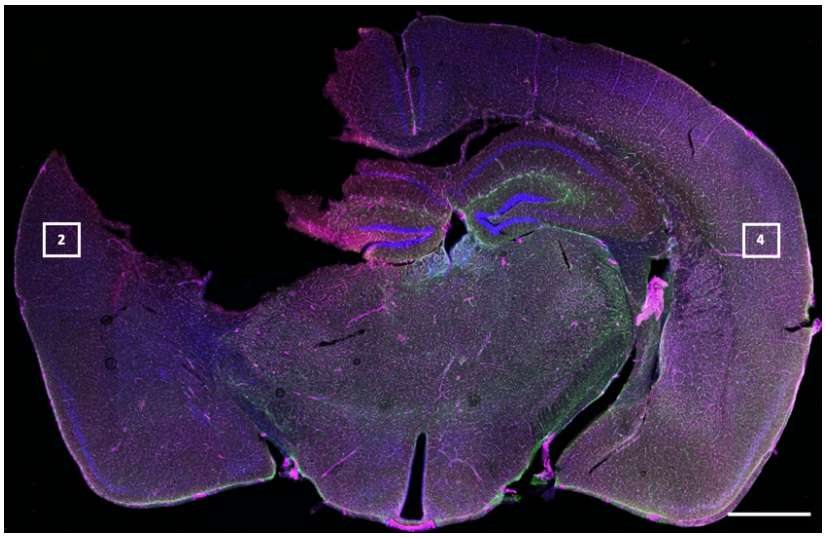

Figure 13: Astrocyte coverage analysis at ROI 1 in the ipsilateral cortex and ROI 2 in the contralateral cortex of a coronal brain section. Scale bar = 1 mm.

2.7.3.6.2 Blood Brain Barrier (BBB) Disruption

To analyze the integrity of the BBB, the presence of parenchymal albumin was assessed; albumin with its weight of 66.5 kDa cannot cross the intact BBB, therefore the quantity of intraparenchymal albumin is a surrogate marker for BBB disruption. Images obtained of sections stained with albumin (main intravascular component) and laminin (representing the vascular basement membrane) were imported into ImageJ as a maximum intensity projection of the Z-stack images. The total albumin and laminin fluorescence was measured using the mean grey value, as well as the albumin signal outside the laminin vessel boundaries (see **Figure 14)**. The pure extravascular albumin fluorescence was then determined more precisely per image using an individually determined threshold to subtract the unspecific background signal, which was also previously added to the mean grey value. Two ROIs (each 300 µm x 300 µm) were analyzed: ROI 1 ipsilateral in the

center of the striatum 300 µm away from the lesion margin and ROI 2 ipsilateral in the center of the cortex 300 µm away from the lesion margin (see **Figure 15**). Both ROIs were also normalized to the contralateral side. The ROIs were purposely selected to have some distance to the lesion rim, as the directly adjacent vessels were largely severed by the shear forces of the trauma and therefore could not be assessed. All time points from 24 hours to six months after TBI were analyzed. Unfortunately, there were not enough brain sections left for an analysis at 12 months after TBI.

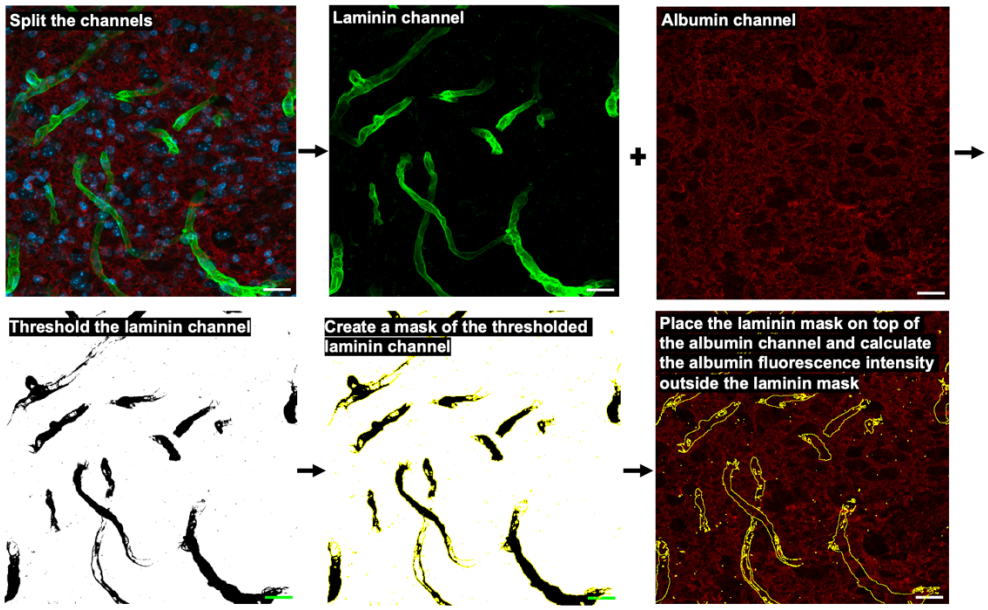

Figure 14: Step by step flow diagram of the blood brain barrier leakage analysis with the laminin (green), albumin (red) and dapi (blue) staining at ROI 1 of a 7 d post TBI mouse. Scale bar = 20 µm.

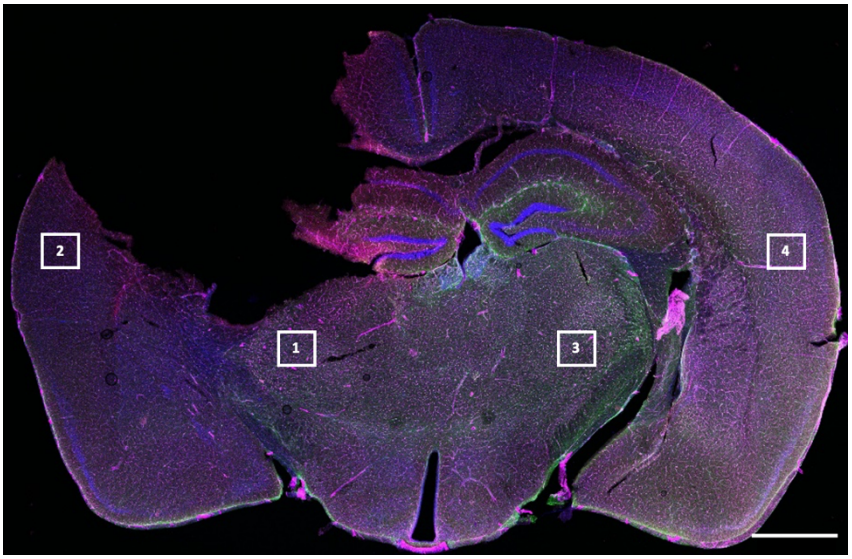

Figure 15: Blood brain barrier leakage analysis at ROI 1 and 2 in the ipsilateral and ROI 3 and 4 in the contralateral hemisphere of a coronal brain section. Scale bar = 1 mm.

2.7.3.7 Assessment of Amyloid-β Plaques

To investigate neurodegenerative processes after TBI, the formation of Amyloid-β (Aβ) plaques after chronic TBI was studied. Aβ is a characteristic pathological protein in Alzheimer's disease that aggregates and forms plaques in the brain of individuals with Alzheimer's disease [191]. The 6E10 antibody is designed to specifically recognize a pathological sequence of the Aβ peptide without reacting with other proteins or structures in the brain tissue [268]. The following time points were analyzed: naive young, naive 12 months, Sham 24 hours, Sham 12 months, 7 days and 12 months post TBI.

The Aβ and NeuN staining was captured with a 10x objective (EC Plan-Neofluar 10x/0.30 Pol M27), with an image matrix of 1024 x 1024 pixels, 16 bits per pixel, voxel size 2.7621 x 2.7621 x 10 μm^3. Whole brain images were acquired in Z-stacks as tile scans, imported into Fiji and assessed in maximum intensity projections. Total Aβ fluorescence was measured in mean grey values over the complete hemisphere and normalized to naïve and sham animals (**see Figure Figure 16**).

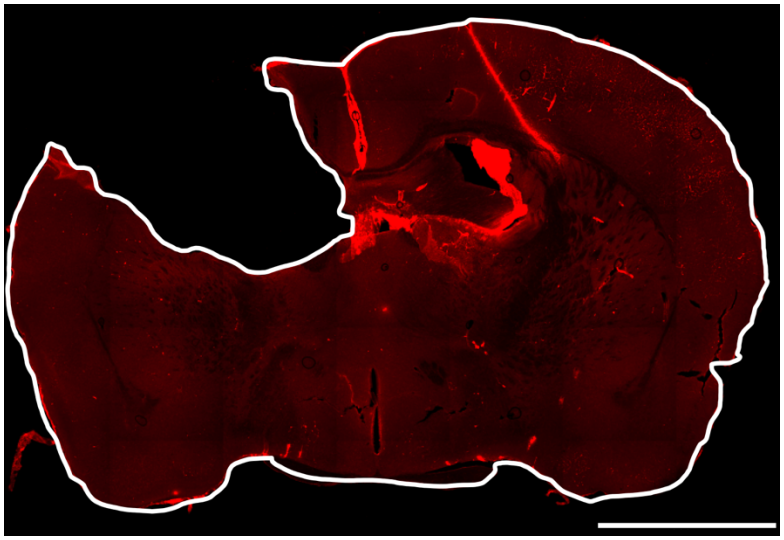

Figure 16: Amyloid-β plaque analysis of the whole hemisphere of a coronal brain section: Scale bar = 1 mm.

2.8 Statistical Analysis

Statistical analysis was performed using GraphPad Prism (version 9.0, San Diego, California, USA). The sample size was calculated using the following parameters: alpha error = 0.05, beta error = 0.2. Normally distributed data is expressed as mean ± standard deviation (SD) and non-normally distributed data as median + 95% confidence interval (CI). All data sets were first tested for normal distribution using the Shapiro-Wilk normality test. To compare two groups, the Student t-test was used for normally distributed data and the Mann-Whitney Rank Sum test (= Wilcoxon Rank Sum test) for non-normally distributed data. To compare more than two groups, the One-Way Anova was used for normally distributed data and the Kruskal-Wallis test (= ANOVA on ranks) for non-normally distributed data. Several measurements within a group were tested for significant differences using the analysis of variance for multiple measurements (ANOVA repeated measurements). Differences between the groups were considered statistically significant below a p-value of 0.05.

3. Results

3.1 Standardization

To assess standard deviation and secondary lesion growth, lesion volume was assessed at 15 minutes after TBI (primary damage) and at 24 hours in 9 6-week-old C57BL/6 mice per group. 15 minutes after CCI, lesion volume amounted to 14 ± 4 mm^3 while lesion size increased to 37.0 ± 6.0 mm^3 after 24 hours (**Figure 17A**). Additionally, the CCI caused an ipsilateral hemispheric swelling of 102.9 ± 5.2 % which represented a 2.9% increase in volume of the ipsilateral relative to the contralateral hemisphere in the 15 minute time point and 111.4 ± 3.9 %, hence a 11.4% increase in volume of the ipsilateral in the 24 hour time point (**Figure 17B)**. The larger ipsilateral hemisphere volume following CCI in comparison to the contralateral hemisphere supports this (**Figure 17C and D**). Therefore, it can be concluded that with this CCI model, the surgeon is able to generate a TBI reliably and reproducibly in mice with a low standard deviation, enabling assessment of dynamic, chronic pathological alterations post TBI.

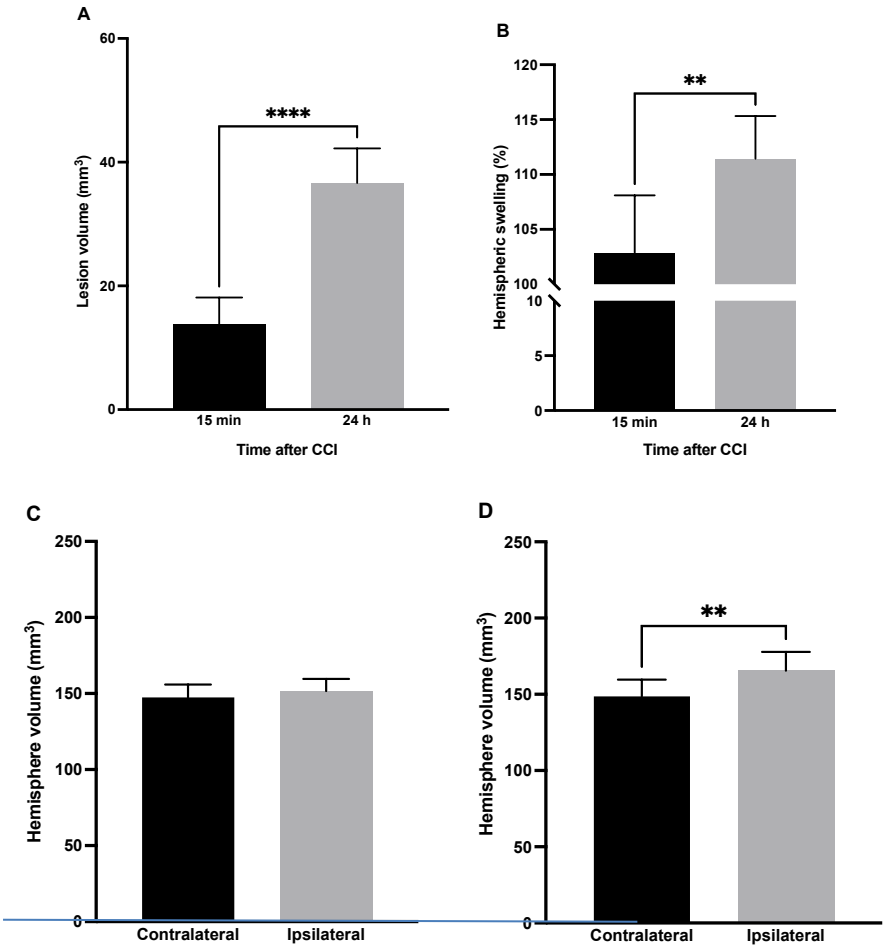

Figure 17: Standardization of the controlled cortical impact model. (A) CCI standardization lesion volume at 15 min and 24 h after CCI. (B) CCI hemispheric swelling at 15 min and 24 h after CCI. (C) Volume of ipsilateral and contralateral hemispheres 15 min after CCI. (D) Volume of ipsilateral and contralateral hemispheres 24 h after CCI. Data are shown as Mean ± SD; t-test, *=p<0.05 vs. naïve/sham, **=p<0.01 vs. naïve/sham, ***=p<0.001 vs. naïve/sham, ****=p<0.0001 vs. naïve/sham, n=1 per naïve, n=5 per sham, n=5 per TBI.

3.2 Assessment of Acute to Chronic Inflammatory Changes

3.2.1 Astrogliosis

Mean GFAP fluorescence intensity was measured at different time points (from 15 minutes to 12 months post TBI) in the complete ipsilateral compared to the contralateral hemisphere (**Figure 18A**) and in seven specific ROIs in the ipsilateral and the respective ROIs in the contralateral hemisphere (**Figure 19A**), to observe the spatial distribution and intensity of scar formation after a head trauma.

Naïve and sham animals were examined first to see if there were any significant differences between them. There were no differences (**Figure 18B and Figure 19B**), so they were combined to form the control group.

In the first analysis, the GFAP fluorescence intensity of the whole TBI hemisphere was greater compared to the contralateral hemisphere at all time points, except for 24 hours post TBI (**Figure 18C**). Quantification of GFAP expression showed a baseline GFAP fluorescence intensity of 2.9 x 10^6 $\pm$ 7.1 x 10^5 AU in control mice (**Figure 18C**). The highest GFAP signal was observed in the ipsilateral hemisphere at seven days post TBI with a mean GFAP fluorescence of 7.1 x 10^6 $\pm$ 1.2 x 10^6 AU (Figure 18C, $p<0.0001$ vs. control), followed by a decrease after one month and a second increase/smaller peak after three months post TBI (**Figure 18C**, mean GFAP fluorescence: 4.7 x 10^6 $\pm$ 7.8 x 10^5 AU). Even after 12 months, the GFAP fluorescence intensity was still significantly elevated in the ipsilateral hemisphere as compared to control animals (**Figure 18C**, mean GFAP fluorescence: 4.1 x 10^6 $\pm$ 1.4 x 10^6 AU, $p<0.05$ vs. control). When normalizing the ipsilateral hemisphere to the contralateral hemisphere to equalize staining differences between groups, the same trend can be observed (**Figure 18D**); a GFAP intensity peak occurred at seven days after CCI (**Figure 18D,** mean GFAP fluorescence 168.4 $\pm$ 34.8% of contralateral, $p<0.0001$), a second smaller peak after three months (**Figure 18D**, mean GFAP fluorescence 152.2 $\pm$ 16.7% of contralateral, $p<0.0001$ compared to control). Even at 12 months after TBI, GFAP fluorescence intensity was significantly elevated compared to the control group (**Figure 18D**, mean GFAP fluorescence 108.2 $\pm$ 16.6% of contralateral, $p=0.201$ compared to naïve/sham). This indicates that once the scar is formed after a head trauma, astrocytes settle into a state of astrogliosis and maintain the scar long after TBI, without returning to the baseline GFAP fluorescence intensities of the control animals even at 12 months after TBI.

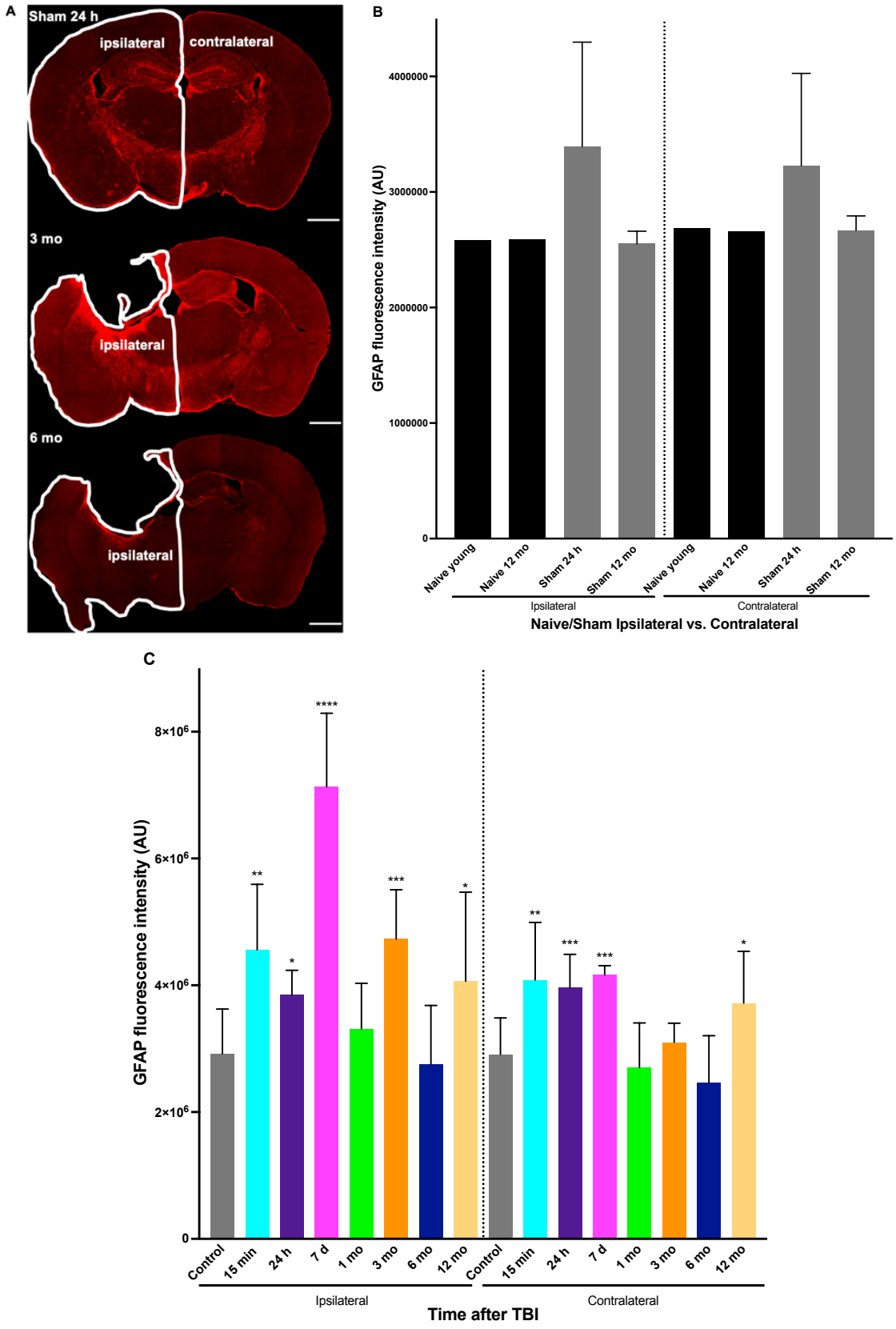
A
Sham 24 h
ipsilateral
contralateral
3 mo
ipsilateral
6 mo
ipsilateral
B
GFAP fluorescence intensity (AU)
4000000
3000000
2000000
1000000
0
Naive young
Naive 12 mo
Sham 24 h
Sham 12 mo
Naive young
Naive 12 mo
Sham 24 h
Sham 12 mo
Ipsilateral
Contralateral
Naive/Sham Ipsilateral vs. Contralateral
C
GFAP fluorescence intensity (AU)
8×10^6
6×10^6
4×10^6
2×10^6
0
****
**
*
***
*
**
***
***
*
Control
15 min
24 h
7 d
1 mo
3 mo
6 mo
12 mo
Control
15 min
24 h
7 d
1 mo
3 mo
6 mo
12 mo
Ipsilateral
Contralateral
Time after TBI

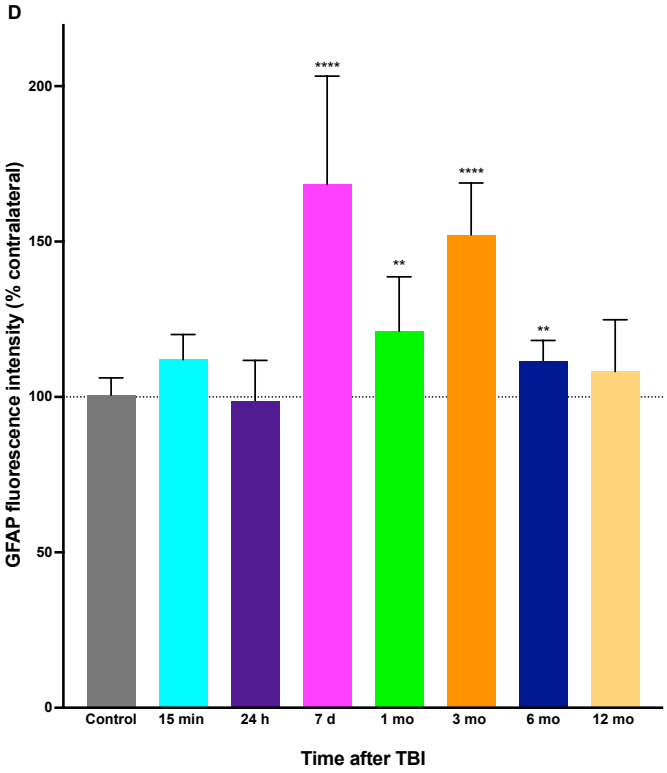

Figure 18: GFAP fluorescence intensity analysis of complete ipsilateral vs. contralateral hemisphere of control and time points 15 min, 24 h, 7 d, 1 mo, 3 mo, 6 mo and 12 mo post TBI. (A) Exemplary GFAP fluorescence intensity stainings of coronal brain sections of sham 24 h, 3 mo and 6 mo post TBI mice, scale bar = 1 mm. (B) GFAP fluorescence intensity in naïve and sham mice in the ipsilateral and contralateral hemisphere. (C) GFAP fluorescence intensity of the ipsilateral vs. the contralateral hemisphere for control and all time points. (D) GFAP fluorescence intensity ipsilateral normalized to contralateral hemisphere for control and all time points. Data are shown as Mean ± SD; t-test, *=p<0.05 vs. control, **=p<0.01 vs. control, ***=p<0.001 vs. control, ****=p<0.0001 vs. control, n=1 per naïve, n=5 per sham, n=5 per TBI.

In the second analysis, the GFAP fluorescence intensity was measured in seven different ROIs in the ipsilateral hemisphere and the corresponding ROIs in the contralateral hemisphere (see locations in **Figure 19A**) to analyze the spatial distribution of astrogliosis. To do so, ROIs 1-3 were chosen directly at the lesion margin in the striatum, ROIs 4-6 1000 µm away from the lesion margin and ROI 7 directly at the lesion margin in the cortex and corresponding contralateral ROIs (ROIs 8-14). GFAP fluorescence intensity reached its peak in the striatum at the lesion margin (ROIs 1-3). Remarkably, ROI 7 – which was also close to the lesion margin but in the cortex – did not exhibit as high GFAP signals and, in turn had fluorescence intensities comparable to ROIs 4-6 which were located 1000 µm away from the lesion margin in the striatum (**Figure 19C**). GFAP fluorescence intensity in the ROIs assessed showed two similar peaks as the global assessment: at seven days and three months post TBI in the ipsilateral hemisphere with the highest peak at three months in ROI 2 (**Figure 19C**). In ROIs 1-3, GFAP intensity persisted to be high even a year after TBI, although there was no significant difference to control animals. Overall, GFAP fluorescence in the more distal regions (ROIs 4-7) in the ipsilateral hemisphere and all ROIs in the contralateral hemisphere, resembled a GFAP fluorescence found in controls (**Figure 19C and D**). Thus, overall, no increased astrogliosis was observed in the cortex, 1000 µm away from the lesion margin or anywhere in the contralateral hemisphere (**Figure 19C and D**). The same trend is observed when normalizing the ipsilateral to the contralateral hemisphere to adjust for staining differences (**Figure 19E**). To compare the ROIs with the highest scar formation more precisely, ROI 1 and 3 were plotted separately (**Figure 19F**

and G). There was an astrogliosis peak at seven days and three months and a continuously elevated GFAP fluorescence up until 12 months after TBI. In total, the data suggest that astrogliosis remains persistently increased for up to 12 months following TBI and that the scar formation is most pronounced close to the lesion.

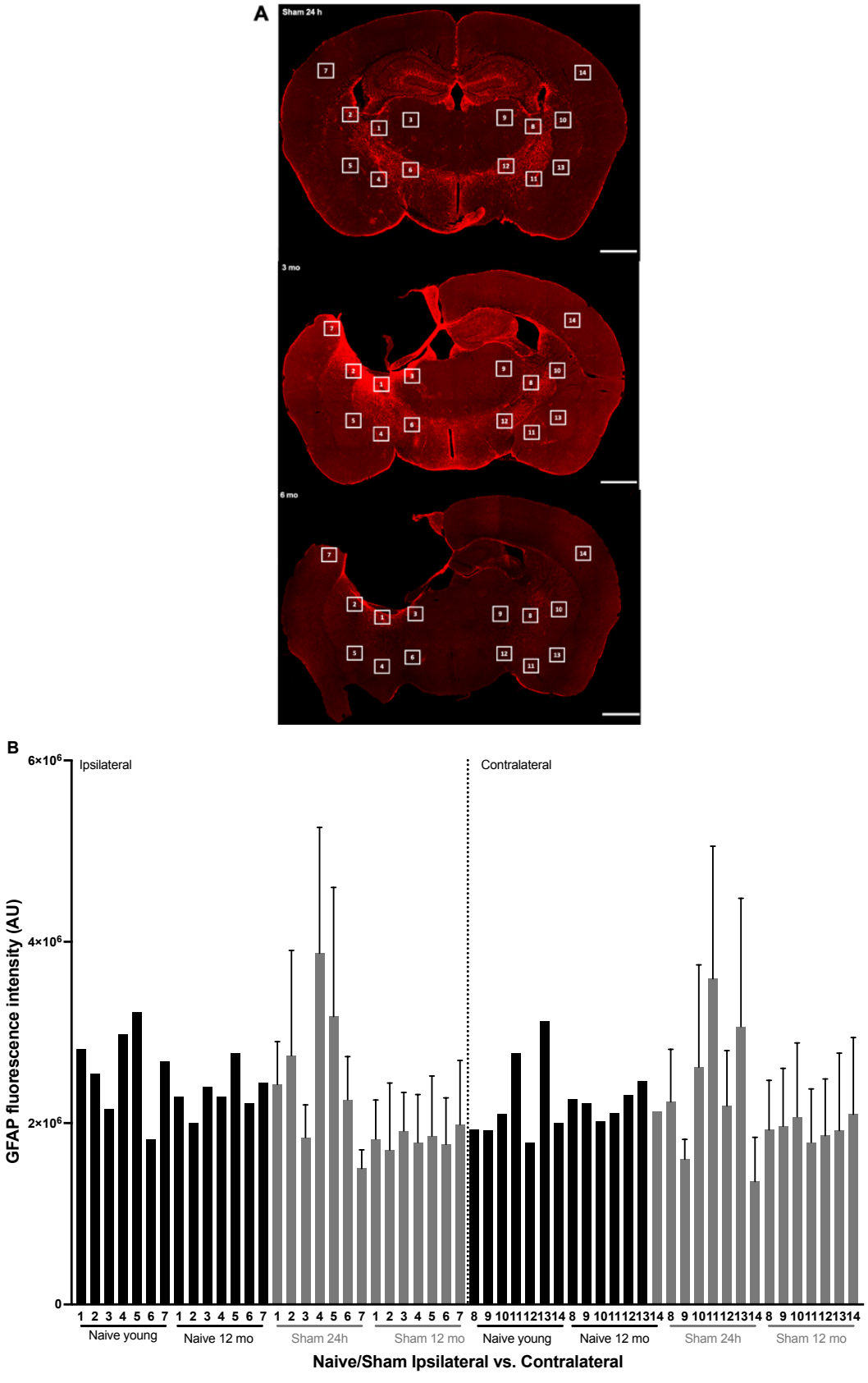

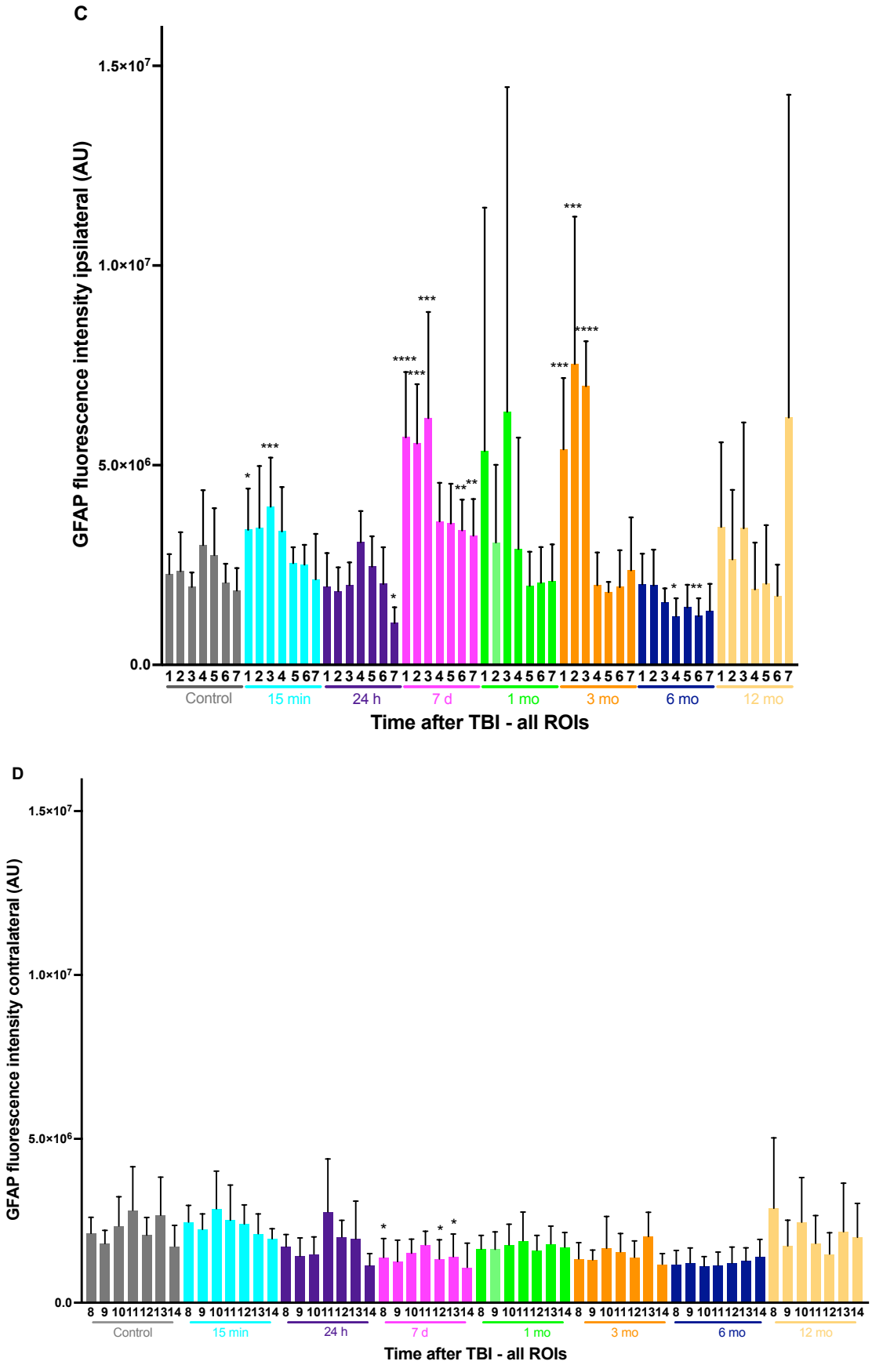
C
GFAP fluorescence intensity ipsilateral (AU)
1.5×10^7
1.0×10^7
5.0×10^6
0.0
Control
15 min
24 h
7 d
1 mo
3 mo
6 mo
12 mo
Time after TBI - all ROIs
D
GFAP fluorescence intensity contralateral (AU)
1.5×10^7
1.0×10^7
5.0×10^6
0.0
Control
15 min
24 h
7 d
1 mo
3 mo
6 mo
12 mo
Time after TBI - all ROIs

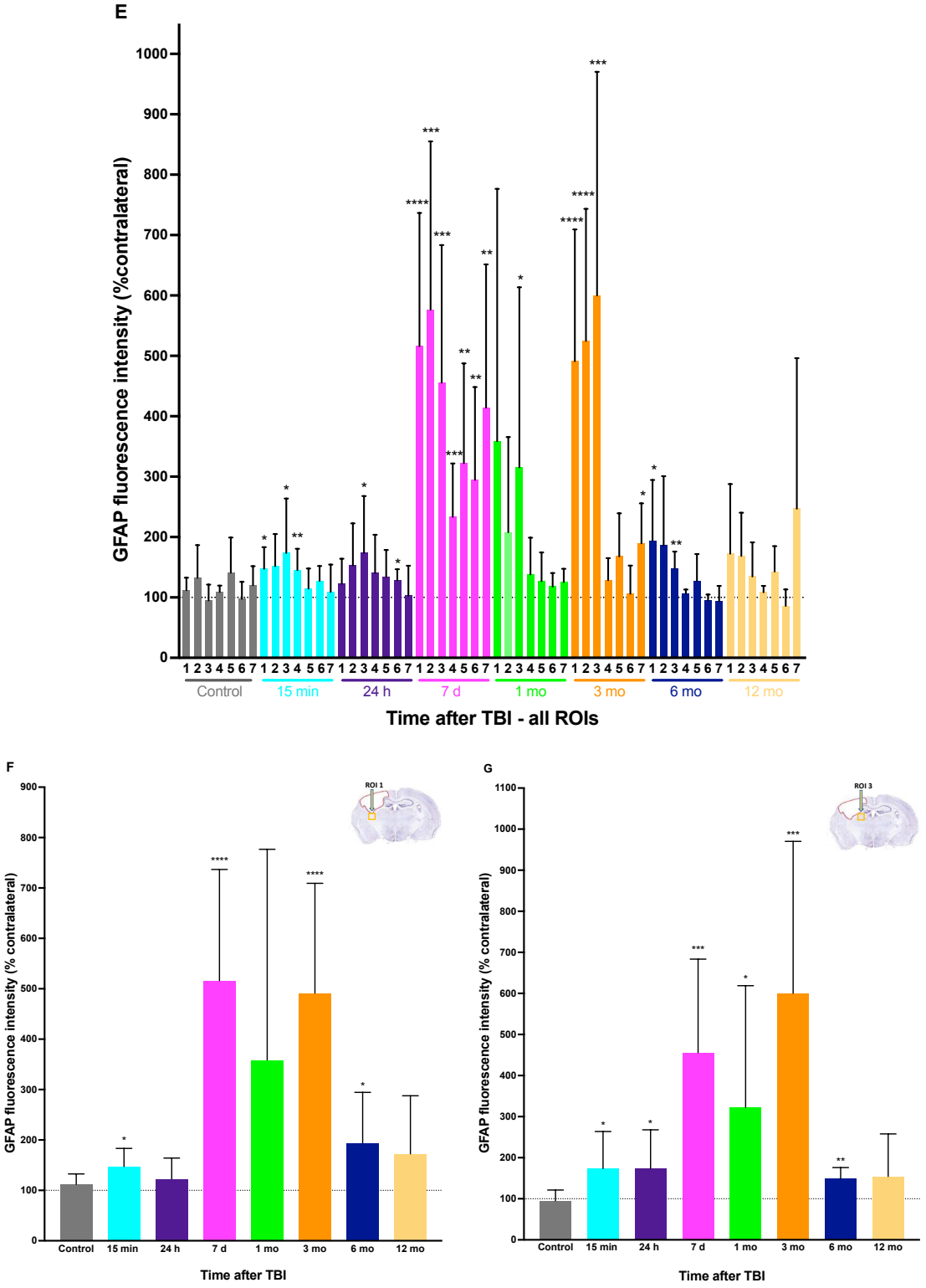

Figure 19: **GFAP fluorescence intensity analysis in different ROIs of control and time points 15 min, 24 h, 7 d, 1 mo, 3 mo, 6 mo and 12 mo post.** (A) Exemplary GFAP fluorescence intensity staining's of coronal brain sections with seven different ROIs in the ipsilateral and the corresponding ROIs in the contralateral hemisphere of sham 24 h, 3 mo and 6 mo post TBI mice, scale bar = 1 mm. (B) GFAP fluorescence intensity in naïve and sham mice across seven ROIs in the ipsilateral vs. the respective ROIs in the contralateral hemisphere. (C) GFAP fluorescence intensity in the ipsilateral hemisphere across the seven ROIs. (D) GFAP fluorescence intensity in the contralateral hemisphere. (E) GFAP fluorescence intensity of the ipsilateral normalized to contralateral hemisphere across seven ROIs. (F) GFAP fluorescence intensity of the ipsilateral normalized to the contralateral hemisphere at ROI 1. (G) GFAP fluorescence intensity of the ipsilateral normalized to the contralateral hemisphere at ROI 3. Data are shown as Mean ± SD; t-test, *=p<0.05 vs. control, **=p<0.01 vs. control, ***=p<0.001 vs. control, ****=p<0.0001 vs. control, n=1 per naïve, n=5 per sham, n=5 per TBI.

3.2.2 Microglia Density

Examining inflammatory changes in relation to microglia density over time following TBI was one of the study's other objectives. Thus, the antibody Iba-1 (ionized calcium-binding adapter molecule 1) was used to stain and identify microglia, the resident immune cells of the central nervous system [270]. The mean fluorescence intensity of Iba-1 was measured in five ROIs in the ipsilateral hemisphere and the mirror-inverted ROIs in the contralateral hemisphere in naïve and sham animals and at time points 15 minutes, 24 hours, 7 days, 1 month, 3 months, 6 months, and 12 months after TBI (**Figure 20A**). This approach facilitated the assessment of temporal changes in microglial distribution across various post-TBI time points, providing insights into the dynamic nature of neuroinflammatory processes in the injured brain.

As can be seen in **Figure 20B**, the quantification of microglia density by Iba-1 pixel based analysis yielded no significant difference between naïve and sham animals; before TBI, the mean Iba-1 fluorescence intensity in the control animals was $2.8 \times 10^6 \pm 2.4 \times 10^5$ AU in all ROIs in both hemispheres.

In the ipsilateral hemisphere, an acute increase in microglia density is observed acutely after TBI, at 15 minutes, followed by a fast decrease with the minimum microglia density across all ROIs at 24 hours post TBI (**Figure 20C**). The maximum microglia density in the ipsilateral hemisphere is observed at seven days and one month post TBI, followed by a steady decrease until six months and a slight increase again at 12 months post TBI (**Figure 20C**). The density of Iba-1 staining in the contralateral hemisphere is not significantly elevated compared to control animals at any time point after TBI, except for significant elevations at 15 minutes, one month and 12 months after TBI (**Figure 20D**).

Overall, when compared to the contralateral, the density of microglia peaks seven days after TBI and starts to quickly decline after one month (**Figure 20E**). It reaches a plateau between six and 12 months, at which point there are no longer any significant differences between the injured animals and the control group (**Figure 20E**). The ROIs with the highest Iba-1 density compared to the contralateral hemisphere are ROIs 1 (**Figure 20E and F**) and 3 (**Figure 20E and G**) at the lesion margin in the striatum. Also here, a microglia density peak at seven days post TBI occurred, with a $176.4 \pm 29.8\%$ (ROI 1, $p<0.0001$ vs. control, **Figure 20F**) and a $103.9 \pm 27.2\%$ increase in microglia density (ROI 3, $p=0.0022$ vs. control, **Figure 20G**) when compared to control animals. At later time points, microglia density steadily decreases but remains elevated compared to control animals even at six months post TBI (ROI 1: $23.6 \pm 12.2\%$ increase, $p=0.08$ vs. control, Figure 20F and ROI 3: $2.8 \pm 17.2\%$ increase, $p=0.87$ vs. control, **Figure 20G**), until it reaches baseline levels at 12 months post TBI (ROI 1: $p=0.43$ vs. control, **Figure 20F** and ROI 3: $p=0.07$ vs. control, **Figure 20G**). All these investigations point towards an increased microglia activation with a maximum at seven days post TBI and a decrease over time; however, it takes 12 months TBI until baseline levels are reached.

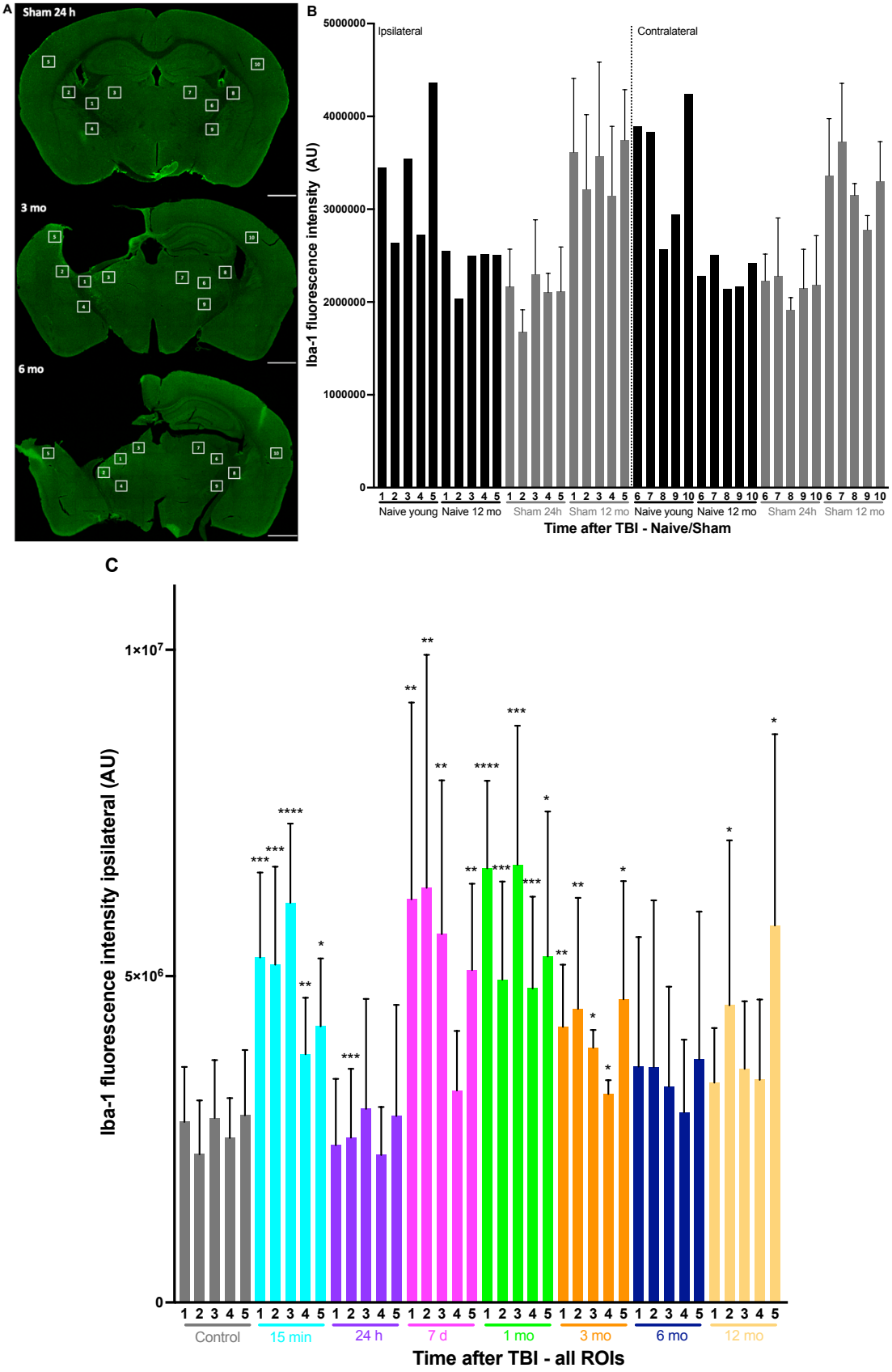
A
Sham 24 h
3 mo
6 mo
B
Ipsilateral
Contralateral
Iba-1 fluorescence intensity (AU)
5000000
4000000
3000000
2000000
1000000
0
Naive young
Naive 12 mo
Sham 24h
Sham 12 mo
Naive young
Naive 12 mo
Sham 24h
Sham 12 mo
Time after TBI - Naive/Sham
C
Iba-1 fluorescence intensity ipsilateral (AU)
1×10^7
5×10^6
0
Control
15 min
24 h
7 d
1 mo
3 mo
6 mo
12 mo
Time after TBI - all ROIs

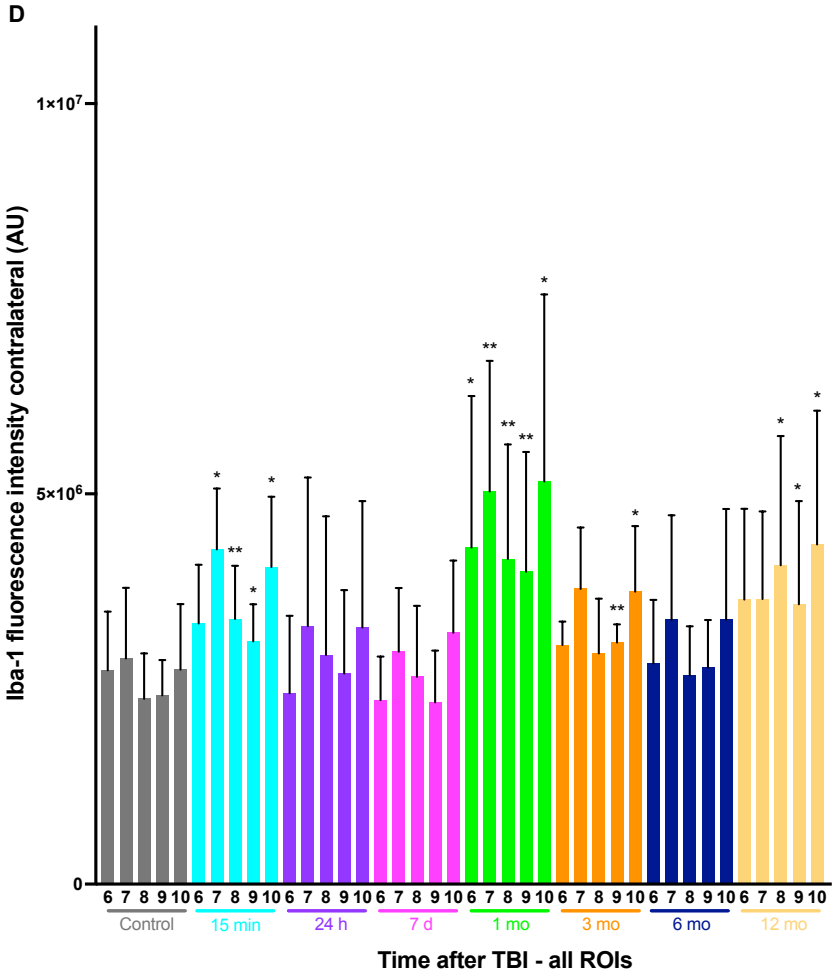
D
1×10^7
5×10^6
0
Iba-1 fluorescence intensity contralateral (AU)
6 7 8 9 10 6 7 8 9 10 6 7 8 9 10 6 7 8 9 10 6 7 8 9 10 6 7 8 9 10 6 7 8 9 10 6 7 8 9 10
Control
15 min
24 h
7 d
1 mo
3 mo
6 mo
12 mo
Time after TBI - all ROIs

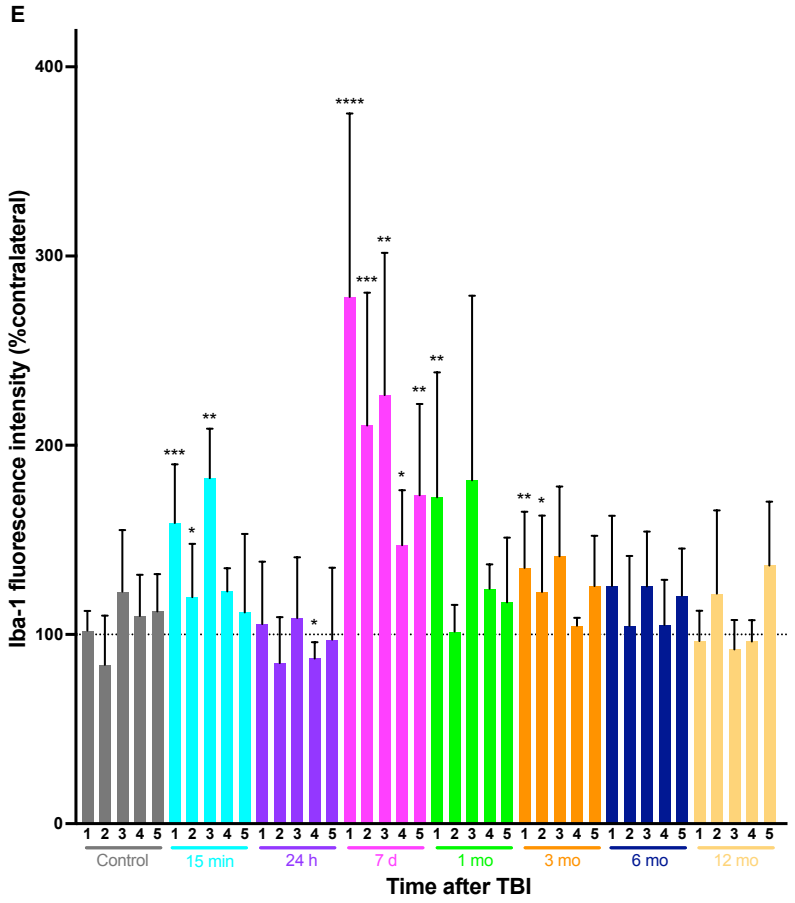
E
400
300
200
100
0
Iba-1 fluorescence intensity (%contralateral)
1 2 3 4 5 1 2 3 4 5 1 2 3 4 5 1 2 3 4 5 1 2 3 4 5 1 2 3 4 5 1 2 3 4 5 1 2 3 4 5
Control
15 min
24 h
7 d
1 mo
3 mo
6 mo
12 mo
Time after TBI

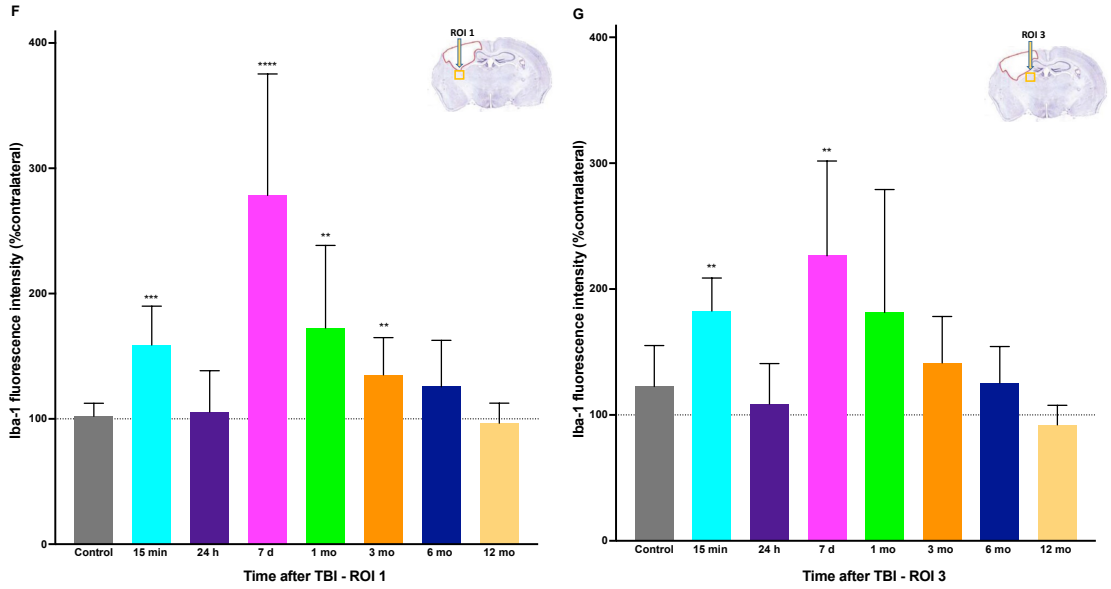

Figure 20: Iba-1 fluorescence intensity analysis in different ROIs of control and time points 15 min, 24 h, 7 d, 1 mo, 3 mo, 6 mo and 12 mo post TBI. (A) Exemplary Iba-1 fluorescence intensity staining's of coronal brain sections with five ROIs in the ipsilateral and the respective ROIs in the contralateral hemisphere of sham 24 h, 3 months, and 6 months post TBI mice, scale bar = 1 mm. (B) Iba-1 fluorescence intensity in naïve and sham mice in the five ROIs in the ipsilateral vs. the five respective ROIs in the contralateral hemisphere. (C) Iba-1 fluorescence intensity of the ipsilateral hemisphere. (D) Iba-1 fluorescence intensity of the contralateral hemisphere. (E) Iba-1 fluorescence intensity of the ipsilateral normalized to the contralateral hemisphere. (F) Iba-1 fluorescence intensity of the ipsilateral normalized to the contralateral hemisphere at ROI 1. (G) Iba-1 fluorescence intensity of the ipsilateral normalized to the contralateral hemisphere at ROI 3. Data are shown as Mean ± SD; t-test, *=p<0.05 vs. control, **=p<0.01 vs. control, ***=p<0.001 vs. control, ****=p<0.0001 vs. control, n=1 per naïve, n=5 per sham, n=5 per TBI.

3.2.3 Microglia Morphology

3.2.3.1 Maximum Span Across Hull, Microglia Circularity, and Microglia Area

The evaluation of microglial morphology was carried out after microglia were identified using Iba-1 labeling to clarify any possible relationships between inflammatory modifications and changes in microglial phenotype in response to TBI. In order to measure the activation of microglia after TBI, we used fractal analysis to evaluate the maximum span across hull, circularity and cell area at the lesion margin in the striatum (ROI 1) and cortex (ROI 2), as well as in the contralateral hemisphere in the cortex (ROI 4), at seven days and six months following injury and in sham 24-hour animals.

Fractal analysis revealed that the cell area and maximum span of microglia decreased over time (**Figure 21B and D**), indicating a significant activation of microglia near the borders of the lesion and in the contralateral hemisphere in the cortex. The cell area and the maximum span across hull decreased in all ROIs from sham 24 hours to seven days post TBI and remained comparably low around those values up to six months post TBI without returning to baseline values. The greatest decrease in the maximum span across hull was observed in ROI 2 with a percentage decrease of 36.7% at seven days (mean: 239.6 ± 32.9, p<0.0001) and 33.6% at six months (mean: 252.5 ± 87.8, p<0.0001) post TBI, when compared to the sham 24 hours group (mean: 378.3 ± 61.5) (**Figure 21B**). The greatest decrease in microglia cell area compared to the sham 24 hours group (median: 3,710.3 (3316, 5351)) was observed in ROI 1 with a percentage decrease of 66.1% at seven days (median: 1,480.0 (1115, 1775), p=0.0163) and 55.5% at 6 months (median: 1,650.5 (1213, 1734), p=0.0053) post TBI (**Figure 21D**). Remarkably, even the microglia

in the contralateral cortex (ROI 4) displayed a reduction in maximum span across hull and cell area; however, in comparison to ROIs surrounding the ipsilateral hemisphere contusion, this loss was less noticeable but still significantly decreased (**Figure 21B and D**).

In case of activation, microglia contract, therefore circularity increases [230, 271]. In our TBI cohort, there was a significant increase in circularity in ROI 2, six months after TBI (p=0.0449, **Figure 21C**), but not at other time points or ROIs. Overall, microglia in proximity to the lesion are smaller, have a decreased span across the hull at seven days and six months post TBI, and are more circular six months after TBI; microglia in the contralateral hemisphere exhibit a comparable but less pronounced alteration in comparison to sham.

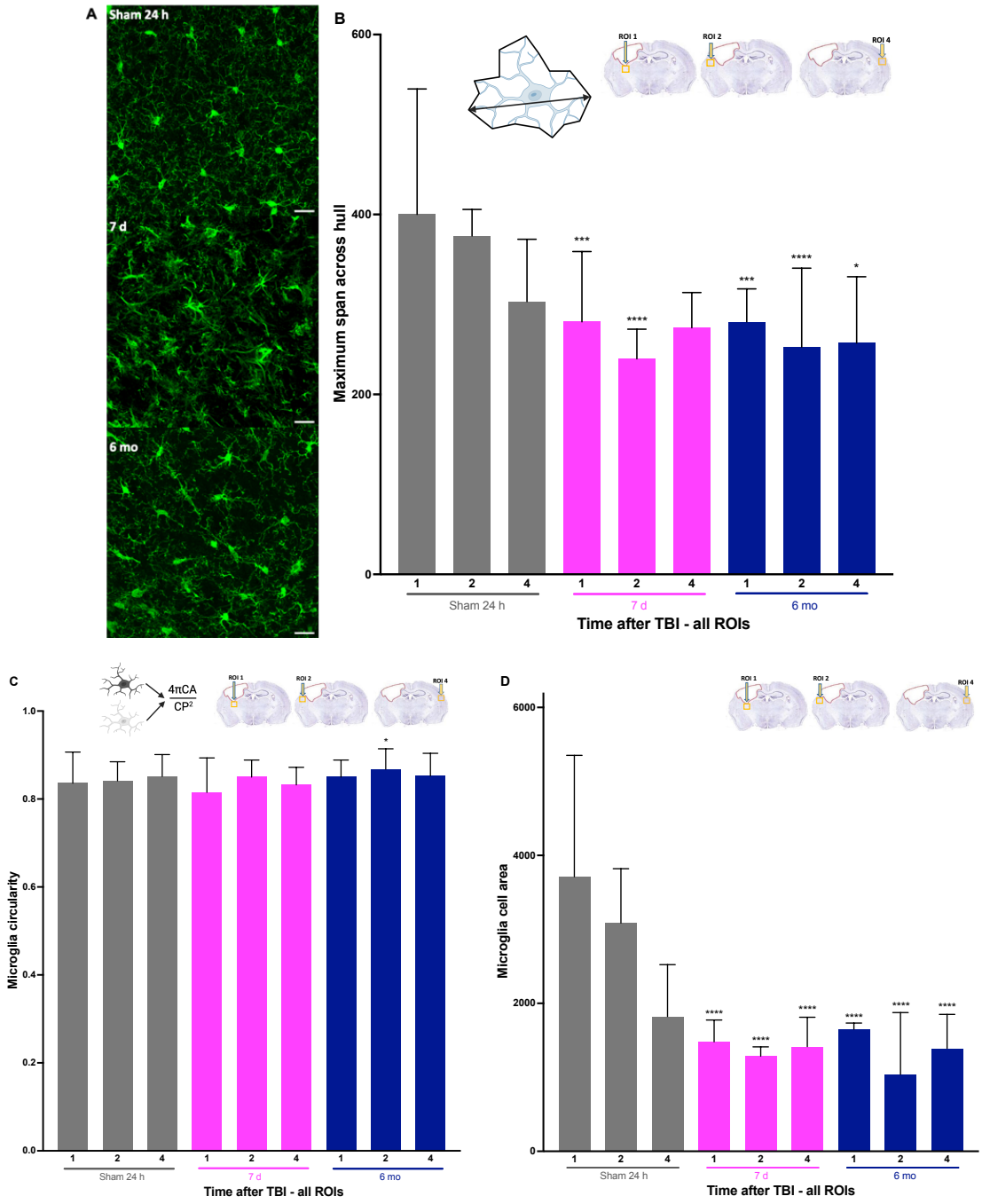

Figure 21: **Microglia morphology fractal analysis in ROI 1, 2 and 4 at time points sham 24 h, 7 d and 6 months post TBI**. (A) Exemplary Iba-1 stainings at ROI 1 of the sham 24 h, the 7 d and the 6 months post TBI mice, scale bar = 20 µm. (B) Maximum span across hull at ROI 1 and 2 in the ipsilateral and ROI 4 in the contralateral hemisphere at time points in the sham 24 h, 7 d, and 6 mo post TBI groups. (C) Microglia circularity at ROI 1 and 2 in the ipsilateral and ROI

4 in the contralateral hemisphere at time points sham 24 h, 7 d and 6 mo post TBI. (D) Microglia cell area at ROI 1 and 2 in the ipsilateral and ROI 4 in the contralateral hemisphere at time points sham 24 h, 7 d and 6 mo post TBI. Data for graphs B and C are shown as Mean ± SD; t-test, and for graph D as Median ± 95% CI; Wilcoxon Rank Rum Test, *=p<0.05 vs. sham, **=p<0.01 vs. sham, ***=p<0.001 vs. sham, ****=p<0.0001 vs. sham, n=5 per sham, n=5 per TBI. Microglia images created with BioRender.com.

3.2.3.2 Microglia Ramifications

Microglia ramifications or the number of intersections of their processes serve as important indicators for the duration and timing of microglia activation and their involvement in the immune response after TBI [272]. Microglia ramifications were therefore quantified using sholl analysis in the identical ROIs and time points as in the fractal analysis mentioned previously. In comparison to sham 24 hours, the number of microglia branch points was reduced at almost all distances from the soma at seven days and six months post-TBI (**Figure 22A-C**), suggesting microglia activation. At a distance of 20 µm from the soma, ROIs 1, 2, and 4 were specifically analyzed because, as compared to sham, they appeared to have the largest reduction in microglia ramifications at this distance (**Figure 22D-F**). The number of microglia intersections decreased the most in ROI 1, from a median of 17.0 intersections in sham 24 hours to a minimum of 8.7 at seven days post-TBI (p<0.0001) and a modest increase to 10.4 intersections at six months post TBI (p=0.0002) (**Figure 22D**). A similar but less pronounced decrease of microglia intersection points was seen in ROI 2 and 4 (**Figure 22E and F**).

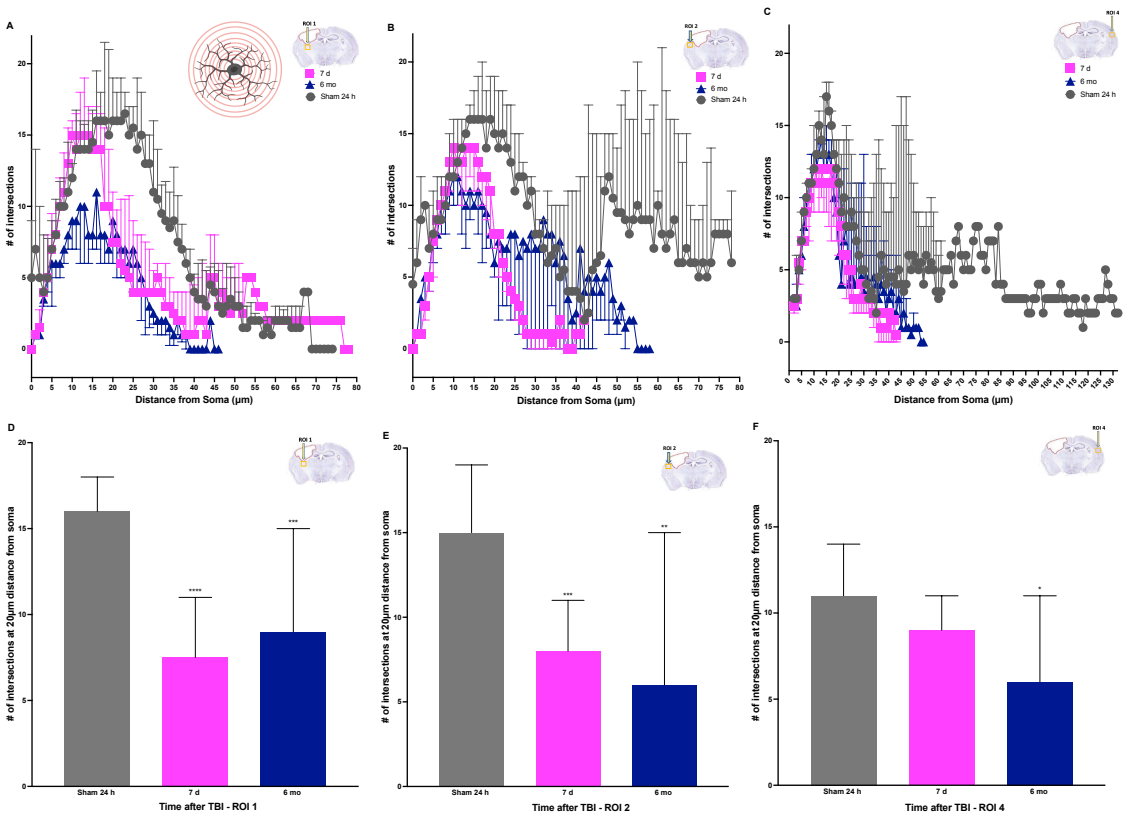

Figure 22: Microglia ramification sholl analysis in ROI 1, 2 and 4 at time points sham 24 h, 7 d and 6 mo post TBI. (A) # of intersections at different distances from the soma in ROI 1 in the ipsilateral striatum at time points sham 24 h, 7 d and 6 mo post TBI. (B) # of intersections at different distances from the soma in ROI 2 in the ipsilateral cortex at time points sham 24 h, 7 d and 6 mo post TBI. (C) # of intersections at different distances from the soma in ROI 4 in the contralateral cortex at time points sham 24 h, 7 d and 6 mo post TBI. (D) # of intersections at 20 μm distance from the soma in ROI 1 in the ipsilateral striatum at time points sham 24 h, 7 d and 6 mo post TBI. (E) # of intersections at 20 μm distance from the soma in ROI 2 in the ipsilateral cortex at time points sham 24 h, 7 d and 6 mo post TBI. (F) # of intersections at 20 μm distance from the soma in ROI 4 in the contralateral cortex at time points sham 24 h, 7 d and 6 mo

post TBI. Data are shown as Median ± 95% CI; Wilcoxon Rank Rum Test, *=p<0.05 vs. sham, **=p<0.01 vs. sham, ***=p<0.001 vs. sham, ****=p<0.0001 vs. sham, n=5 per sham, n=5 per TBI. Microglia image created with BioRender.com.

3.2.4 Microglia Activation

To examine how the immune system reacts to tissue damage following an injury, CD68, a marker of microglia and macrophage activation, was used. This is a damage associated microglial marker involved in phagocytosis and implies microglia are actively engulfing cellular debris caused by a pathology [74]. Consequently, we examined the CD68 fluorescence intensity in five ROIs in the ipsilateral and the corresponding ROIs in the contralateral hemisphere: ROIs 1-3 were situated along the striatal lesion margin, ROI 4 was 600 µm distant from the lesion in the striatum and ROI 5 was along the lesion margin in the cortex (**Figure 23A**). Next, we carried out a 2D (at the same 5 ROIs, **Figure 10**) and 3D (at 2 ROIs along the lesion margin in the striatum and cortex, **Figure 11**) colocalization study of CD68 with activated microglia to determine which microglia were activated and where,.

3.2.4.1 Assessment of Microglia Activation by CD68 Fluorescence Intensity and 2D CD68/Iba-1 Colocalization

The CD68 fluorescence intensity analysis was conducted following the observation of no significant differences between the sham-operated and naïve animals, prompting their combination as control in the subsequent study (**Figure 23B**). During the acute phase of a traumatic brain injury (15 minutes and 24 hours), the CD68 fluorescence intensity in the ipsilateral hemisphere remained at control levels (mean of all ROIs at 15 minutes: 2.3 x 10^6 AU, at 24 hours: 2.9 x 10^6 AU, control: 2.3 x 10^6 AU, **Figure 23C**). Following this, there was an increase at seven days after the injury (mean of all ROIs 6.4 x 10^6 AU, **Figure 23C**), a decrease that occurred one month later (4.0 x 10^6 AU, **Figure 23C**), and then a continuous reduction at later time points where CD68 remained just above baseline levels in all ROIs (**Figure 23C**). CD68 fluorescence intensity in the contralateral hemisphere did not differ from control mice (**Figure 23D**).

When the ipsilateral CD68 fluorescence intensity is reported as percent of the contralateral hemisphere, a similar pattern with a peak at seven days is observed (mean CD68 fluorescence intensity of all ROIs at 7 days: 235.7% of contralateral, **Figure 23E**). ROIs 1 and 3 (**Figure 23F** and G), the two ROIs closest to the striatal lesion, displayed the strongest CD68 signals compared to control. In ROI 1 (**Figure 23F**) and ROI 3 (**Figure 23G**), ipsilateral CD68 levels were nearly identical to the contralateral side´s signal in the control group as well as 15 minutes and 24h after TBI; later after TBI, there is a significant increase with a maximum at seven days (ROI 1: 7 days post-TBI: 370.0 ± 257.4% of the contralateral, p=0.0053, 1 month: 196.2 ± 50.7%, p=0.0001, ROI 3: seven days post-TBI: 251.0 ± 98.4% of the contralateral, p=0.0066, 1 month: 172.0 ± 53.0%, p=0.1777, **Figure 23F and G**). 12 months post-TBI, C68 fluorescence intensity levels returned to baseline values to 98.0 ± 27.6%, p=0.3838 in ROI 1 and 92.9 ± 21.5%, p=0.3838 in ROI 3.

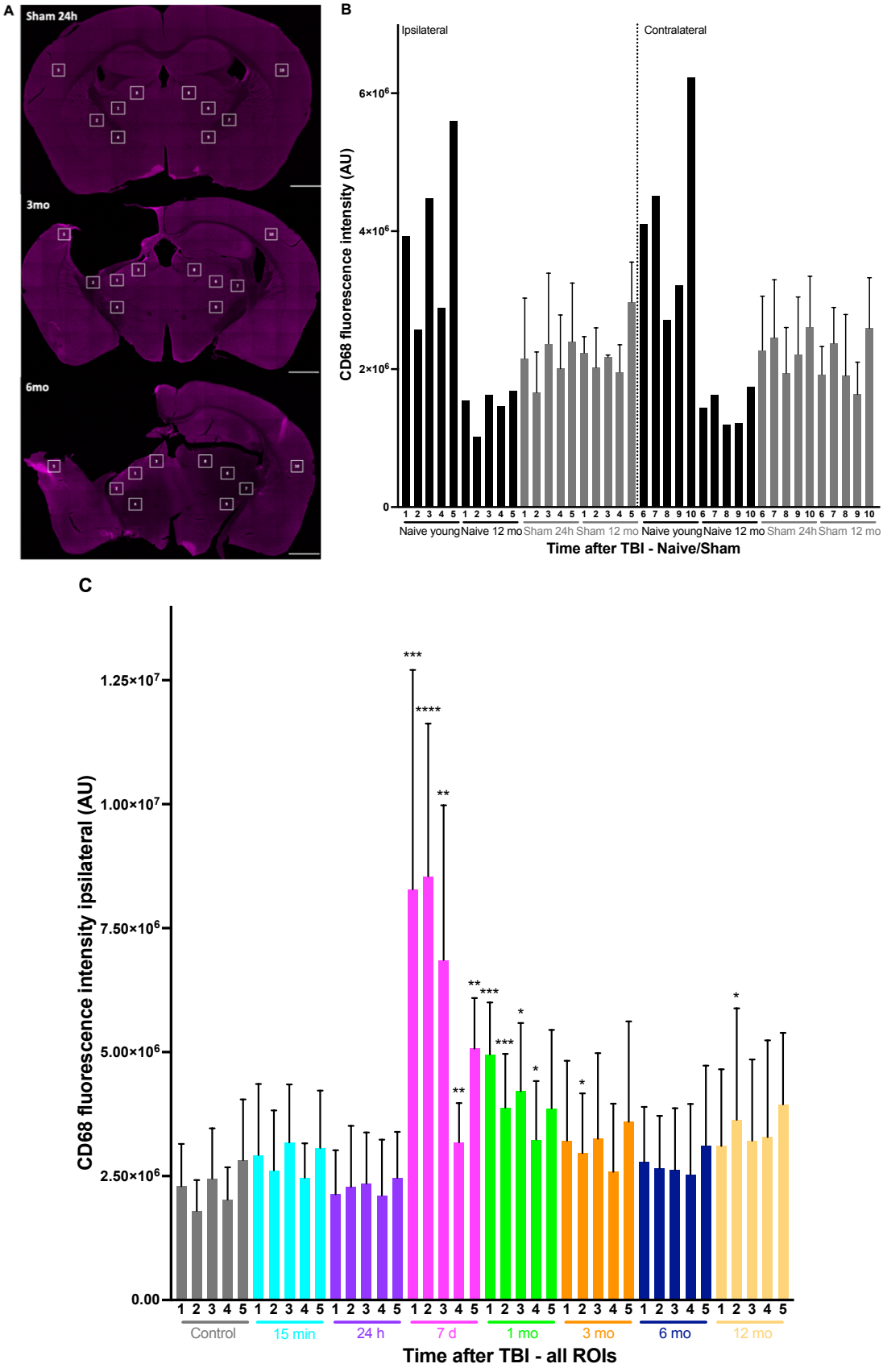
A
Sham 24h
3mo
6mo
B
Ipsilateral
Contralateral
CD68 fluorescence intensity (AU)
6×10^6
4×10^6
2×10^6
0
Naive young
Naive 12 mo
Sham 24h
Sham 12 mo
Time after TBI - Naive/Sham
C
CD68 fluorescence intensity ipsilateral (AU)
1.25×10^7
1.00×10^7
7.50×10^6
5.00×10^6
2.50×10^6
0.00
Control
15 min
24 h
7 d
1 mo
3 mo
6 mo
12 mo
Time after TBI - all ROIs

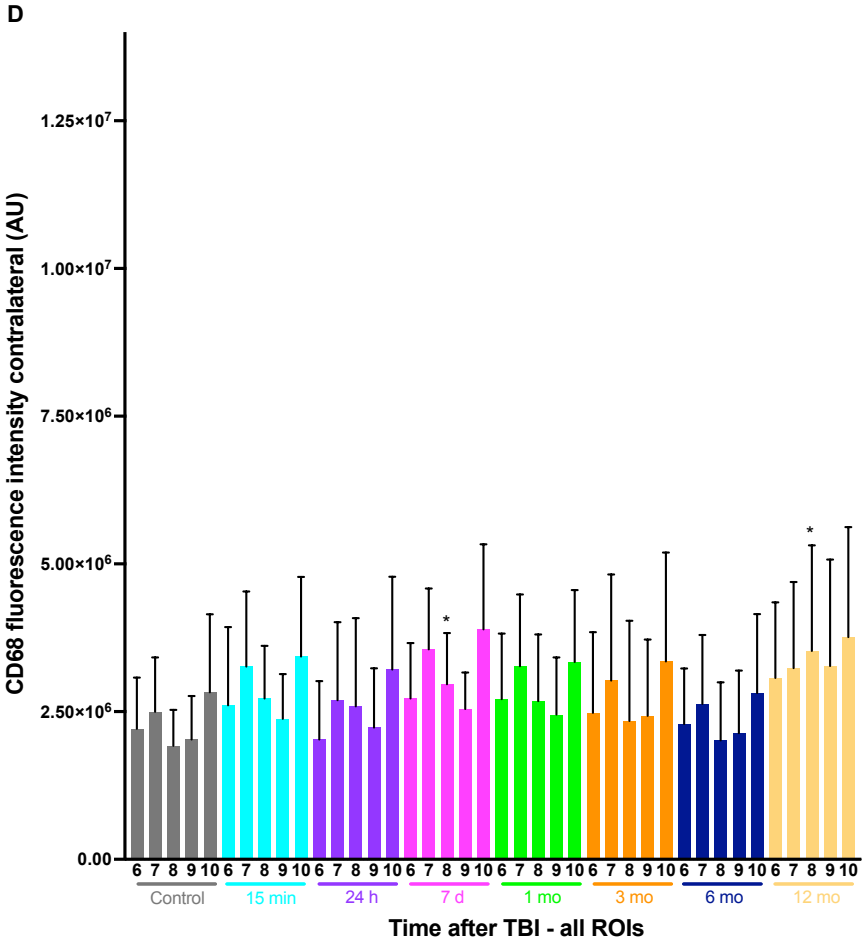
D
CD68 fluorescence intensity contralateral (AU)
1.25×10^7
1.00×10^7
7.50×10^6
5.00×10^6
2.50×10^6
0.00
6 7 8 9 10 6 7 8 9 10 6 7 8 9 10 6 7 8 9 10 6 7 8 9 10 6 7 8 9 10 6 7 8 9 10
Control
15 min
24 h
7 d
1 mo
3 mo
6 mo
12 mo
Time after TBI - all ROIs

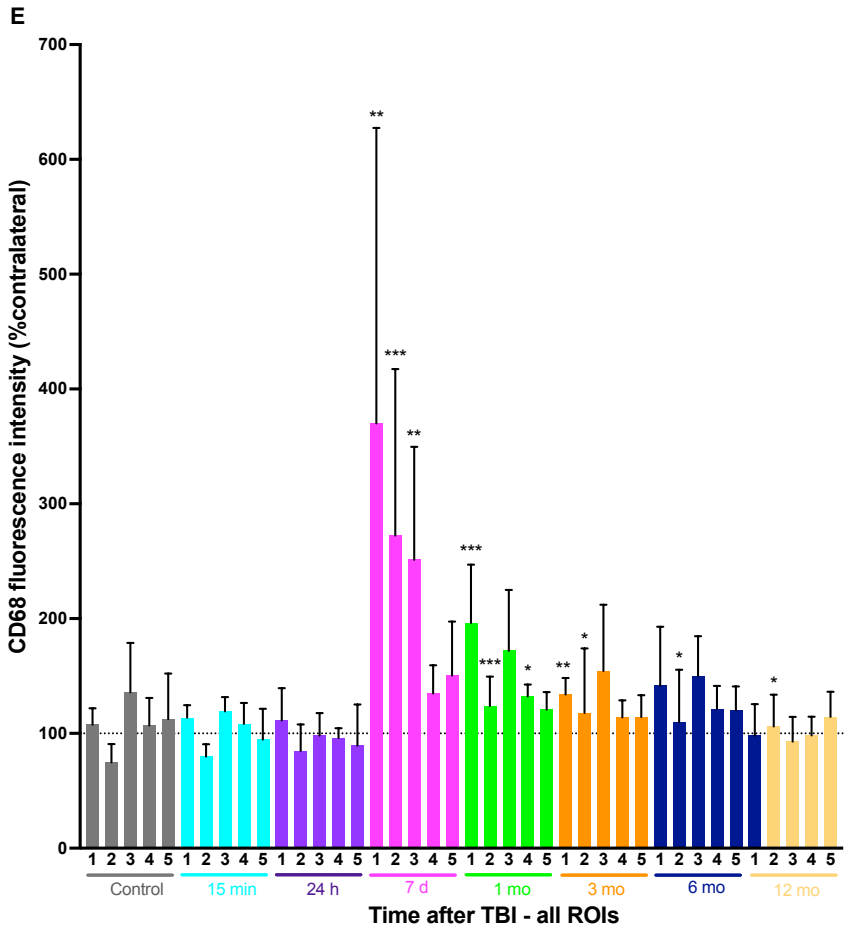
E
CD68 fluorescence intensity (%contralateral)
700
600
500
400
300
200
100
0
1 2 3 4 5 1 2 3 4 5 1 2 3 4 5 1 2 3 4 5 1 2 3 4 5 1 2 3 4 5 1 2 3 4 5 1 2 3 4 5
Control
15 min
24 h
7 d
1 mo
3 mo
6 mo
12 mo
Time after TBI - all ROIs

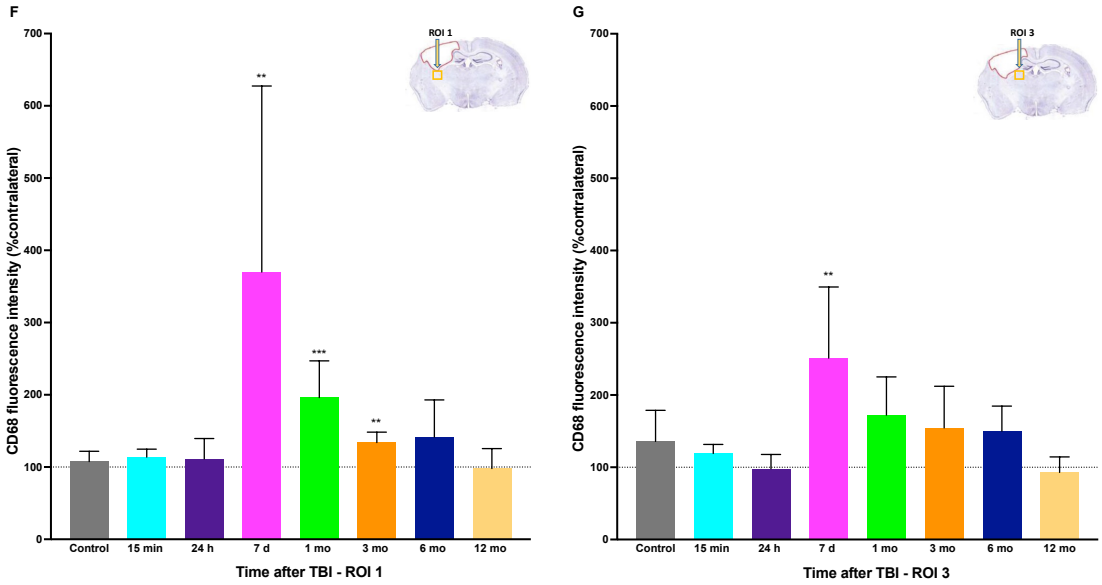

Figure 23: CD68 fluorescence intensity analysis in different ROIs for control and time points 15 min, 24 h, 7 d, 1 mo, 3 mo, 6 mo and 12 mo post TBI. (A) Exemplary CD68 fluorescence intensity staining's of coronal brain sections with five ROIs in the ipsilateral and the respective ROIs in the contralateral hemisphere of sham 24 h, 3 mo and 6 mo post TBI mice, scale bar = 1 mm. (B) CD68 fluorescence intensity in naïve and sham mice at the five ROIs in the ipsilateral vs. the five respective ROIs in the contralateral hemisphere. (C) CD68 fluorescence intensity of the ipsilateral hemisphere across five ROIs. (D) CD68 fluorescence intensity of the contralateral hemisphere across five ROIs. (E) CD68 fluorescence intensity of the ipsilateral normalized to the contralateral hemisphere across five ROIs. (F) CD68 fluorescence intensity of the ipsilateral normalized to the contralateral hemisphere at ROI 1. (G) CD68 fluorescence intensity of the ipsilateral normalized to the contralateral hemisphere at ROI 3. Data are shown as Mean ± SD; t-test, *=p<0.05 vs. control, **=p<0.01 vs. control, ***=p<0.001 vs. control, ****=p<0.0001 vs. control, n=1 per naïve, n=5 per sham, n=5 per TBI.

To analyze microglia activation, a 2D colocalization of CD68 and Iba-1 stained sections was performed in five ROIs in the ipsilateral and the corresponding ROIs in the contralateral hemisphere (see **Figure 10** and **Figure 24A**). Again, naïve and sham groups were merged as a control group as no significant difference in the CD68/Iba-1 ratio was seen between them (mean CD68/Iba-1 ratio for ROIs 1-5 for control: 90.3 ± 35.5 AU **Figure 24B**). In the ipsilateral hemisphere, the CD68/Iba-1 ratio reaches its maximum at seven days after TBI in ROI 1 (137.8 ± 19.0 AU p=0.0097 vs. control) and 2 (148.6 ± 36. 9 AU p=0.0074 vs. control) and then returns to baseline/control values in the following time points at one month, three months six months and 12 months (**Figure 24C**). In the contralateral hemisphere, no ROI showed a significant higher microglia activation than the control group at any time point after TBI (**Figure 24D**).

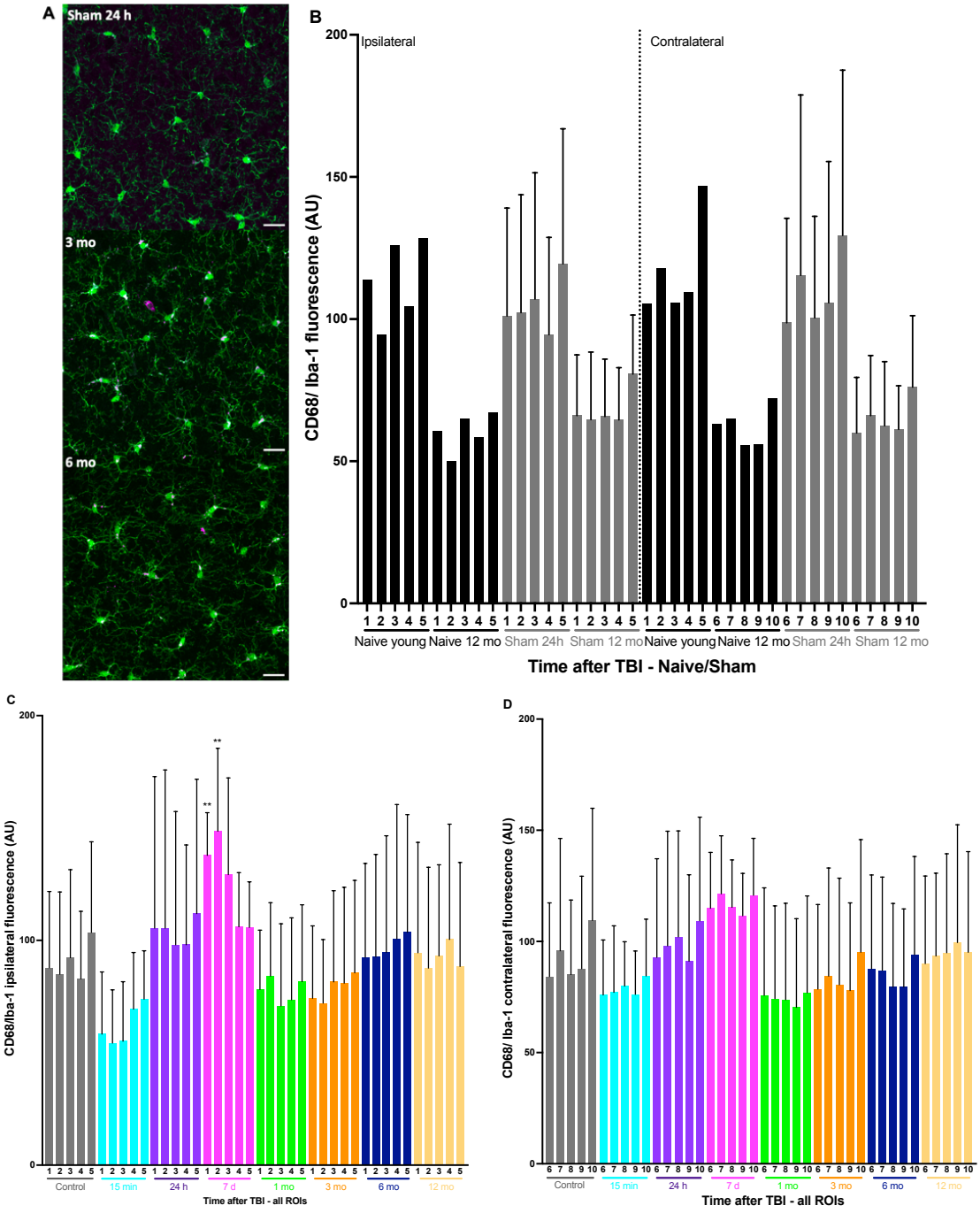

Figure 24: **CD68/Iba-1 fluorescence intensity analysis in different ROIs for control and time points 15 min, 24 h, 7 d, 1 mo, 3 mo, 6 mo and 12 mo post TBI.** (A) Exemplary CD68 (magenta) and Iba-1 (green) fluorescence intensity staining's in ROI 1 of sham 24 h, 3 mo and 6 mo post TBI mice, scale bar = 20 μm. (B) CD68/Iba-1 fluorescence intensity in naïve and sham mice at the five ROIs in the ipsilateral vs. the five respective ROIs in the contralateral hemisphere. (C) CD68/Iba-1 fluorescence intensity of the ipsilateral hemisphere. (D) CD68/Iba-1 fluorescence intensity of the contralateral hemisphere.. Data are shown as Mean ± SD; t-test, *=p<0.05 vs. control, **=p<0.01 vs. control, ***=p<0.001 vs. control, ****=p<0.0001 vs. control, n=1 per naïve, n=5 per sham, n=5 per TBI.

3.2.4.2 Assessment of Microglia Activation by 3D CD68/Iba-1 Colocalization

To further characterize the spatial pattern of microglia activation, a 3D analysis of CD68 and Iba-1 colocalization was carried out. **Figure 25A** illustrates the 3D analysis for sham 24-hours and time points 24 hours and six months after TBI. The analysis was performed in ROI 1 and 2 at the

lesion margin in the striatum and cortex and the counterparts in the contralateral hemisphere (ROI 3 and 4) (see **Figure 11**) for a control group (naïve and sham animals, **Figure 25B**) and the following time points after TBI: 24 hours, seven days, and six months. Ipsilaterally, the CD68 and Iba-1 positive signal peaks in ROI 1 at 24 hours after TBI (21.6 ± 8.1 mm^3, p=0.0005, **Figure 25C**), followed by a slight decrease at seven days (18.4 ± 10.5 mm^3, p=0.0076) and six months (16.6 ± 5.6 mm^3, p=0.0005); however, at six months there is still a consistently higher microglia activation compared to control animals (3.5 ± 2.14 mm^3). Also, the contralateral hemisphere reveals a significant increase in activated microglia compared to controls (for ROI 3 - control group: 2.5 ± 1.0 mm^3; 24 hours: 8.4 ± 4.4 mm^3, p=0.0102, seven days: 9.5 ± 7.4 mm^3, p=0.0470, six months: 10.4 ± 2.9 mm^3, p<0.0001, for ROI 4 - control group: 2.6 ± 1.8 mm^3; 24 hours: 9.0 ± 2.9 mm^3, p=0.0015, seven days: 16.3 ± 17.9 mm^3, p=0.0924, six months: 10.4 ± 3.1 mm^3, p=0.0006).

Overall, the 3D colocalization of CD68 with microglia indicates that microglia activation peaks in the ipsilateral hemisphere 24 hours to seven days after a traumatic brain injury (TBI) and remains elevated for up to six months after the injury without declining to pre-trauma levels. There is also a significant, albeit lower activation in the contralateral hemisphere, which peaks at 6 months after the injury.

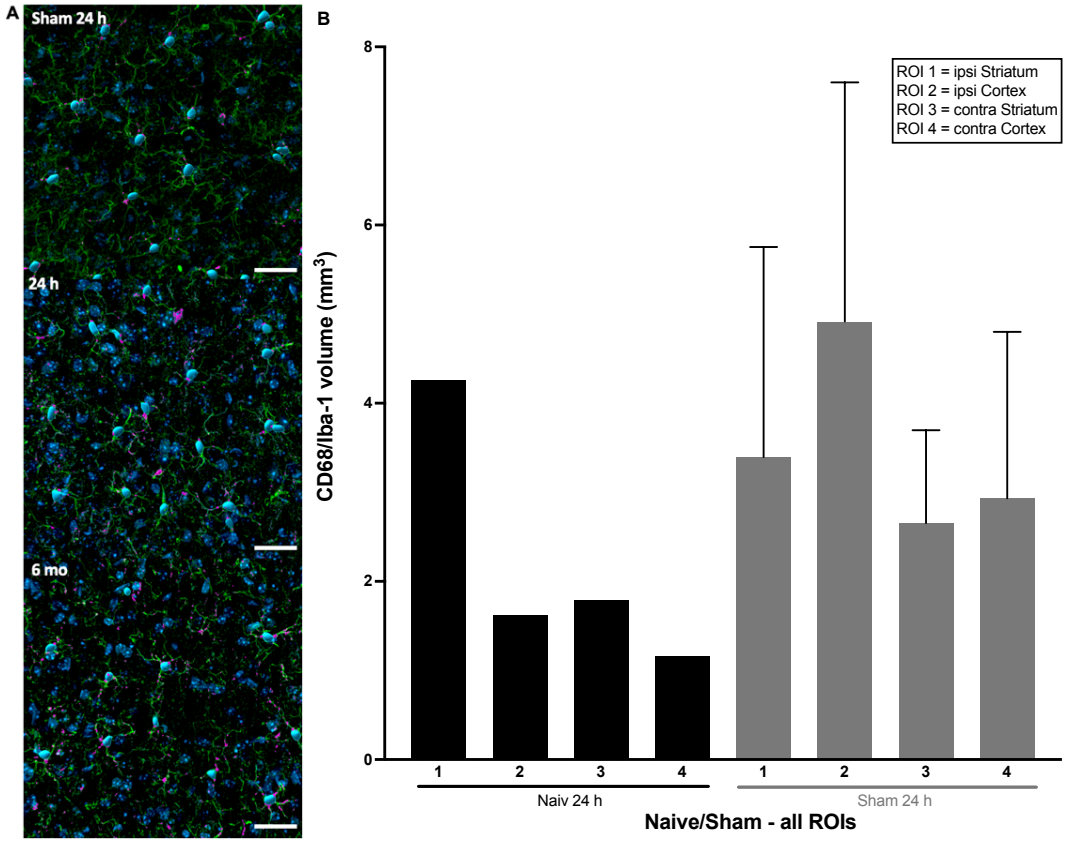

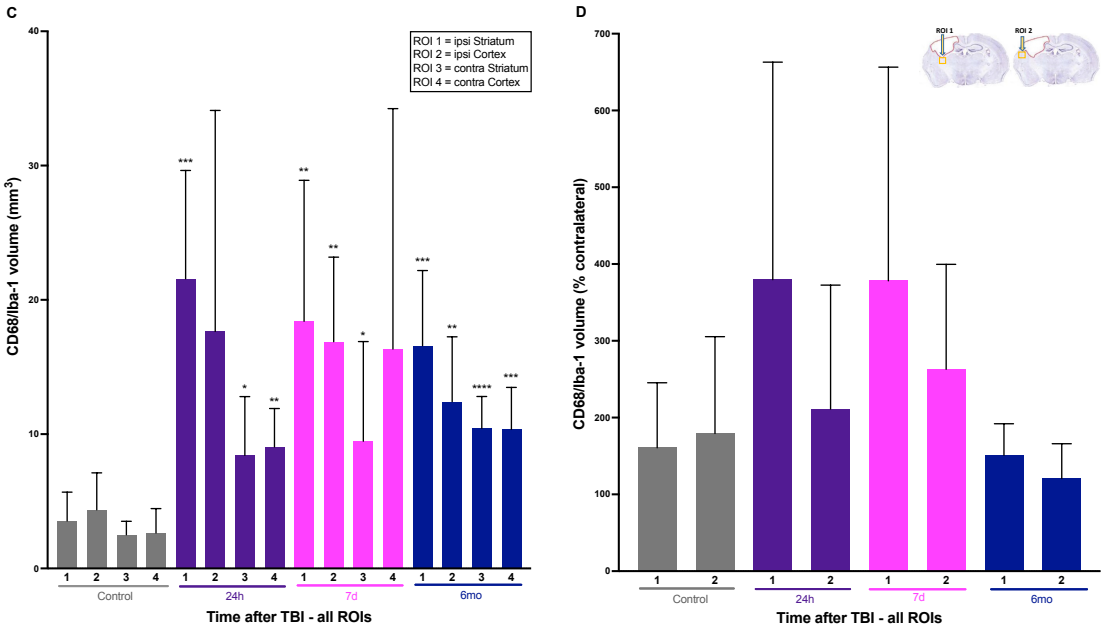

Figure 25: **CD68/Iba-1 volume analysis in ROI 1, 2, 3 and 4 for control and time points 24 h, 7 d, and 6 months post TBI.** (A) Sample pictures of the Imaris analysis showing different 3D images of CD68 (magenta), Iba-1 (green) and Dapi (blue) stainings in sham 24 h, 24 h and 6 months post TBI mice, scale bar = 20 μm (B) CD68/Iba-1 volume in naïve and sham mice at the two ROIs in the ipsilateral vs. the two respective ROIs in the contralateral hemisphere. (C) CD68/Iba-1 volume at the two ROIs in the ipsilateral and the two respective ROIs in the contralateral hemisphere for control and time points 24 h, 7 d and 6 mo post TBI. (D) CD68/Iba-1 volume of the ipsilateral normalized to the contralateral hemisphere at the two ROIs for control and time points 24 h, 7 d and 6 mo post TBI. Data are shown as Mean ± SD; t-test, *=p<0.05 vs. control, **=p<0.01 vs. control, ***=p<0.001 vs. control, ****=p<0.0001 vs. control, n=1 per naïve, n=5 per sham, n=5 per TBI.

3.3 Assessment of the Cerebral Microvasculature

3.3.1 Astrocyte Coverage of Micro Vessels

The neurovascular unit (NVU) is a structural and functional component of the central nervous system that describes the close interaction between neurons, glial cells (astrocytes and microglia), and blood vessels [159]. Dysfunction in this unit has been linked to a number of neurological conditions, including traumatic brain injury [157]. A central part of the NVU is an adequate coverage of cerebral micro vessels with astrocytic end feet. This was examined using the CD31, an endothelial cell marker that lines the inner surface of blood vessels [273] and Aqp4, a water channel protein that is primarily expressed in astrocytic end feet [267]. These markers were examined in the cortex at the lesion margin (ROI 2) and in the mirror-inverted ROI in the contralateral hemisphere (ROI 4) (see **Figure 13**).

Firstly, the Aqp4 fluorescence intensity was measured (**Figure 26A to C**). The Aqp4 fluorescence intensity in the ipsilateral hemisphere (ROI 2) increased minimally but still significantly from a baseline of 1.0 x 10^7 ± 1.8 x 10^6 AU in control animals to 1.3 x 10^7 ± 9.4 x 10^5 AU at 24 hours after trauma (p=0.0146 vs. control, **Figure 26C**). Seven days after the TBI, it fell to 1.2 x 10^7 ± 2.5 x 10^6 AU (p=0.3839), about the same as pre-trauma levels. Six months after TBI (1.3 x 10^7 ± 3.6 x 10^6 AU, p=0.1161 vs. control), there was no difference compared to the control group (**Figure 26C**). The contralateral hemisphere did not show any significant increase or decrease of Aqp4

fluorescence intensity at any time point, with values consistently comparable to those of control animals (**Figure 26C**).

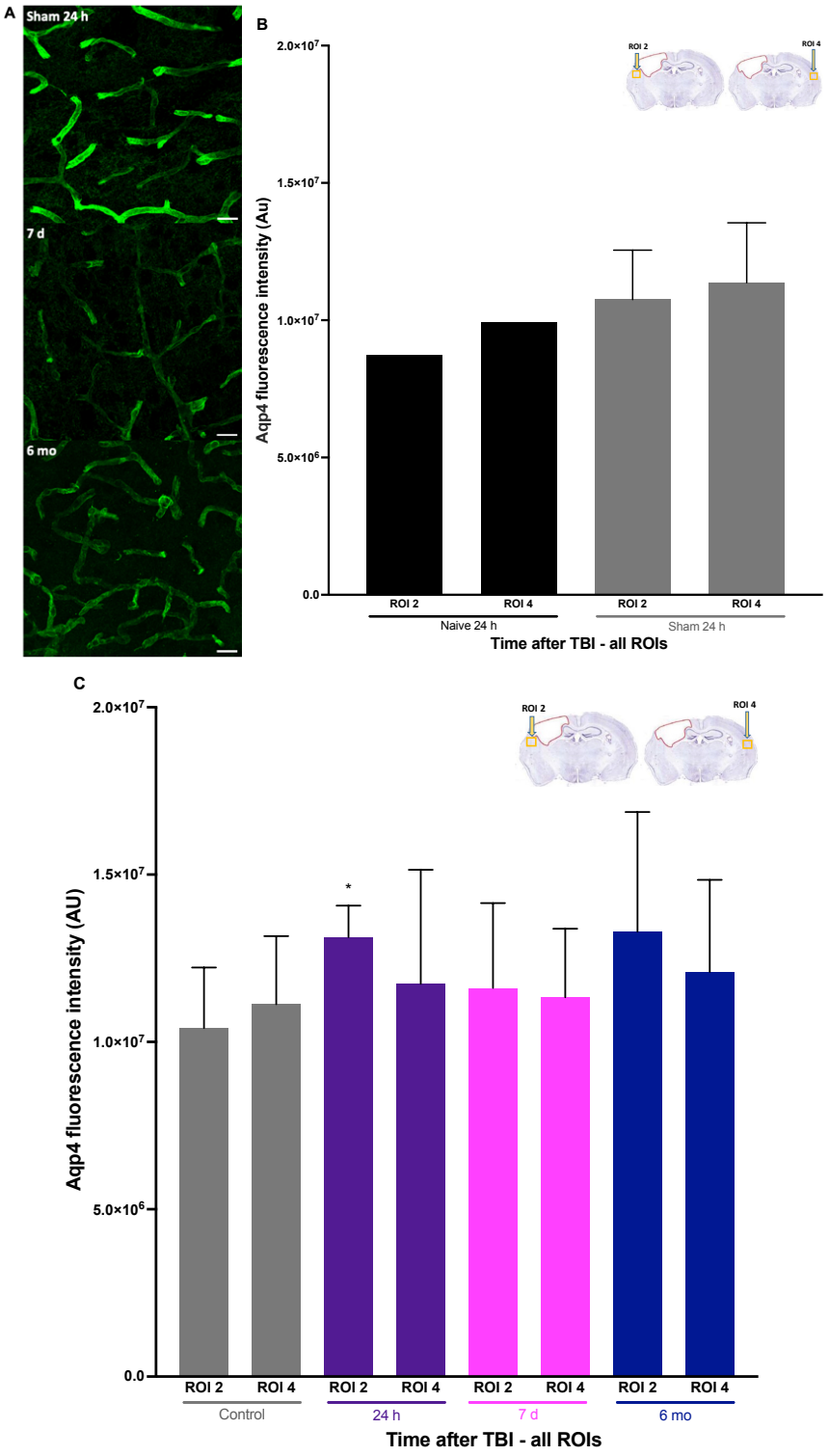

Figure 26: **Aqp4 analysis in ROI 2 and 4 in the cortex for control and time points 24 h, 7 d and 6 mo post TBI.** (A) Exemplary Aqp4 fluorescence intensity staining's at ROI 2 in the ipsilateral cortex in sham 24 h, 7 d and 6 mo post TBI mice, scale bar = 20 μm. (B) Aqp4 fluorescence intensity in naïve and sham mice at ROI 2 in the ipsilateral vs. the respective ROI 4 in the contralateral hemisphere. (C) Aqp4 fluorescence intensity at ROI 2 in the ipsilateral and ROI 4 in the contralateral hemisphere for control and time points 24 h, 7 d and 6 mo post TBI. (Data are shown as Mean ± SD; t-test, *=p<0.05 vs. control, **=p<0.01 vs. control, ***=p<0.001 vs. control, ****=p<0.0001 vs. control, n=1 per naïve, n=5 per sham, n=5 per TBI.

Next, the intensity of CD31 fluorescence was measured. Once more, there was no discernible difference between naïve and sham animals (**Figure 27B**), hence they were combined as a control group. The endothelial cell marker, CD31, demonstrated a significant decline in the ipsilateral hemisphere (ROI 2), with a minimum at 24 hours post TBI of 7.0 x 10^6 ± 1.6 x 10^6 AU, p=0.0103 vs. control, compared to the pre-trauma baseline of 9.8 x 10^6 ± 1.2 x 10^6 AU (**Figure 27C**). After that, CD31 fluorescence intensity increased to pretrauma levels (8.7 x 10^6 ± 3.7 x 10^6 AU at seven days, p=0.5122; 10.6 x 10^6 ± 2.1 x 10^6 AU at 6 months, p=0.4969). In the contralateral hemisphere there were no significant variations from control animals at any of the time points (**Figure 27C**).

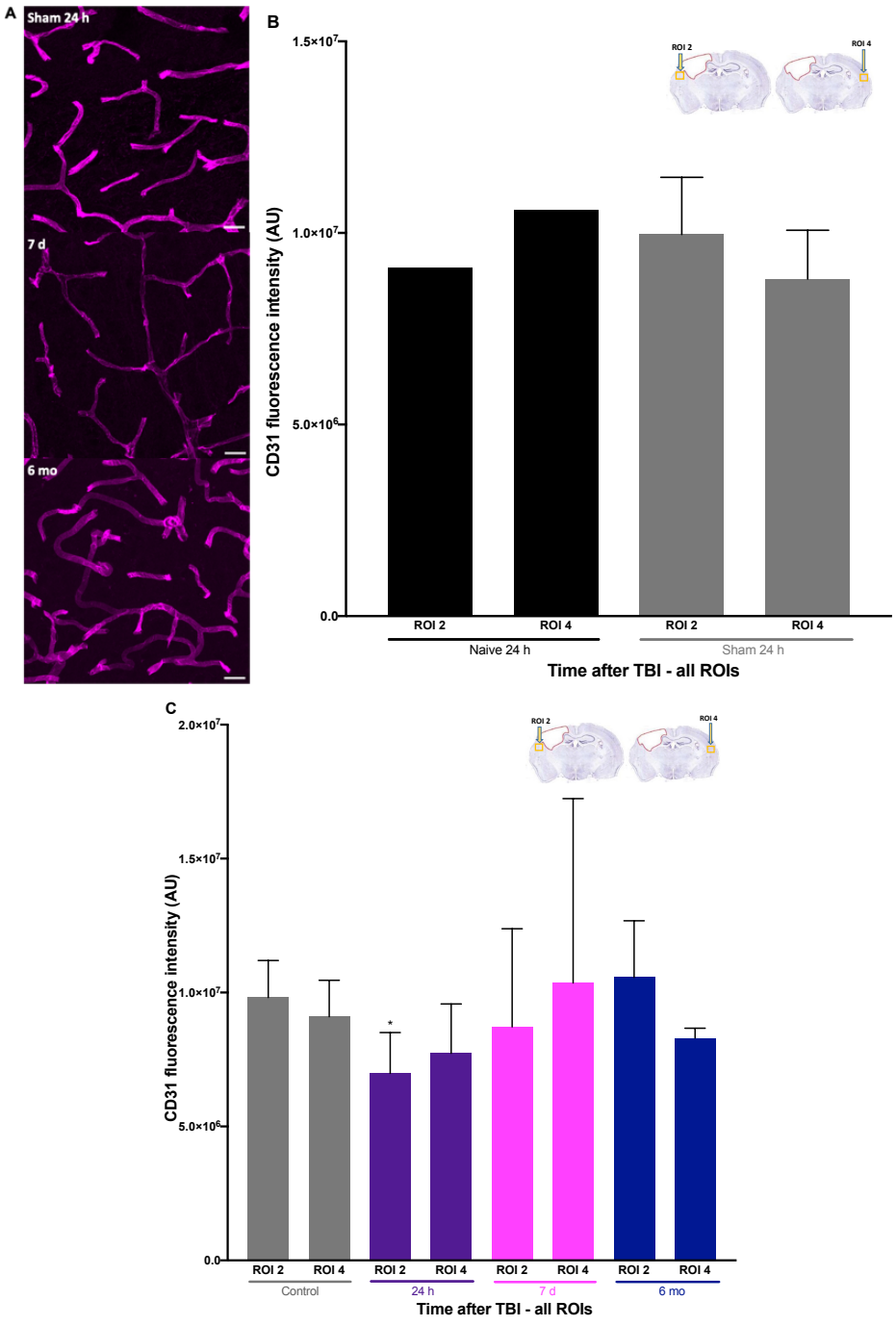

Figure 27: **CD31 analysis in ROI 2 and 4 in the cortex for control and time points 24 h, 7 d and 6 mo post TBI.** (A) Exemplary CD31 fluorescence intensity staining's at ROI 2 in the ipsilateral cortex in sham 24 h, 7 d and 6 mo post TBI mice, scale bar = 20 μm. (B) CD31 fluorescence intensity in naïve and sham mice at ROI 2 in the ipsilateral vs. the

respective ROI 4 in the contralateral hemisphere. (C) CD31 fluorescence intensity at ROI 2 in the ipsilateral and ROI 4 in the contralateral hemisphere for control and time points 24 h, 7 d and 6 mo post TBI. Data are shown as Mean ± SD; t-test, *=p<0.05 vs. control, **=p<0.01 vs. control, ***=p<0.001 vs. control, ****=p<0.0001 vs. control, n=1 per naïve, n=5 per sham, n=5 per TBI.

Using the CD31 and Aqp4 markers, the proportion of the endothelial cell surface that was covered by astrocytes was examined to assess the astrocyte coverage of microvessels. In healthy brains, 98% of the endothelial surface is covered by Aqp4 astrocytic endfeet [182, 274], thus the coverage analysis serves as a surrogate marker to evaluate the NVU integrity. Based on the ipsilateral hemisphere (ROI 2), the mean baseline coverage in the control was 65.8 ± 8.1% (**Figure 28C**) with no difference in the percentage of CD31 covered by Aqp4 between naïve and sham mice (**Figure 28B**). 24 hours after TBI, there was no significant difference (67.6 ± 15.7%, p=0.8089) to the baseline coverage, but after seven days, there was a tendency toward a decreased vascular coverage of 56.3 ± 7.2%, p=0.0729 but there was still no significant difference to the control (**Figure 28C**). Six months after the TBI, values returned to baseline levels (p=0.5311). However, the percentage coverage after half a year remained lower than it was in the absence of a TBI when comparing the same ROIs with each other (**Figure 28C**). The result was comparable in the contralateral hemisphere (ROI 4), showing a significant decline, seven days following TBI (52.5 ± 9.3%, p=0.0007, **Figure 28C**). Overall, in both the ipsilateral and contralateral hemisphere, the astrocyte coverage of endothelial cells decreased at 7 days after TBI; over a course of six months after TBI, this decrease recovered back to baseline.

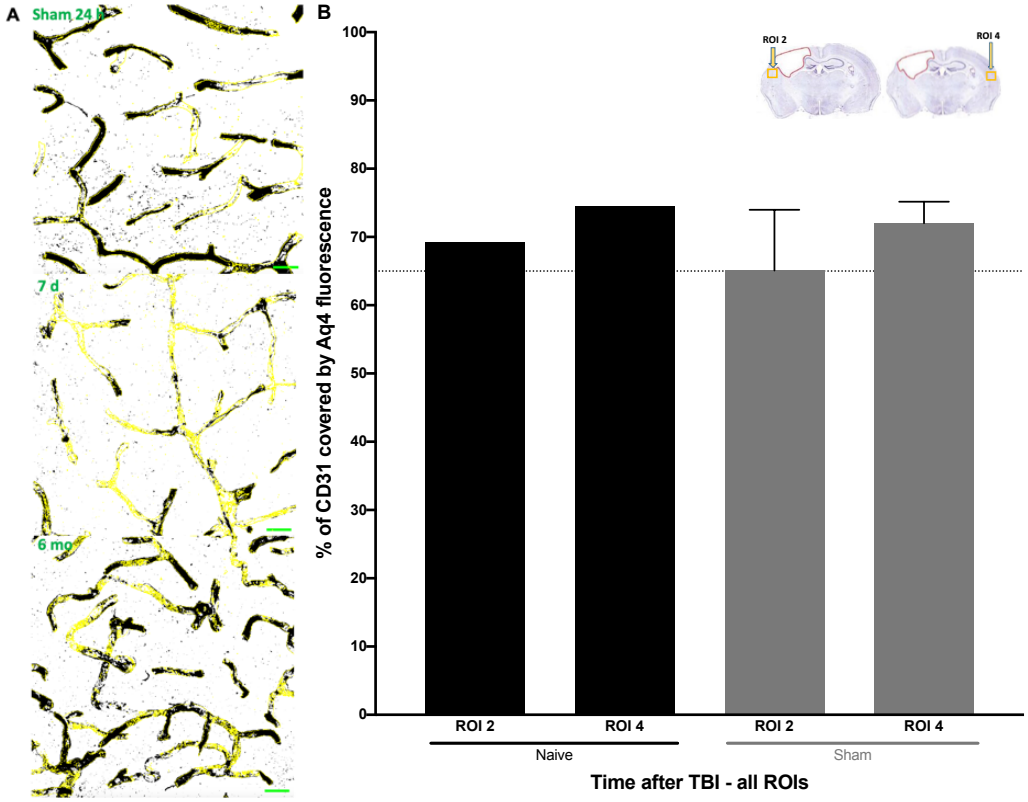

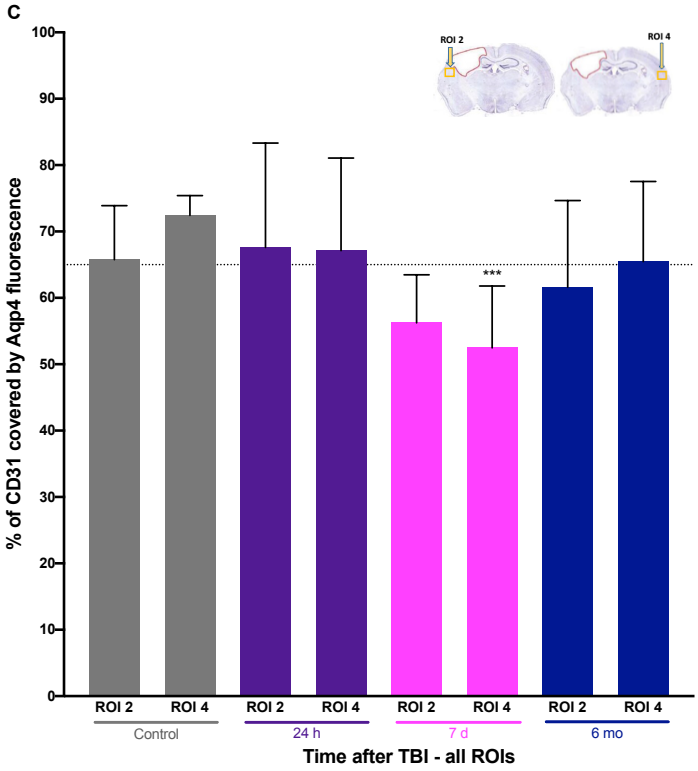

Figure 28: **Percentage of CD31 covered by Aqp4 analysis in ROI 2 and 4 in the cortex for control and time points 24 h, 7 d and 6 mo post TBI.** (A) Exemplary thresholded CD31 (black) with a masked Aqp4 (yellow) channel at ROI 2 in the ipsilateral cortex in sham 24 h, 7 d and 6 mo post TBI mice, scale bar = 20 μm. (B) Percentage of CD31 covered by Aqp4 fluorescence in naïve and sham mice at ROI 2 in the ipsilateral vs. the respective ROI 4 in the contralateral hemisphere. (C) Percentage of CD31 covered by Aqp4 fluorescence at ROI 2 in the ipsilateral and ROI 4 in the contralateral hemisphere for control and time points 24 h, 7 d and 6 mo post TBI. Data are shown as Mean ± SD; t-test, *=p<0.05 vs. control, **=p<0.01 vs. control, ***=p<0.001 vs. control, ****=p<0.0001 vs. control, n=1 per naïve, n=5 per sham, n=5 per TBI.

3.3.2 Blood-Brain Barrier Disruption

BBB dysfunction is a thought to play a major role in the pathophysiology of posttraumatic brain damage [74]. Therefore, we assessed BBB integrity by Laminin staining, which is part of the basal membrane of brain blood vessels [275] that provides structural support to the endothelial cells and aids in regulating the permeability of the BBB. To further demonstrate BBB leakage following traumatic brain injury, albumin, the biggest intravascular molecule that can only cross into the perivascular space when the BBB is compromised, was utilized as a marker [74]. Two separate ROIs were used to determine the albumin that was discovered to be outside of the laminin-marked vessels: ROI 1 in the striatum at the lesion border and ROI 2 in the cortex at the lesion border, with the matching ROIs 3 and 4 in the contralateral hemisphere (see **Figure 15**).

Extravascular albumin fluorescence intensity in the sham and the naïve groups did not differ, therefore they were combined as the control group in the subsequent analyses (**Figure 29B**). In the ipsilateral hemisphere, extravascular albumin in ROI 1 (**Figure 29C**) significantly increased at 24 hours (maximum albumin fluorescence intensity: 5.3 ± 2.3 x 10^6 AU, p=0.0021); in the following six months after TBI, albumin fluorescence intensity declined. ROI 2 in the cortex displays two minor peaks of extravascular albumin at 24 hours and seven days after traumatic brain injury (highest albumin fluorescence intensity: 2.4 ± 1.4 x 10^6 AU and 2.5 ± 1.4 x 10^6 AU, respectively, **Figure 29C**), after which there is a sharp decline to baseline values from one month to six months after trauma.

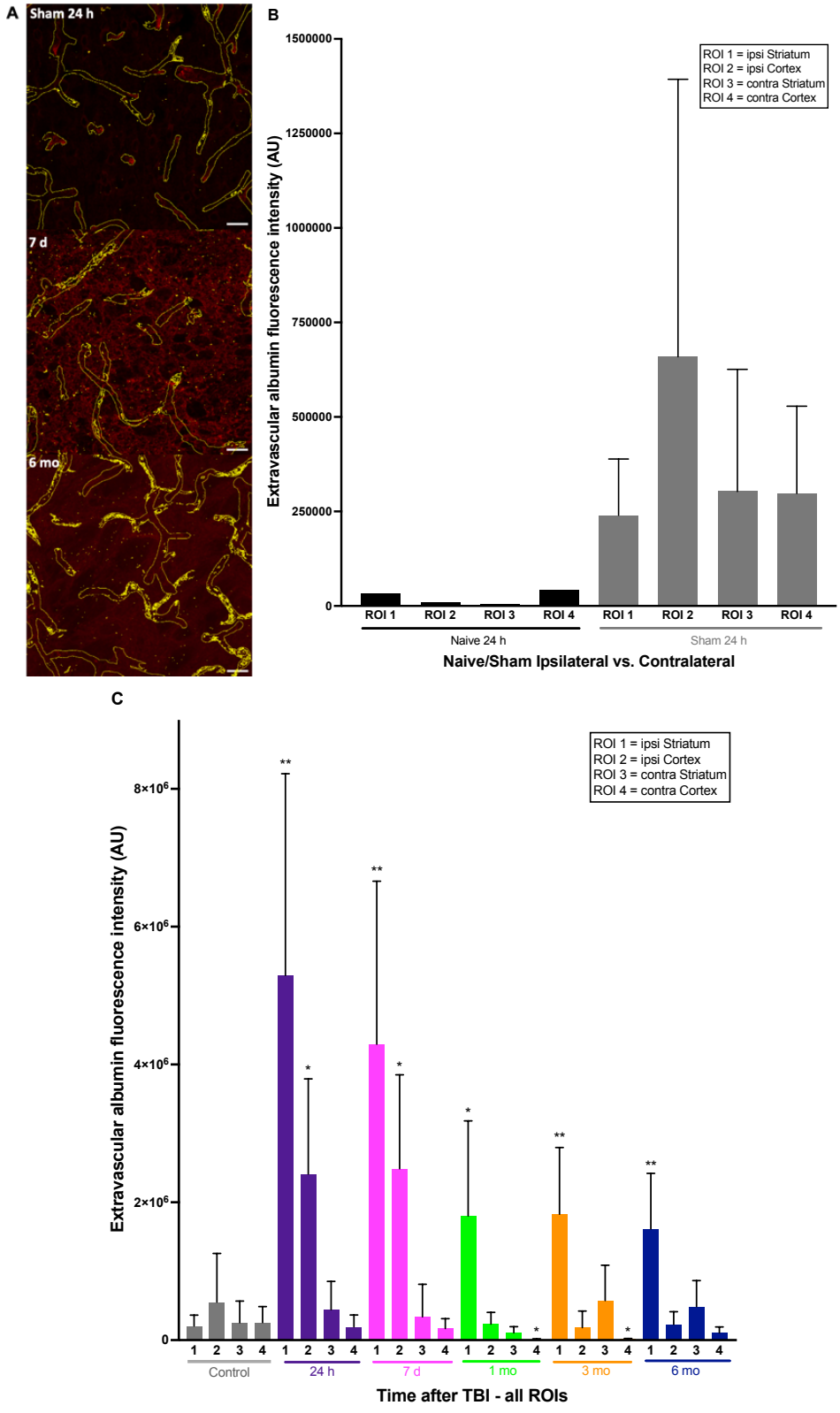

Figure 29: **Extravascular albumin analysis in ROI 1, 2, 3 and 4 for control and time points 24 h, 7 d, 1 mo, 3 mo and 6 mo post TBI.** (A) Exemplary albumin fluorescence intensity staining's at ROI 2 in the ipsilateral cortex in sham 24 h, 7 d and 6 mo post TBI mice, scale bar = 20 μm. (B) Extravascular albumin fluorescence intensity in naïve and sham mice at the two ROIs in the ipsilateral vs. the two respective ROIs in the contralateral hemisphere. (C) Extravascular albumin fluorescence intensity at ROI 1 and 2 in the ipsilateral and the respective ROI 3 and 4 in the contralateral hemisphere for control and time points 24 h, 7 d 1 mo, 3 mo and 6 mo post TBI. Data are shown as Mean ± SD; t-test, *=p<0.05 vs. control, **=p<0.01 vs. control, ***=p<0.001 vs. control, ****=p<0.0001 vs. control, n=1 per naïve, n=5 per sham, n=5 per TBI.

3.4 Neurodegeneration

Dementia and persistent neurodegeneration have been linked to traumatic brain injury [42]. Among the chronic neurodegenerative disorders that may follow TBI, the association with Alzheimer disease (AD) has the strongest support [190]. We investigated the anti-beta-amyloid precursor protein (betaAPP) monoclonal antibody 6E10, which is normally elevated in AD models [276], at 24 hours and 12 months post TBI across the whole brain. The fluorescence intensity of the amyloid beta-peptide in the naïve and sham groups did not differ significantly (**Figure 30B**). As shown in **Figure 24C**, acutely after TBI, at 24 hours, there was already a 138% increase in amyloid beta-peptide fluorescence intensity when normalized to the control ($p<0.0001$) and 12 months after a 40% increase ($p<0.0001$). However, due to lack of tissue in the 12-month groups, only three animals could be assessed for this analysis, therefore the results need to be interpreted cautiously.

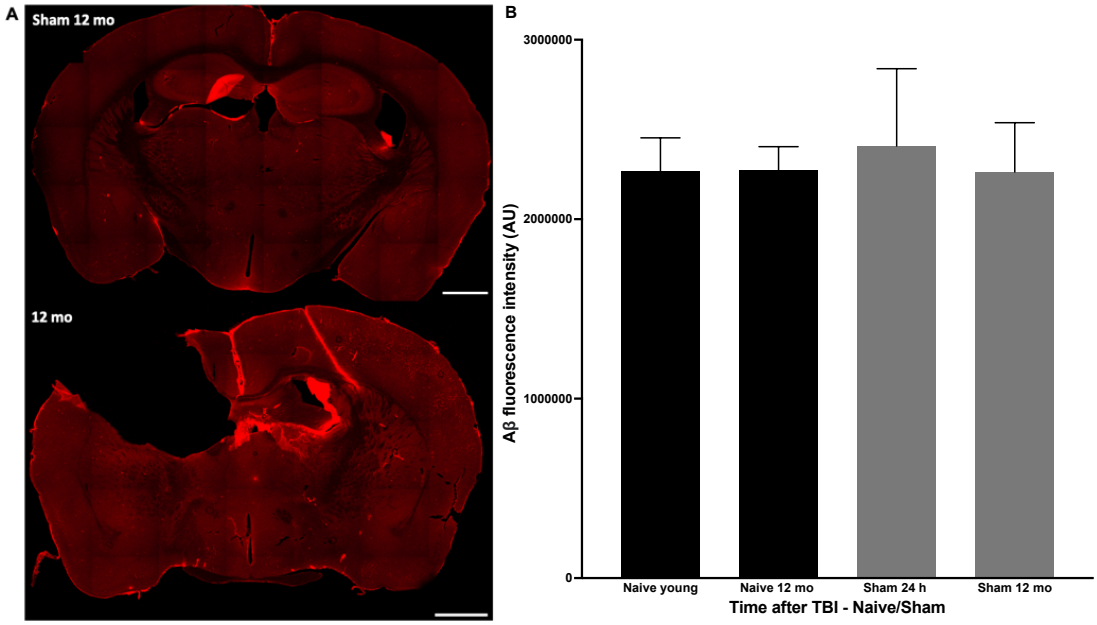

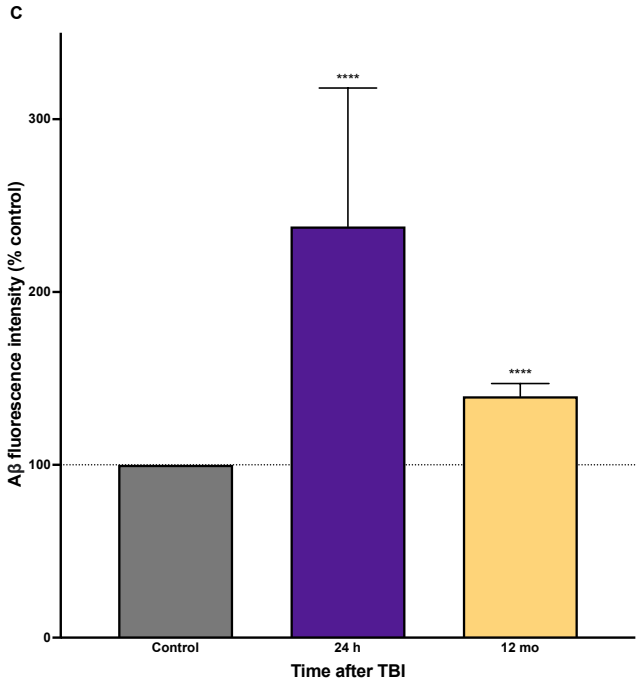

Figure 30: **Aβ fluorescence analysis for control and time points 24 h and 12 months post TBI.** (A) Exemplary Aβ fluorescence intensity stainings of coronal brain sections of sham 12 months and 12 months post TBI mice, scale bar = 1 mm. (B) Aβ fluorescence intensity in naïve and sham mice of the whole brain section. (C) Aβ fluorescence intensity of the whole brain section normalized to control at time points 24 h and 12 months post TBI. Data are shown as Mean ± SD; t-test, *=p<0.05 vs. control, **=p<0.01 vs. control, ***=p<0.001 vs. control, ****=p<0.0001 vs. control, n=3 per naïve/sham 24 h, n=9 per sham 12 months, n=3 per TBI 24 h, n=9 per TBI 12 mo.

Traumatic brain injury also causes neuronal loss [277]. Thus, NeuN was used as a neuronal cell body marker and counted in the ipsilateral cortex next to the lesion margin (ROI 2) and in the corresponding area of the contralateral cortex (ROI 4), to asses neuronal cell loss after TBI. There were no variations in the NeuN cell count between sham and naïve mice (**Figure 31B**). 24 hours post TBI, neuronal cell count decreased, reaching a minimum at seven days, and then returning to baseline levels at six months after TBI (**Figure 31C**). TBI results in both acute and subacute neuronal loss up to seven days after the injury, with recovery occurring six months later.

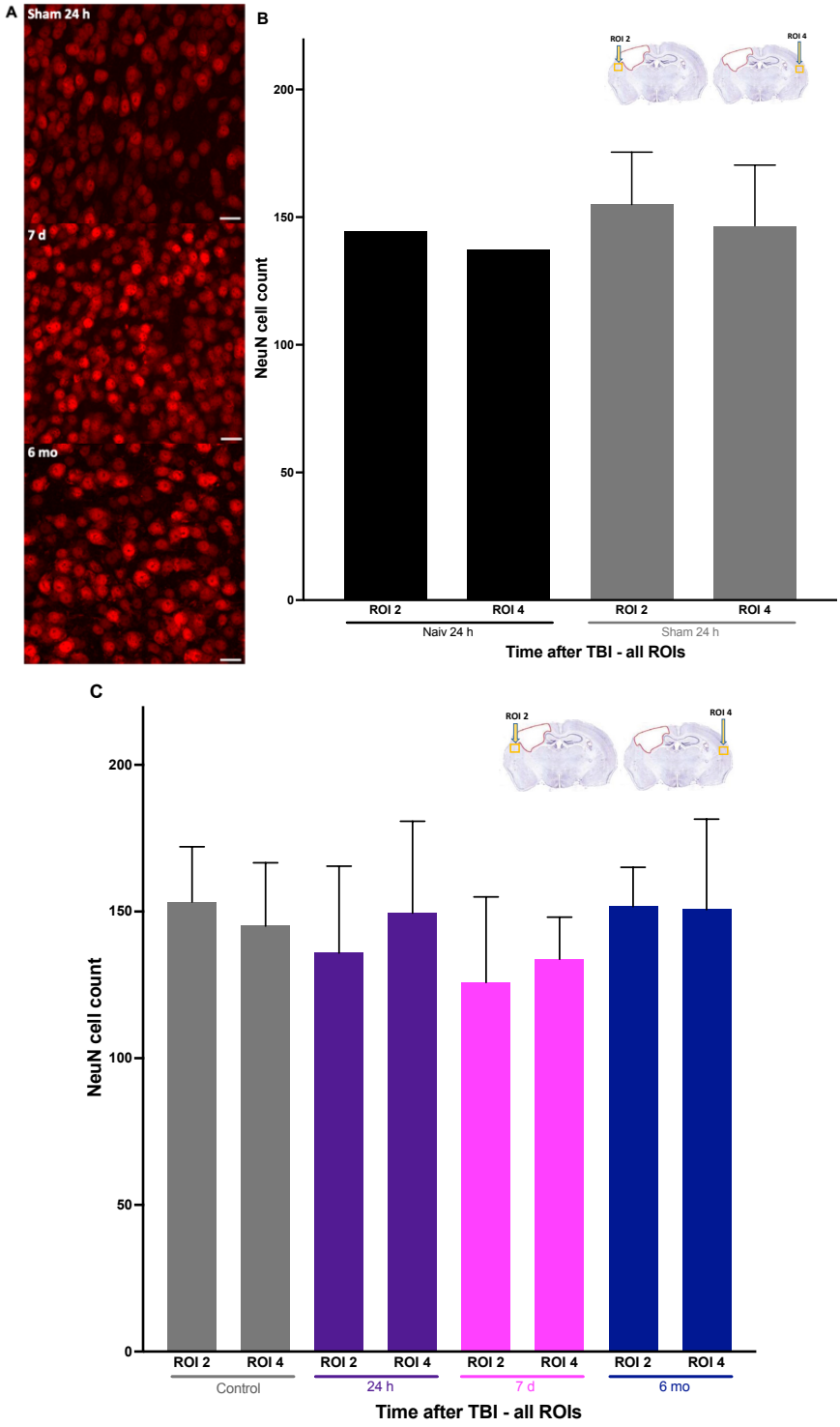

Figure 31: **NeuN analysis at ROI 2 and 4 in the cortex for control and time points 24 h, 7 d and 6 mo post TBI.** (A) Exemplary NeuN stainings in sham 24 h, 7 d and 6 mo post TBI mice, scale bar = 20 μm. (B) NeuN cell count in naïve and sham mice at ROI 2 in the ipsilateral vs. the respective ROI 4 in the contralateral hemisphere. (C) NeuN cell count at ROI 2 in the ipsilateral and the respective ROI 4 in the contralateral hemisphere for control and time points 24 h, 7 d and 6 mo post TBI. Data are shown as Mean ± SD; t-test, *=p<0.05 vs. control, **=p<0.01 vs. control, ***=p<0.001 vs. control, ****=p<0.0001 vs. control, n=1 per naïve, n=5 per sham, n=5 per TBI.

4. Discussion

4.1 Discussion of the Methods

4.1.1 Selection of the Experimental Animal Species

The current study utilized male C57Bl/6 mice as the experimental model. Mice are most commonly chosen for TBI research due to several advantages over rats: they reproduce quickly and cost-effectively, and their genetic makeup can be modified to create specific strains. Additionally, our lab has extensive experience conducting CCI experiments in mice, allowing for comparisons with previous studies [256, 257, 258, 278, 279, 280, 281, 282, 283, 284, 285, 286, 287, 288, 289, 290, 291, 292].

Young adult male mice were selected to avoid the potential influence of female hormones like estrogen and progesterone, which can affect secondary brain injury and outcomes in TBI models [293, 294, 295]. Since this study is the first of its kind, the main goal was to focus on understanding the long-term alterations and timeline after TBI, however future research will need to include female and older mice as well as humans for broader validation. Furthermore, it will be crucial to explore the relevance of these findings in larger animal models, such as those in gyrencephalic brains, as opposed to the lissencephalic brains of mice. This will provide critical insights into the potential translational value of the results for humans. The mouse model also raises some concerns, such as the animal's small size, which makes surgical preparation and manipulation more difficult. Nonetheless, this can be addressed with the intraoperative application of surgical microscopes, microsurgical methods, and sufficient surgical training. Moreover, although drug metabolism in mice differs significantly from humans, this was not a concern in this purely observational study without pharmacological interventions [296, 297]. Overall, considering the advantages and drawbacks, the mouse model was deemed appropriate and well-suited to meet the objectives of this study.

4.1.2 Selection of the Traumatic Brain Injury Model and Survival Times

Traumatic brain injury presents a complex and multifaceted pathology influenced by numerous cerebral and extracerebral factors, making it impossible for any single experimental model to fully replicate all aspects of its pathophysiology. Over the decades, several animal models have been developed to study TBI mechanisms, each with distinct strengths and limitations [298, 299, 300]. Importantly, the choice of model must consider not only the specific research objectives but also the model's ability to replicate relevant aspects of human TBI. A model of isolated head damage was chosen because the goal of the current investigation was to assess the impact of a single brain trauma, even though some individuals experience TBI in the context of multiple/multi-organ injuries.

One of the significant challenges with animal models is their inherent specificity: each model reflects a particular pathoanatomic type of injury and is influenced by factors such as the species' age, sex, and genetic background [117, 301]. These variables limit the ability of any single model to capture the full spectrum of primary and secondary damage observed in human TBI. The diversity of injury mechanisms and the multitude of factors contributing to individual outcomes in patients further underscore this limitation.

For the present study, the controlled cortical impact (CCI) model was selected. This model, established by Lighthall and refined for rodents, provides a high degree of reproducibility, inter- and intra-observer stability and experimental control by allowing precise adjustments to all parameters determining contusion size, such as impact depth, velocity, and duration [249, 300]. An impact depth of 1 mm, an impact velocity of 8 m/s, and a dwelling time of 150 m/s was chosen for the current study. These parameters produce a midsized to large contusion with a well-quantifiable secondary lesion expansion of roughly 60% of the initial tissue lesion [64, 256, 257] which is present in over 2/3 of severe human TBI cases [37]. Furthermore, the CCI mainly leads to contusional brain damage, which is a crucial aspect of the pathophysiology of human TBI [75]. On the other hand, diffuse axonal injury and other damage patterns are not the main characteristics of the CCI model. Moreover, this model also replicates secondary injury processes, including intracranial hypertension [256, 257, 284] cerebral ischemia [281], progressive neuronal death, neuroinflammation, and brain edema [257, 302], aligning well with data from human clinical observations. Likewise, this model produces consistent neurological deficits with low mortality, facilitating behavioral assessments and longitudinal studies [256, 292]. In addition to rodents such as rats [303, 304, 305], mice [306, 307], and ferrets [249, 308], the CCI has been effectively applied in large animal models like swine [309, 310, 311] and non-human primates [312], where the pathophysiology was equivalent to that of small animal studies, making it the ideal model for this study.

On the other hand, the free weight-drop model developed by Marmarou and colleagues induces diffuse axonal injury, hippocampal cell death, parenchymal rupture, and subarachnoid hemorrhages but no contusions [252, 313]. This model, commonly used in larger rodents like rats, involves dropping a defined weight, enclosed in a Plexiglas tube, vertically onto the closed skull. A steel "helmet" or metal plate is affixed to the skull bone where the weight strikes to prevent bone fractures (open TBI). While it allows adjustments in severity by altering drop height and weight, limitations include potential re-hits [314] and lack of fixation [315]. Similarly, the fluid percussion injury (FPI) model generates TBI through a fluid pressure wave delivered via a pendulum that impacts a fluid-filled tube placed over the epidural space after craniotomy [316, 317]. FPI is commonly used in experimental TBI research because it mimics clinical contusion without skull fractures and leads to neuronal damage, vascular disruption, and hemorrhages. However, it offers limited biomechanical control and fails to capture the full complexity of human TBI. This led to the pursuit of alternate models of TBI [318].

Considering all the previously discussed factors, we chose to use the CCI model due to our interest in the pathophysiology of contusions, the model's excellent repeatability, the extensive experience with this model in our lab for more than 20 years, and the fact that it adequately models the bulk of pathophysiological factors associated with TBI in humans. While limitations exist—such as the inability to consistently induce diffuse axonal injury or model multiorgan trauma—the CCI model captures critical aspects of TBI relevant to the study's aims. By focusing on a well-defined injury type and secondary processes, the CCI model provides a robust platform for understanding pathophysiological mechanisms and evaluating potential therapeutic interventions, while acknowledging the broader complexity and heterogeneity of human TBI.

Building on the strengths of the CCI model, this study is unique in its investigation of the acute, subacute, and chronic phase of TBI. Time points for histochemical analyses were selected at 15 minutes, 24 hours, 1 month, 3 months, 6 months, and 12 months post-injury. While larger groups and additional time points could be selected, this is not always feasible due to budgetary limitations and ethical concerns about animal welfare. Notably, no other animal study to date in this research field includes this many time points, particularly in the chronic phase, as most research

focuses predominantly on acute changes following TBI. By expanding the analysis to long-term time points, this study aims to elucidate how the effects of TBI evolve over time, providing novel insights into the trajectory of long-term consequences and mechanisms of injury. This comprehensive approach underscores the importance of chronic-phase research to fully understand and address the prolonged impact of TBI on affected individuals.

4.1.3 Possible Confounding Factors Affecting Traumatic Brain Injury Outcome in Experiments

Aside from the type of TBI model, other aspects that are crucial for the long-term outcome after TBI must be considered, including age and sex of laboratory animals, chemicals used for anesthesia, and the frequency of TBI.

4.1.3.1 Age and the Impact of Aging on Traumatic Brain Injury

The age of experimental animals significantly influences the outcomes of TBI studies. Older brains show higher susceptibility to tissue damage and impaired recovery post-TBI, with increased neuronal loss and larger lesion volumes compared to younger brains [130, 319]. Moreover, aging leads to elevated protein expression levels involved in tissue response and morphological changes in the brain [320, 321]. For example, RNA sequencing revealed that astrocytes alter their transcriptome and become reactive in a region-dependent way during ageing [322]. Microglia also change morphologically and functionally over time, leading to senescence or dystrophic conditions [323]. These findings highlight the age-dependent nature of TBI pathology. However, commonly used animal models often fail to replicate the complexities of aging, including comorbidities and hormonal fluctuations [324], which are common in elderly populations and significantly impact TBI outcomes [325]. The inclusion of naive and sham young and old mice as controls in this study highlights the effort to identify and decipher age-related alterations in the research. Despite these limitations, experimental research underscores the importance of age as a critical factor in understanding TBI pathophysiology and tailoring therapeutic interventions for aging populations. Therefore, this study must be elaborated in aging mice as well as this study only used young mice.

4.1.3.2 Sex Differences

Sex differences significantly influence the outcomes and progression of TBI, making them a critical consideration in experimental research and clinical studies. Epidemiological studies indicate that TBI is more common in men than in women [17, 27], but the unequal distribution of sexes in research samples can lead to biased interpretations [326, 327, 328]. Hormonal differences, particularly the effects of progesterone and estrogens like estradiol, play a significant role in TBI outcomes, influencing inflammation and injury response [329, 330, 331]. Males often exhibit heightened inflammatory responses, including elevated levels of pro-inflammatory cytokines and a more robust activation of microglia and astrocytes, which can exacerbate secondary damage [332]. In contrast, females tend to show a more balanced or even protective inflammatory response, likely due to the neuroprotective effects of estrogens, which have been shown to reduce oxidative stress, limit blood-brain barrier disruption, and modulate immune cell activity [332]. Experimental studies also report sex-based variations in lesion size [332] and behavioral outcomes post-TBI. Males frequently display larger lesions and greater neuronal loss, while females may experience greater sensitivity to sensory stimuli and different recovery trajectories [332, 333, 334]. These findings emphasize the importance of considering sex differences in TBI research to improve the accuracy and applicability of experimental results. A significant limitation of this study

is the exclusive use of male mice, which excludes potential insights into sex-specific differences and limits the generalizability of the findings to both sexes. The decision to use only male mice was based on proof-of-principle considerations, as well as ethical and financial constraints, including efforts to reduce the total number of animals used in accordance with animal welfare guidelines. Male mice were chosen to establish a clear timeline and understanding of the progression of TBI in a controlled setting. Now that the trajectory of TBI has been characterized in younger male mice, future studies should focus on investigating female mice to elucidate sex-specific differences. Such research will be critical to highlighting how sex influences TBI pathology, inflammation, and recovery, ultimately improving the relevance of experimental results to diverse patient populations.

4.1.3.3 Anesthesia

The choice of drugs used for anesthesia is an important consideration in experimental TBI research, as there are many substances that have been proven to directly influence brain physiology and therefore may potentially confound results. Prolonged exposure to isoflurane or sevoflurane has been shown to induce brain damage by triggering mechanisms like mitochondrial apoptosis, neuroinflammation, and neuronal death [335, 336]. Isoflurane, which was used in this study, disrupts ion homeostasis, decreases the activity of neural enzymes, alters cellular morphology and can increase intracranial pressure [337, 338, 339]. Microglial processes were noticeably longer in both acute (one to two days post-surgery) and chronic studies (four months post-surgery) when isoflurane was utilized [340]. In this study, the operation times for inducing TBI were not precisely the same across all animals, as variations in the difficulty of performing the craniotomy occasionally extended the procedure. Efforts were made to standardize and closely match operation durations through training and protocol refinement. However, differences in operation and anesthesia duration could still influence long-term TBI outcomes, introducing a potential limitation to the study.

Additionally, it is noteworthy that while sham mice displayed some elevated histochemical staining compared to naïve mice in certain analyses, these increases were never statistically significant. This subtle elevation could potentially be attributed to the effects of anesthesia or the craniotomy procedure itself. The craniotomy may induce some degree of indirect injury to the brain, particularly as the drilling process might occasionally minimally touch the dura, potentially influencing the brain's response. Other studies have already shown that the sham injury procedure can result in mild neuroinflammation, especially if a craniotomy is performed [341, 342]. Such factors underscore the importance of including sham and naïve mice, meticulous surgical technique and careful interpretation of sham controls in experimental TBI models.

4.1.3.4 Frequency of Traumatic Brain Injury

While this study focused on a single severe TBI, it is crucial to emphasize that the mechanisms and outcomes of a single severe TBI are distinct from those of mild or repetitive mild traumatic brain injuries (rmTBI). Chronic traumatic encephalopathy (CTE), which is often associated with repetitive mild TBIs, represents a fundamentally different pathological process than the chronic trauma consequences studied here. In cases of rmTBI, research has demonstrated a strong association with long-term neurodegenerative conditions such as CTE, dementia, and Alzheimer’s disease, particularly in individuals exposed to repeated head impacts, such as athletes and military personnel [245, 343]. Additionally, an increased density of CD68+ cells and a changed microglial phenotype was found in post-mortem brains of American football players [344]. Overall,

research has shown that cumulative damage from rmTBI leads to exacerbated brain injury, with amplified inflammatory responses and neurodegeneration compared to single-impact injuries [344]. Timing between injuries also plays a crucial role; repeated impacts within 24 hours significantly worsen outcomes, whereas intervals of 48 hours or more result in damage similar to single injuries [345, 346]. These complexities and the clinical significance of rmTBI underline the need to expand this single TBI study on rmTBI.

4.1.4 Immunohistological Analysis

4.1.4.1 Strengths and Limitations of the Neuroinflammation Analysis

The use of GFAP, Iba-1, and CD68 antibodies in this study provided valuable insights into neuroinflammation and glial activation following TBI, enabling a detailed analysis of both acute and chronic phases. Each antibody offered distinct advantages that aligned with the study's goals. GFAP was instrumental in identifying and quantifying astrogliosis, providing clear visualization of astrocyte activation and distribution patterns [264]. Iba-1 allowed for comprehensive evaluation of microglial density, morphology, and spatial distribution [262], while CD68 served as a reliable marker for identifying activated microglia and macrophages, correlating with their phagocytic activity and immune response [263]. The combination of these markers offered a multidimensional perspective on neuroinflammation, encompassing both structural and functional changes in glial cells.

However, there are some restrictions on these immunohistochemical markers. For instance, while GFAP is a widely used and specific marker for detecting reactive astrocytes [130], its reliability as an indicator of astrogliosis severity has been questioned. Various studies have highlighted variability and unreliability in GFAP expression across astrocytic populations [347, 348, 349] including the identification of "GFAP-negative" astrocytes [350, 351, 352]. This designation may stem from GFAP expression levels being below detection thresholds or from technical factors such as paraformaldehyde fixation masking GFAP, particularly in gray matter regions [353]. Despite these limitations, GFAP remains valuable for investigating injury-induced astrogliosis, though findings should ideally be corroborated with additional markers to account for astrocyte heterogeneity and ensure a comprehensive analysis.

Similarly, Iba-1, while considered a gold standard for visualizing microglia, presents challenges that may complicate interpretation. One limitation is its lack of specificity, as Iba-1 also stains perivascular macrophages, which can lead to difficulty distinguishing between these cells and microglia in certain contexts [354, 355]. This overlap can obscure the precise characterization of microglial-specific responses, particularly in regions where perivascular macrophages are abundant or have been recruited during an immune response. Additionally, Iba-1 staining does not provide direct information about the functional state of microglia, such as their cytokine production or antigen-presenting capabilities, limiting its utility in fully characterizing the spectrum of microglial activation states [354, 356].

CD68 is a well-established marker for identifying activated microglia and macrophages due to its association with lysosomal activity [263]. However, this specificity also narrows its scope, as CD68 primarily highlights phagocytic activity and does not adequately capture other activation states of microglia and macrophages, such as those involving inflammatory signaling or neuroprotective roles [357, 358]. This limitation means that CD68 alone cannot fully depict the functional

diversity of microglial responses to TBI. Furthermore, reliance on CD68 may underrepresent populations of microglia or macrophages that are metabolically active but not engaged in phagocytosis.

The imaging protocol itself, while robust, introduced certain limitations. Most of the analysis focused on pre-determined regions of interest (ROIs) that were normalized to contralateral areas, but this approach may overlook systemic TBI effects that influence both hemispheres. This limitation applies not only to the current analysis but extends to all subsequent analyses where specific ROIs were chosen, potentially missing nuanced or localized effects in other brain regions. Additionally, another limitation of this study applying to all immunohistochemical analyses was that while the normalization of fluorescence intensity to the contralateral hemisphere helped address variability, it cannot entirely eliminate the influence of systemic TBI effects that might impact both hemispheres.

Ultimately, while GFAP, Iba-1, and CD68 successfully captured key aspects of the neuroinflammatory response, their inherent limitations underscore the need for complementary approaches. Methods such as single-cell sequencing or multiplex imaging could enhance our understanding of the complex and dynamic glial responses following TBI, offering deeper insights into the nuanced roles of glial cells in the context of both injury and recovery.

4.1.4.2 Strengths and Limitations of Cerebral Microvessel and BBB Analysis

This study utilized advanced techniques to investigate the integrity of cerebral microvessels and blood-brain barrier (BBB) functionality following TBI, providing critical insights into the structural and functional changes that occur in these systems over time. By employing markers such as CD31, laminin, and aquaporin-4 (Aqp4), the analysis successfully captured detailed information about vascular endothelial integrity [265] and astrocytic end-foot coverage [182], while parenchymal albumin staining served as a reliable surrogate marker for BBB disruption [74]. Together, these approaches highlighted key aspects of neurovascular unit (NVU) disruption and chronic BBB impairment, shedding light on their roles in prolonged neuroinflammation, disrupted cerebral blood flow (CBF), and cognitive decline.

The strengths of this analysis lay in its ability to assess microvascular and astrocytic components of the NVU simultaneously, offering a comprehensive view of the structural interplay between astrocytes and endothelial cells. The use of high-resolution imaging and quantitative fluorescence analysis provided precise metrics for evaluating endothelial coverage by astrocyte end-feet and the extent of BBB permeability. Normalizing these measures to the contralateral hemisphere helped to account for individual variability of TBI. The time-course approach, spanning acute to chronic phases post-injury, further enhanced the study's capacity to track the progression of cerebral microvessel and BBB disruption, providing valuable temporal insights into the mechanisms underlying long-term brain vulnerability.

However, there are limitations inherent to the methodology and markers employed. CD31 is an effective marker for endothelial cells, yet it does not capture other critical components of the NVU, such as pericytes, which play a pivotal role in BBB maintenance and neurovascular coupling [359, 360]. Similarly, while Aqp4 effectively highlights astrocytic end-feet, its expression may be influenced by regional variability or technical factors such as non-specific staining, particularly in areas with high background fluorescence, as evident in this study. Notably, the Aqp4 staining in this study demonstrated suboptimal coverage, as astrocytic end-feet typically cover approximately 98% of blood vessels in a healthy brain [182]. In contrast, our control group only demonstrated

66% coverage, indicating that a significant portion of Aqp4 coverage was missed. This discrepancy underscores potential limitations in the staining protocol or tissue preparation, which may have affected the reliability of the Aqp4 signal and reduced its ability to accurately reflect astrocytic coverage of the vasculature. Moreover, the exclusion of striatal regions due to staining challenges represents another limitation, as the striatum is known to be particularly susceptible to TBI-induced changes. This gap may have limited the study's ability to fully characterize the spatial heterogeneity of microvascular responses.

The reliance on albumin as a marker of BBB disruption also has its constraints. While albumin leakage into the parenchyma is a clear indicator of BBB permeability, it does not provide detailed information on the specific mechanisms driving the disruption, such as endothelial cell damage, tight junction protein degradation, or astrocytic dysfunction [361]. Moreover, the analysis at later time points (e.g., 12 months post-TBI) would have enhanced the understanding of the chronic progression of BBB dysfunction and its potential recovery.

In summary, while the analysis of cerebral microvessels, astrocytic end-feet, and BBB integrity provided valuable insights into the pathophysiology of TBI, its limitations underscore the need for complementary methods. Incorporating additional markers, such as those for tight junction proteins or pericytes, and employing broader imaging techniques like whole-brain analyses or single-cell sequencing, could yield a more comprehensive understanding of cerebral microvessels, astrocytic end-feet and BBB dynamics. Future studies addressing these gaps could enhance our ability to identify therapeutic targets for mitigating long-term vascular and BBB dysfunction in TBI survivors.

4.1.4.3 Strengths and Limitations of the Neurodegeneration Analysis

The analysis of neurodegenerative changes in this study highlighted both strengths and limitations in the methodology, particularly regarding the use of the 6E10 antibody to investigate amyloid-beta (Aβ) accumulation. This antibody, which targets a fragment of the amyloid precursor protein (APP) [268], was chosen for its ability to identify Aβ pathology, a hallmark of Alzheimer's disease (AD) and a potential consequence of TBI [191, 194]. However, the use of the 6E10 antibody also posed certain limitations. While it effectively stained Aβ deposits, it did not capture all aspects of the pathology. Aβ plaques and diffuse accumulations may vary in their binding affinity to this antibody, and the analysis may have missed some forms of Aβ, such as oligomers or truncated variants, which are also relevant in TBI associated AD pathology [362, 363]. Additionally, variability in the staining quality, as evidenced by uneven fluorescence intensity and potential background interference, could have affected the accuracy and consistency of the results. This was particularly notable in areas with high autofluorescence or damaged tissue, where distinguishing specific antibody binding from nonspecific signals proved challenging.

Despite these limitations, the inclusion of the 6E10 antibody in this study allowed for a focused exploration of Aβ dynamics in the context of TBI. While it may not encompass the full spectrum of Aβ-related neurodegenerative changes, its findings contribute to the growing body of evidence linking TBI to AD pathology. Future studies could complement this approach by using additional antibodies targeting different Aβ species or by integrating other markers of neurodegeneration [364], such as tau pathology [365, 366], to provide a more comprehensive picture of the chronic impacts of TBI on brain health.

Furthermore, the analysis of neuronal cell count using NeuN staining provided insights into the extent and temporal progression of neuronal loss following TBI. However, this analysis also had its imitations. NeuN staining is restricted to neuronal cell bodies, potentially overlooking other

critical neuronal components such as dendrites and axons, which are also susceptible to TBI [367, 368]. Additionally, the focus on specific ROIs near the lesion may not fully capture the broader spatial heterogeneity of neuronal damage throughout the brain [369]. Despite these constraints, the findings provide an important foundation for understanding neuronal dynamics post-TBI and underscore the need for complementary methods to assess more comprehensive neuronal and network-level changes.

4.2 Discussion of the Results

4.2.1 Neuroinflammation

4.2.1.1 Astrogliosis

The results of this study highlight the persistent and dynamic nature of astrogliosis following TBI, evidenced by increased GFAP fluorescence intensity in the ipsilateral hemisphere over a period of up to 12 months. Two distinct peaks in GFAP intensity were observed, one at seven days and another at three months post-injury, suggesting an ongoing and phased astrocytic response. Elevated GFAP levels were most pronounced near the lesion margin, particularly in the striatum, whereas regions further away from the lesion and within the contralateral hemisphere showed GFAP levels comparable to controls. Notably, GFAP fluorescence intensity did not return to baseline levels even at 12 months, indicating that astrogliosis persists long-term following TBI and contributes to sustained scar formation.

Comparing these findings with previous studies, several consistencies and distinctions emerge. Consistent with earlier research, this study confirms that astrogliosis is an early and sustained response to TBI, with astrocytes playing a central role in glial scar formation [120, 133, 134, 135]. The observed peak in astrocytic activity at seven days aligns with other studies documenting early hypertrophy and proliferation of astrocytes post-injury [114, 124, 139, 156]. However, the persistence of elevated GFAP levels at 12 months contrasts with studies suggesting resolution of astrogliosis within months [139], highlighting the importance of lesion severity, methodological differences, and regional specificity in interpreting these outcomes.

The persistent elevation in GFAP and spatially localized scar formation underscore the potential for chronic astrocytic dysfunction to influence long-term neurological outcomes. It is generally believed that one of the factors preventing full recovery of the damaged tissue is the barrier created by astrocytes that prevents axonal regrowth. Alternatively, Anderson et al. [370] showed that by preventing astroglia scar formation axonal growth was inhibited in the injured spinal cord. However, as astrocytes modulate the extracellular matrix and inflammatory environment, their prolonged activation could hinder axonal regeneration, synaptic repair, and overall neural recovery [120, 151, 152, 154, 155]. This aligns with evidence suggesting that dysregulated glial responses may contribute to neurodegeneration and cognitive deficits in TBI survivors [114, 141, 146, 147, 148, 149]. These findings highlight the need for additional research to further understand the precise processes by which glial cells influence post-injury recovery and to address the contradictory findings in this area.

These results reinforce the need for therapeutic strategies targeting the chronic phase of TBI. By modulating astrocytic activity and addressing the sustained inflammatory state, there may be potential to improve structural and functional recovery post-TBI. Strategies to address astrocytic

ECM alterations could promote axonal regeneration and improve recovery. Future research should further elucidate the interplay between astrocytic and microglial responses over time, with a focus on identifying windows for intervention that can mitigate the long-term impact of neuroinflammation on brain health.

4.2.1.2 Microglia

The study comprehensively assesses microglial density, morphology, and activation following TBI over various time points, revealing dynamic neuroinflammatory responses. Iba-1 fluorescence intensity quantification revealed microglial density in the ipsilateral hemisphere, reaching a peak along the lesion border seven days after TBI and progressively reverting to baseline by 12 months. Contralateral hemisphere changes were minimal, however with significant increases at 15 minutes, one month, three months, and 12 months after TBI. Morphological analyses revealed a reduction in microglial cell area and maximum span across hull, indicative of activation, with similar values at both seven days and six months post-injury near the lesion borders and in the contralateral cortex. The increased circularity of microglia in the cortex near the lesion border at six months and the Sholl analysis, which verified decreased microglial ramifications at seven days and six months, especially in the striatum and cortex near lesion borders, are additional indicators of microglial activation. CD68 analysis, a marker of microglial activation, corroborated these findings, showing a peak in immune activation at seven days post-TBI in the ipsilateral hemisphere, followed by a gradual decline to baseline at 12 months. CD68/Iba-1 colocalization in 2D and 3D analyses provided spatial insights, with the 3D approach highlighting a peak in activation at 24 hours, followed by sustained yet diminishing activity at seven days and six months post-TBI, which was most pronounced in the ipsilateral but still significantly increased in the contralateral hemisphere. Overall, the results underscore a distinct temporal and spatial pattern of microglial activation, peaking within the first week, persisting until 6 months and resolving over the course of 12 months.

The findings from this study align with and expand upon the body of existing research on chronic neuroinflammation following TBI. Previous studies have demonstrated that microglial activation persists in the chronic phase, characterized by sustained amoeboid morphology and prolonged secretion of pro-inflammatory cytokines [120, 136, 137, 138]. Additionally, microglial activation has been observed in human studies to last for several years, in some cases even up to 18 years following the initial brain trauma, especially in cases of moderate-to-severe traumatic brain injury [136, 137, 371]. Thus, temporal dynamics of neuroinflammation following TBI have been extensively studied, yet gaps remain in our understanding of how microglial activation evolves across specific time points after TBI. Various studies suggest that microglial density and activation typically peak within the first week post-injury, coinciding with the subacute inflammatory response [114, 372], a finding that is consistent with our study results. Over the following weeks to months, a gradual decline in microglial activation is generally observed, although the extent of this decline varies based on injury severity, species, and the specific brain regions analyzed. For example, an experimental closed-head TBI study highlighted that microglial activation and density remain elevated compared to baseline levels even at 6 to 12 months post-injury throughout the entire brain [114], suggesting that neuroinflammation may persist well into the chronic phase, maintaining a state of low-grade inflammation that promotes neurodegenerative processes [12, 127, 227]. Another single moderate-level CCI study demonstrated microglial activation throughout 1-year post-injury, expressed by major histocompatibility complex class II, CD68, and NADPH oxidase histological assessment at the margins of the expanding lesion [41]. The persistent microglial

activation was also associated with progressive hippocampal neurodegeneration, lesion expansion, and loss of myelin. These findings coincide with this study, but in contrast, we observed that microglial density and activation had already reached control levels by 12 months.

One area of divergence in different studies is the involvement of the contralateral hemisphere. While some studies did not investigate the contralateral hemisphere [41], other studies reported variable changes in distant and contralateral brain regions from the TBI [114, 126, 136, 373]. This study provides further evidence that both ipsilateral and contralateral regions exhibit prolonged neuroinflammation, suggesting a more widespread systemic response than previously suspected. However, this study also shows that the ipsilateral hemisphere is impacted much more significantly than the contralateral, reinforcing the notion that TBI-induced damage is more pronounced in the hemisphere directly affected by the injury. This finding may have important implications for understanding the extent and nature of neuroinflammatory processes following traumatic brain injury.

Importantly, no prior study has systematically examined microglial activation across this comprehensive range of time points, from 15 minutes, 24 hours, seven days, one month, three months, six months, to 12 months post-TBI, making this investigation unique in its ability to elucidate the temporal progression of neuroinflammation from the acute to chronic phases. This enhanced understanding of the inflammatory timeline has significant implications for therapeutic interventions, as it provides critical insights into when and how anti-inflammatory strategies might be most effective in modulating the neuroinflammatory response to optimize recovery and minimize long-term damage.

The persistence of microglial activation underscores the need for future research to identify optimal windows for intervention and uncover critical pathways for therapeutic targeting, focusing on modulating the balance between pro-inflammatory and anti-inflammatory responses and understanding the mechanisms driving the transition of glial cells from protective to detrimental roles. Moreover, the chronic nature of these changes highlights the importance of long-term monitoring and individualized rehabilitation for TBI survivors, addressing not only acute recovery but also the lasting cognitive and structural deficits associated with prolonged neuroinflammation [114, 141, 142, 143, 146, 147]. Additionally, the development of biomarkers to monitor chronic neuroinflammation in vivo could enhance early detection and intervention. The parallels between chronic neuroinflammation in TBI and neurodegenerative diseases like Alzheimer's and Parkinson's [148, 149, 150] further underscore the broader implications of these findings, suggesting shared pathways that might be targeted for dual benefit. By bridging gaps in our understanding of chronic neuroinflammation, this research provides a foundation for developing therapies aimed at mitigating the long-term effects of TBI and improving patient outcomes.

4.2.2 Cerebral Microvasculature

This study investigated the integrity and dynamics of the cerebral microvasculature, astrocytic coverage of microvessels, and BBB disruption in both the ipsilateral and contralateral hemispheres at acute and chronic time points post-TBI.

The assessment of Aqp4 fluorescence intensity revealed subtle temporal changes in astrocytic end feet coverage following TBI. In the ipsilateral hemisphere, Aqp4 intensity increased significantly at 24 hours, suggesting a rapid astrocytic response to trauma. However, this was followed by a decline at seven days and a return to baseline levels by six months. These findings indicate

an early upregulation of astrocytic water channels as a compensatory mechanism which normalizes over time, potentially supporting homeostasis and tissue repair, stabilizing the extracellular environment and mitigating edema. Interestingly, the contralateral hemisphere showed no significant changes, highlighting the localized nature of astrocytic responses to focal injury. CD31 fluorescence intensity, a marker of endothelial cells, showed a significant decrease at 24 hours post-TBI in the ipsilateral hemisphere, consistent with acute microvascular damage. The recovery to baseline levels by seven days and six months suggests a partial restoration of endothelial integrity. However, the transient reduction in astrocytic coverage of endothelial surfaces, peaking at seven days post-TBI, particularly significant in the contralateral hemisphere, underscores a period of vulnerability in NVU integrity, that may render the brain particularly susceptible to secondary injury, such as inflammation, oxidative stress, or ischemia. This study's findings align with previous research indicating acute disruptions in cerebral microvasculature and subacute disruptions of astrocytic end feet coverage following TBI [161, 162, 163, 183, 184]. However, our results extend the existing body of knowledge by providing a more granular temporal analysis.

The study's examination of extravascular albumin fluorescence intensity provided compelling evidence for BBB disruption following TBI. In the ipsilateral hemisphere, albumin fluorescence intensity peaked at 24 hours in the striatum and showed minor but still significant elevations in the cortex, followed by a progressive decline over the next six months without reaching control levels in the striatum. The contralateral hemisphere did not show increased extravascular albumin fluorescence intensity compared to the control. These results align with the known acute breakdown of the BBB post-TBI and its gradual repair over time [175, 178, 188, 187]. However the two stages of BBB breakdown with one peak after a few hours, followed by a decline and secondary delayed peak after three to seven days, as described in various studies, has not been found [120, 185, 186]. It is likely that albumin leaks acutely during the first few days post-injury and subsequently remains within the tissue, rather than continuing to extravasate, as a persistently open BBB over the long term cannot be definitively demonstrated based on the available data. This interpretation warrants caution, as while the observed fluorescence intensity indicates the presence of albumin in the tissue over an extended period, this does not necessarily imply ongoing BBB leakage. Instead, the data support the notion that extravasated plasma components, such as albumin, may persist in the tissue and contribute to prolonged pathological mechanisms, including inflammation and secondary injury processes. Moreover, there is insufficient data to determine whether the persistent extravascular albumin in this study is a primary processes due to shear injury, impairments in the regulation of the BBB, cerebral blood flow and metabolic processes, or a secondary pathological event after TBI due to aberrant brain activity, metabolic abnormalities, inflammation-related mechanisms, and astrocytic dysfunction [47, 177].

These findings have several important implications. First, the identification of a vascular and astrocytic vulnerability window highlights a potential timeframe for therapeutic interventions aimed at stabilizing NVU integrity. Strategies to enhance astrocyte-endothelial interactions during this phase could mitigate secondary injury and promote recovery. For example, therapies targeting the upregulation of Aqp4 through gene or protein therapy could enhance water regulation and support vascular stability. Additionally, interventions aimed at reducing endothelial stress or promoting angiogenesis, such as the vascular endothelial growth factor (VEGF) or anti-oxidative compounds, could enhance microvascular repair [161, 374, 375].

The observed dynamics of BBB disruption, with early albumin leakage followed by delayed secondary leakage up to six months post-TBI, open new questions about the mechanisms driving prolonged BBB dysfunction. This pattern may reflect ongoing inflammation, delayed endothelial

repair, or cyclical vascular stress. Understanding these mechanisms could help refine therapeutic windows and develop more effective interventions. Pharmacological agents such as matrix metalloproteinase inhibitors, which are known to protect BBB integrity [376, 377, 378] or targeted delivery of neuroprotective agents [379, 380, 381] during this delayed phase, could represent promising avenues for future research.

Despite advances in knowledge about cerebral microvasculature from this study, several questions remain unanswered. For instance: which molecular pathways drive the delayed reduction in astrocytic coverage and prolonged BBB leakage, which role does systemic inflammation play in NVU and BBB changes and how does NVU disruption affect long-term neurofunctional outcomes? By addressing these unanswered questions and leveraging the therapeutic opportunities identified, future research could significantly advance our understanding of TBI pathology and improve patient outcomes.

4.2.3 Neurodegeneration

This study comprehensively evaluated the relationship between TBI and subsequent risks of neuronal loss and amyloid-beta pathology. The results suggest that a single severe TBI is associated with acute and chronic neuronal loss and increased amyloid-beta fluorescence intensity in the brain, key hallmarks of neurodegenerative processes [191, 194].

Acutely, at 24 hours post-injury, there was a dramatic increase in Aβ fluorescence intensity, indicating a rapid pathological response to trauma. This early surge may reflect an acute disruption in amyloid precursor protein processing or clearance mechanisms, potentially exacerbated by inflammation and oxidative stress. At the chronic time point of 12 months, Aβ fluorescence intensity remained elevated, suggesting that TBI initiates long-lasting disruptions in amyloid metabolism. These findings align with prior studies that associate TBI with increased vulnerability to AD [42, 127, 189, 190]. However, the results of this study extend beyond the time frames typically examined in prior experimental studies. While earlier experimental investigations often focused on short-term outcomes (e.g., up to 28 days [242]), this study underscores the chronic nature of TBI-induced amyloid pathology, consistent with evidence from human postmortem studies showing persistent Aβ and tau pathology decades post-injury [240, 241, 242]. It is worth noting, however, that the limited sample size for the 12-month group (n=3) necessitates cautious interpretation of these findings and warrants further replication in larger cohorts to confirm these results.

Acute neuronal loss, analyzed by the NeuN cell count, was evident as early as 24 hours post-injury and peaked at seven days, marking a critical subacute phase of neuronal vulnerability. Interestingly, neuronal cell counts returned to baseline levels by six months post-TBI, suggesting a degree of neuroplastic recovery or compensatory mechanisms in the chronic phase. This biphasic pattern of neuronal loss and recovery is consistent with prior observations of TBI-induced neurodegeneration and highlights the dynamic nature of neuronal survival and repair processes [13, 203, 204, 205]. The temporal alignment of peak Aβ accumulation with acute neuronal loss raises questions about the interplay between amyloid pathology and neuronal degeneration in the aftermath of TBI.

Moreover, the experiments conducted in our lab by Dr. Xiang Mao showed that gradual neurocognitive changes were closely linked to significant histopathological alterations, specifically progressive brain atrophy and hippocampal damage in mice [64] (see **Figure 2**). The CCI resulted in notable and progressive impairments across several domains, including body weight reduction, motor deficits, memory decline, and depressive-like behavior [64]. Over time, the extent of tissue

loss increased steadily, peaking at 360 days post-injury. Histological analysis revealed significant atrophy in the ipsilateral hemisphere, ipsilateral white matter tracts, and both the ipsilateral and contralateral lateral hippocampus [64].

These findings carry significant implications for understanding the long-term consequences of TBI. The sustained elevation of Aβ peptide fluorescence intensity up to 12 months post-injury reinforces the idea that TBI could predispose individuals to AD-like pathology. This opens avenues for early therapeutic interventions targeting amyloid processing pathways to mitigate the risk of chronic neurodegeneration after TBI. The transient neuronal loss observed within the first week post-injury suggests a window of heightened vulnerability that may benefit from neuroprotective strategies. Therapies aimed at reducing excitotoxicity, oxidative stress, or inflammation during this critical period could enhance neuronal survival and potentially prevent long-term deficits.

Future research should address several open questions: what molecular pathways drive the sustained elevation of Aβ levels post-TBI, and how do these interact with neuronal loss and recovery mechanisms? How do Aβ accumulation and neuronal loss vary across different brain regions, and how do these patterns correlate with functional impairments?

Potential explanations for the positive correlation between TBI and dementia/AD risk have been put forth. The pathophysiology of dementia has been thought to be significantly influenced by blood-brain barrier disruption [231]. The disruption of the blood-brain barrier caused by TBI may result in leukocyte infiltration and microglial activation. In addition, neurodegenerative disease has been linked to β-amyloid pathology, tau deposition, vascular injury, chronic neuroinflammation, mitochondrial function, and white-matter degeneration in TBI patients [148, 190, 208, 382, 383, 384, 385]. Understanding how these factors interact over time will be crucial for delineating the mechanistic link between TBI and neurodegeneration, ultimately guiding future therapeutic strategies.

Building on these findings, potential therapeutic strategies to mitigate the long-term neurodegenerative consequences of TBI are emerging as critical areas of focus. Targeting chronic neuroinflammation with anti-inflammatory therapies, such as microglial modulators and cytokine inhibitors, offers promise for slowing the progression of post-TBI neurodegeneration [121]. Interventions aimed at reducing protein pathology, including clearing toxic aggregates like amyloid-beta (Aβ) and tau or preventing their formation, may delay the onset of neurodegenerative diseases. For example, anti-amyloid therapies, such as β-secretase inhibitors or monoclonal antibodies, could be explored for their potential to prevent chronic Aβ accumulation [386, 387]. Similarly, neuroprotective agents and rehabilitation strategies during the acute phase might limit neuronal loss and enhance recovery [196, 388]. Furthermore, leveraging biomarkers such as reduced Aβ levels in cerebrospinal fluid or imaging evidence of tau deposition after TBI can enable earlier diagnosis and intervention, potentially improving outcomes for TBI survivors.

The overlapping pathophysiology between TBI and disorders like Alzheimer's disease underscores the urgent need for comprehensive research into these therapeutic strategies. By addressing neuroinflammation, protein aggregation, and vascular dysfunction, we may alter the trajectory of post-TBI neurodegeneration and significantly improve long-term outcomes for affected individuals. In conclusion, this study underscores the intricate and evolving nature of neurodegeneration following TBI, providing a foundation for future investigations into the mechanisms linking TBI to chronic neurodegenerative diseases.

4.3 Conclusion

In conclusion, this study highlights the complex and prolonged neuroinflammatory, vascular, and neurodegenerative responses following TBI (see **Figure 32**). The persistent activation of glial cells, particularly astrocytes and microglia, coupled with ongoing disruptions to the blood-brain barrier and cerebral microvasculature, suggests that TBI triggers a series of chronic pathological processes over many months that may contribute to long-term cognitive deficits and increased susceptibility to neurodegenerative diseases such as Alzheimer's. The findings underscore the need for targeted therapeutic strategies that address these prolonged inflammatory and pathological changes to mitigate the long-term impact of TBI. Further research is essential to refine our understanding of the molecular mechanisms involved, and to identify effective intervention windows that can ultimately reduce the risk of chronic neurodegeneration and improve the quality of life for TBI survivors.

The histopathological and MRI findings from Dr. Xiang Mao provide crucial insights into the progressive nature of tissue damage following TBI and were the foundation for the research question addressed in this study. Specifically, Dr. Xiang Mao's study, conducted in our lab, identified the phenomenon of lesion expansion after experimental TBI that progressed almost linearly over time, prompting us to investigate the cellular pathological processes driving this pathology [64]. It was observed that the defect volume in the traumatized hemisphere significantly increased over time, with the lesion expanding from 7 days up to 12 months post-injury (see **Figure 2**) [64]. Alongside this, progressive hemispheric atrophy, white matter injury (e.g., thinning of the corpus callosum), hydrocephalus characterized by ventricle enlargement, and hippocampal damage were noted [64]. The hippocampus, a structure critical for memory and cognitive function, exhibited significant substantial and progressive tissue loss, starting as early as 7 days post-TBI and worsening up to 12 months [64]. Notably, even the hippocampus in the non-traumatized hemisphere showed changes over time, indicating that TBI-induced neurodegeneration might extend beyond the direct impact site. A key question arising from these findings is: why does the defect volume continue to expand in a near-linear fashion over time? To address this, we sought to identify the cellular mechanisms and reactivity correlates contributing to this lesion expansion, focusing on neuroinflammation, vascular disruption, and neurodegeneration.

Our findings highlight that neuroinflammation, primarily characterized by microglial and astrocyte activation, reaches a peak at 7 days post-TBI. While microglial activation gradually declines by 6 months, astrocytic activation persists up to 12 months, suggesting their prolonged involvement in the chronic injury response. Interestingly, the astrocytic marker Aqp4 showed an early but transient increase in fluorescence intensity within the ipsilateral hemisphere at 24 hours post-TBI, declining by 7 days and normalizing by 6 months. Conversely, vascular disruption appeared more sustained, with CD31 intensity showing acute microvascular damage at 24 hours, recovering by 7 days. Astrocytic end-feet coverage of endothelial surfaces exhibited transient reductions peaking at 7 days. BBB disruption, evidenced by albumin extravasation, peaked acutely at 24 hours and persisted with a progressive decline over 6 months without fully returning to control levels. This finding underscores the prolonged vascular instability and incomplete recovery of the BBB. Chronic neurodegeneration, marked by sustained amyloid-beta accumulation in the traumatized hemisphere, was also observed up to 12 months post-TBI, indicating persistent neuronal damage.

This neurodegeneration, may play a significant role in lesion expansion, potentially contributing to the progressive tissue loss observed histopathologically. Given that the hippocampus is particularly vulnerable to trauma, as evidenced by Dr. Xiang Mao's findings of substantial hippocampal

atrophy in the traumatized hemisphere, it is plausible that the neurodegenerative processes contribute not only to the structural damage but also to the progressive neurocognitive deficits reported. The hippocampus, critical for memory and learning, undergoes significant tissue loss that parallels the sustained Aβ accumulation, suggesting a connection between these findings. Among the various mechanisms identified, the progressive nature of BBB disruption emerges as a particularly compelling cellular correlate for the continued lesion expansion observed histopathologically (see **Figure 32**). While microglia and astrocytes likely contribute to lesion expansion during the acute and subacute phases , their subsequent decline suggests they may not be the primary drivers of ongoing tissue loss (see **Figure 32**). Instead, the combination of persistent BBB disruption and chronic neurodegeneration, potentially exacerbated by hippocampal vulnerability, appears central to the near-linear expansion of the lesion volume up to 12 months post-TBI (see **Figure 32**). The BBB plays a vital role in maintaining homeostasis in the central nervous system, and its integrity is essential to protect neural tissue from blood-derived toxins, immune cells, and inflammatory mediators. Persistent BBB disruption, as observed in this study, likely contributes to a toxic microenvironment in the injured brain, which may drive ongoing lesion expansion after TBI. This emphasizes the need for future studies to further investigate the molecular and cellular pathways underlying these processes, as targeting both vascular instability and neurodegenerative pathways may offer promising therapeutic strategies to mitigate chronic lesion progression and its cognitive consequences.

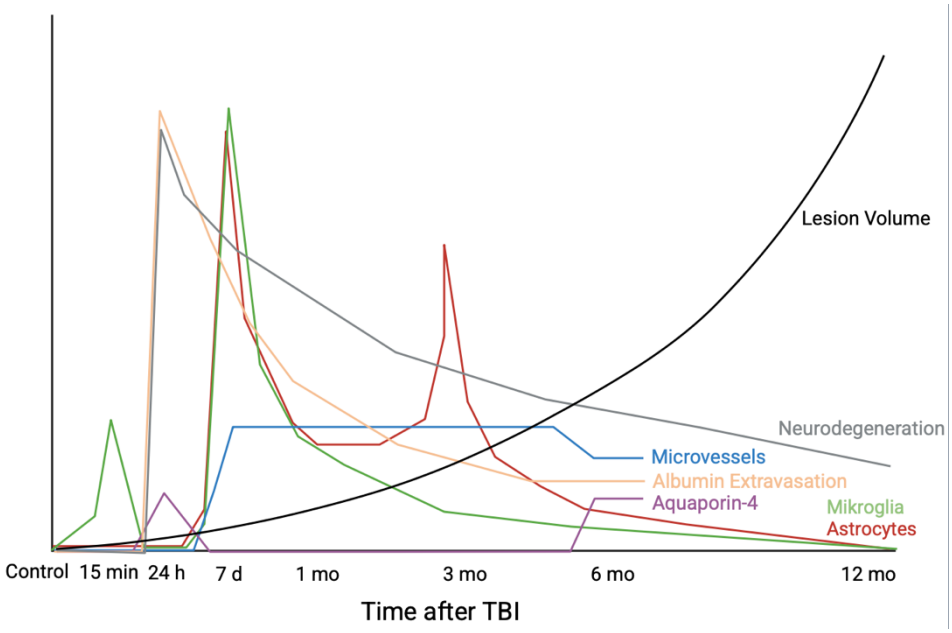

Figure 32: Acute and chronic cellular and histomorphological changes after TBI.

References

1. Lefevre-Dognin, C., et al., *Definition and epidemiology of mild traumatic brain injury.* Neurochirurgie, 2021. **67**(3): p. 218-221.
2. Thornhill, S., et al., *Disability in young people and adults one year after head injury: prospective cohort study.* Bmj, 2000. **320**(7250): p. 1631-5.
3. Giner, J., et al., *Traumatic brain injury in the new millennium: new population and new management.* Neurologia (Engl Ed), 2022. **37**(5): p. 383-389.
4. Nguyen, R., et al., *The International Incidence of Traumatic Brain Injury: A Systematic Review and Meta-Analysis.* Can J Neurol Sci, 2016. **43**(6): p. 774-785.
5. Thurman, D.J., *The Epidemiology of Traumatic Brain Injury in Children and Youths: A Review of Research Since 1990.* J Child Neurol, 2016. **31**(1): p. 20-7.
6. Mathers, C.D. and D. Loncar, *Projections of global mortality and burden of disease from 2002 to 2030.* PLoS Med, 2006. **3**(11): p. e442.
7. Olesen, J., et al., *The economic cost of brain disorders in Europe.* Eur J Neurol, 2012. **19**(1): p. 155-62.
8. Ma, V.Y., L. Chan, and K.J. Carruthers, *Incidence, prevalence, costs, and impact on disability of common conditions requiring rehabilitation in the United States: stroke, spinal cord injury, traumatic brain injury, multiple sclerosis, osteoarthritis, rheumatoid arthritis, limb loss, and back pain.* Arch Phys Med Rehabil, 2014. **95**(5): p. 986-995.e1.
9. Maas, A.I.R., et al., *Traumatic brain injury: progress and challenges in prevention, clinical care, and research.* Lancet Neurol, 2022. **21**(11): p. 1004-1060.
10. Wilson, L., et al., *The chronic and evolving neurological consequences of traumatic brain injury.* Lancet Neurol, 2017. **16**(10): p. 813-825.
11. Di Saverio, S., et al., *Changes in the outcomes of severe trauma patients from 15-year experience in a Western European trauma ICU of Emilia Romagna region (1996-2010). A population cross-sectional survey study.* Langenbecks Arch Surg, 2014. **399**(1): p. 109-26.
12. Seabury, S.A., et al., *Assessment of Follow-up Care After Emergency Department Presentation for Mild Traumatic Brain Injury and Concussion: Results From the TRACK-TBI Study.* JAMA Netw Open, 2018. **1**(1): p. e180210.
13. Wehn, A.C., et al., *RIPK1 or RIPK3 deletion prevents progressive neuronal cell death and improves memory function after traumatic brain injury.* Acta Neuropathol Commun, 2021. **9**(1): p. 138.
14. Rickels, E., et al., *The Long-Term Sequelae of Traumatic Brain Injury Over 10 Years of Follow-Up—A Matched Cohort Study Based on Routine Data of a Statutory Health Insurance Carrier.* Dtsch Arztebl Int, 2023. **120**(16): p. 271-276.
15. James, S.L., et al., *Global, regional, and national burden of traumatic brain injury and spinal cord injury, 1990-2016: a systematic analysis for the Global Burden of Disease Study 2016.* Lancet Neurol, 2019. **18**(1): p. 56-87.
16. Wiles, M.D., *Management of traumatic brain injury: a narrative review of current evidence.* Anaesthesia, 2022. **77 Suppl 1**: p. 102-112.
17. Brazinova, A., et al., *Epidemiology of Traumatic Brain Injury in Europe: A Living Systematic Review.* J Neurotrauma, 2021. **38**(10): p. 1411-1440.
18. Quintard, H., P. Bouzat, and T. Geeraerts, *Towards a new pattern for epidemiology of traumatic brain injury.* Anaesth Crit Care Pain Med, 2021. **40**(1): p. 100808.
19. Majdan, M., et al., *Epidemiology of traumatic brain injuries in Europe: a cross-sectional analysis.* Lancet Public Health, 2016. **1**(2): p. e76-e83.
20. Ramanathan, D.M., et al., *Epidemiological shifts in elderly traumatic brain injury: 18-year trends in Pennsylvania.* J Neurotrauma, 2012. **29**(7): p. 1371-8.

21. Gardner, R.C., et al., *Geriatric Traumatic Brain Injury: Epidemiology, Outcomes, Knowledge Gaps, and Future Directions.* J Neurotrauma, 2018. **35**(7): p. 889-906.

22. Taylor, C.A., et al., *Traumatic Brain Injury-Related Emergency Department Visits, Hospitalizations, and Deaths - United States, 2007 and 2013.* MMWR Surveill Summ, 2017. **66**(9): p. 1-16.

23. Dewan, M.C., et al., *Estimating the global incidence of traumatic brain injury.* J Neurosurg, 2019. **130**(4): p. 1080-1097.

24. Maas, A.I.R., et al., *Traumatic brain injury: integrated approaches to improve prevention, clinical care, and research.* Lancet Neurol, 2017. **16**(12): p. 987-1048.

25. Chang, H.Y.M., et al., *Predicting mortality in moderate-severe TBI patients without early withdrawal of life-sustaining treatments including ICU complications: The MYSTIC-score.* J Crit Care, 2022. **72**: p. 154147.

26. Clark, D., et al., *Casemix, management, and mortality of patients rreseceiving emergency neurosurgery for traumatic brain injury in the Global Neurotrauma Outcomes Study: a prospective observational cohort study.* Lancet Neurol, 2022. **21**(5): p. 438-449.

27. Capizzi, A., J. Woo, and M. Verduzco-Gutierrez, *Traumatic Brain Injury: An Overview of Epidemiology, Pathophysiology, and Medical Management.* Med Clin North Am, 2020. **104**(2): p. 213-238.

28. McGinn, M.J. and J.T. Povlishock, *Pathophysiology of Traumatic Brain Injury.* Neurosurg Clin N Am, 2016. **27**(4): p. 397-407.

29. Chen, P., et al., *Analysis of Clinical Characteristics and Prognosis of Traumatic Brain Injury in Papua New Guinea.* Comput Math Methods Med, 2021. **2021**: p. 4948664.

30. Andriessen, T.M., B. Jacobs, and P.E. Vos, *Clinical characteristics and pathophysiological mechanisms of focal and diffuse traumatic brain injury.* J Cell Mol Med, 2010. **14**(10): p. 2381-92.

31. Teasdale, G. and B. Jennett, *Assessment of coma and impaired consciousness. A practical scale.* Lancet, 1974. **2**(7872): p. 81-4.

32. Roy, D., et al., *Loss of consciousness and altered mental state predicting depressive and post-concussive symptoms after mild traumatic brain injury.* Brain Inj, 2019. **33**(8): p. 1064-1069.

33. Pankatz, L., et al., *Adverse Outcome Following Mild Traumatic Brain Injury Is Associated with Microstructure Alterations at the Gray and White Matter Boundary.* J Clin Med, 2023. **12**(16).

34. Daneshvar, D.H., et al., *Long-term consequences: effects on normal development profile after concussion.* Phys Med Rehabil Clin N Am, 2011. **22**(4): p. 683-700, ix.

35. Rimel, R.W., et al., *Disability caused by minor head injury.* Neurosurgery, 1981. **9**(3): p. 221-8.

36. Brasure, M., et al., *AHRQ Comparative Effectiveness Reviews*, in *Multidisciplinary Postacute Rehabilitation for Moderate to Severe Traumatic Brain Injury in Adults*. 2012, Agency for Healthcare Research and Quality (US): Rockville (MD).

37. Strich, S.J., *Lesions in the cerebral hemispheres after blunt head injury.* J Clin Pathol Suppl (R Coll Pathol), 1970. **4**: p. 166-71.

38. Rosenfeld, J.V., et al., *Early management of severe traumatic brain injury.* Lancet, 2012. **380**(9847): p. 1088-98.

39. McKee, A.C. and D.H. Daneshvar, *The neuropathology of traumatic brain injury.* Handb Clin Neurol, 2015. **127**: p. 45-66.

40. Sahuquillo, J., M.A. Poca, and S. Amoros, *Current aspects of pathophysiology and cell dysfunction after severe head injury.* Curr Pharm Des, 2001. **7**(15): p. 1475-503.

41. Loane, D.J., et al., *Progressive neurodegeneration after experimental brain trauma: association with chronic microglial activation.* J Neuropathol Exp Neurol, 2014. **73**(1): p. 14-29.

42. Faden, A.I., et al., *Progressive inflammation-mediated neurodegeneration after traumatic brain or spinal cord injury.* Br J Pharmacol, 2016. **173**(4): p. 681-91.

43. Baethmann, A., et al., *Mediators of brain edema and secondary brain damage.* Crit Care Med, 1988. **16**(10): p. 972-8.

44. Vespa, P., *Traumatic brain injury is a longitudinal disease process.* Curr Opin Neurol, 2017. **30**(6): p. 563-564.

45. Lund, S.B., et al., *Moderate traumatic brain injury, acute phase course and deviations in physiological variables: an observational study.* Scand J Trauma Resusc Emerg Med, 2016. **24**: p. 77.

46. Toshkezi, G., et al., *Brain repair by hematopoietic growth factors in the subacute phase of traumatic brain injury.* J Neurosurg, 2018. **129**(5): p. 1286-1294.

47. Shlosberg, D., et al., *Blood-brain barrier breakdown as a therapeutic target in traumatic brain injury.* Nat Rev Neurol, 2010. **6**(7): p. 393-403.

48. Humble, S.S., et al., *Prognosis of diffuse axonal injury with traumatic brain injury.* J Trauma Acute Care Surg, 2018. **85**(1): p. 155-159.

49. Wallesch, C.W., et al., *Outcome after mild-to-moderate blunt head injury: effects of focal lesions and diffuse axonal injury.* Brain Inj, 2001. **15**(5): p. 401-12.

50. Eisenberg, H.M., et al., *Initial CT findings in 753 patients with severe head injury. A report from the NIH Traumatic Coma Data Bank.* J Neurosurg, 1990. **73**(5): p. 688-98.

51. Khoshyomn, S. and B.I. Tranmer, *Diagnosis and management of pediatric closed head injury.* Semin Pediatr Surg, 2004. **13**(2): p. 80-6.

52. Martin, G., *Traumatic brain injury: The first 15 milliseconds.* Brain Inj, 2016. **30**(13-14): p. 1517-1524.

53. Cepeda, S., et al., *Traumatic Intracerebral Hemorrhage: Risk Factors Associated with Progression.* J Neurotrauma, 2015. **32**(16): p. 1246-53.

54. Lobato, R.D., et al., *Outcome from severe head injury related to the type of intracranial lesion. A computerized tomography study.* J Neurosurg, 1983. **59**(5): p. 762-74.

55. Bullock, R., J. Golek, and G. Blake, *Traumatic intracerebral hematoma--which patients should undergo surgical evacuation? CT scan features and ICP monitoring as a basis for decision making.* Surg Neurol, 1989. **32**(3): p. 181-7.

56. Chang, E.F., M. Meeker, and M.C. Holland, *Acute traumatic intraparenchymal hemorrhage: risk factors for progression in the early post-injury period.* Neurosurgery, 2007. **61**(1 Suppl): p. 222-30; discussion 230-1.

57. Lobato, R.D., et al., *Sequential computerized tomography changes and related final outcome in severe head injury patients.* Acta Neurochir (Wien), 1997. **139**(5): p. 385-91.

58. Servadei, F., et al., *Evolving brain lesions in the first 12 hours after head injury: analysis of 37 comatose patients.* Neurosurgery, 1995. **37**(5): p. 899-906; discussion 906-7.

59. Gudeman, S.K., et al., *The genesis and significance of delayed traumatic intracerebral hematoma.* Neurosurgery, 1979. **5**(3): p. 309-13.

60. Oertel, M., et al., *Progressive hemorrhage after head trauma: predictors and consequences of the evolving injury.* J Neurosurg, 2002. **96**(1): p. 109-16.

61. Smith, J.S., et al., *The role of early follow-up computed tomography imaging in the management of traumatic brain injury patients with intracranial hemorrhage.* J Trauma, 2007. **63**(1): p. 75-82.

62. Simard, J.M., et al., *Key role of sulfonylurea receptor 1 in progressive secondary hemorrhage after brain contusion.* J Neurotrauma, 2009. **26**(12): p. 2257-67.

63. Hicks, R.R., S.A. Baldwin, and S.W. Scheff, *Serum extravasation and cytoskeletal alterations following traumatic brain injury in rats. Comparison of lateral fluid percussion and cortical impact models.* Mol Chem Neuropathol, 1997. **32**(1-3): p. 1-16.

64. Mao, X., et al., *Progressive Histopathological Damage Occurring Up to One Year after Experimental Traumatic Brain Injury Is Associated with Cognitive Decline and Depression-Like Behavior.* J Neurotrauma, 2020. **37**(11): p. 1331-1341.

65. Losurdo, M., J. Davidsson, and M.K. Sköld, *Diffuse Axonal Injury in the Rat Brain: Axonal Injury and Oligodendrocyte Activity Following Rotational Injury.* Brain Sci, 2020. **10**(4).

66. Saatman, K.E., et al., *Classification of traumatic brain injury for targeted therapies.* J Neurotrauma, 2008. **25**(7): p. 719-38.

67. McAllister, T.W., *Neurobiological consequences of traumatic brain injury.* Dialogues Clin Neurosci, 2011. **13**(3): p. 287-300.

68. Armstrong, R.C., et al., *White matter involvement after TBI: Clues to axon and myelin repair capacity.* Exp Neurol, 2016. **275 Pt 3**: p. 328-333.

69. Gentleman, S.M., et al., *Axonal injury: a universal consequence of fatal closed head injury?* Acta Neuropathol, 1995. **89**(6): p. 537-43.

70. Maas, A.I., N. Stocchetti, and R. Bullock, *Moderate and severe traumatic brain injury in adults.* Lancet Neurol, 2008. **7**(8): p. 728-41.

71. Gennarelli, T.A., et al., *Diffuse axonal injury and traumatic coma in the primate.* Ann Neurol, 1982. **12**(6): p. 564-74.

72. Mesfin, F.B., et al., *Diffuse Axonal Injury*, in *StatPearls*. 2024, StatPearls Publishing

73. Strich, S.J., *Diffuse degeneration of the cerebral white matter in severe dementia following head injury.* J Neurol Neurosurg Psychiatry, 1956. **19**(3): p. 163-85.

74. van Vliet, E.A., et al., *Long-lasting blood-brain barrier dysfunction and neuroinflammation after traumatic brain injury.* Neurobiol Dis, 2020. **145**: p. 105080.

75. Werner, C. and K. Engelhard, *Pathophysiology of traumatic brain injury.* Br J Anaesth, 2007. **99**(1): p. 4-9.

76. Hickenbottom, S.L. and J. Grotta, *Neuroprotective therapy.* Semin Neurol, 1998. **18**(4): p. 485-92.

77. McIntosh, T.K., S. Fernyak, and A.I. Faden, *Endogenous opioids, opiate receptors and traumatic brain injury.* NIDA Res Monogr, 1986. **75**: p. 527-30.

78. McIntosh, T.K., et al., *Endogenous opioids may mediate secondary damage after experimental brain injury.* Am J Physiol, 1987. **253**(5 Pt 1): p. E565-74.

79. Reinert, M., et al., *High level of extracellular potassium and its correlates after severe head injury: relationship to high intracranial pressure.* J Neurosurg, 2000. **93**(5): p. 800-7.

80. Schilling, L. and M. Wahl, *Mediators of cerebral edema.* Adv Exp Med Biol, 1999. **474**: p. 123-41.

81. Sen, A.P. and A. Gulati, *Use of magnesium in traumatic brain injury.* Neurotherapeutics, 2010. **7**(1): p. 91-9.

82. Arango, M.F. and D. Bainbridge, *Magnesium for acute traumatic brain injury.* Cochrane Database Syst Rev, 2008(4): p. Cd005400.

83. Unterberg, A.W., et al., *Edema and brain trauma.* Neuroscience, 2004. **129**(4): p. 1021-9.

84. Ghirnikar, R.S., Y.L. Lee, and L.F. Eng, *Inflammation in traumatic brain injury: role of cytokines and chemokines.* Neurochem Res, 1998. **23**(3): p. 329-40.

85. Arvin, B., et al., *The role of inflammation and cytokines in brain injury.* Neurosci Biobehav Rev, 1996. **20**(3): p. 445-52.

86. Ziebell, J.M. and M.C. Morganti-Kossmann, *Involvement of pro- and anti-inflammatory cytokines and chemokines in the pathophysiology of traumatic brain injury.* Neurotherapeutics, 2010. **7**(1): p. 22-30.

87. Plesnila, N., *The immune system in traumatic brain injury.* Curr Opin Pharmacol, 2016. **26**: p. 110-7.

88. Klatzo, I., *Pathophysiological aspects of brain edema.* Acta Neuropathol, 1987. **72**(3): p. 236-9.

89. Donkin, J.J. and R. Vink, *Mechanisms of cerebral edema in traumatic brain injury: therapeutic developments.* Curr Opin Neurol, 2010. **23**(3): p. 293-9.

90. Garnett, M.R., et al., *Abnormal cerebral blood volume in regions of contused and normal appearing brain following traumatic brain injury using perfusion magnetic resonance imaging.* J Neurotrauma, 2001. **18**(6): p. 585-93.

91. Aarabi, B. and D.M. Long, *Dynamics of cerebral edema. The role of an intact vascular bed in the production and propagation of vasogenic brain edema.* J Neurosurg, 1979. **51**(6): p. 779-84.

92. Ayata, C. and A.H. Ropper, *Ischaemic brain oedema.* J Clin Neurosci, 2002. **9**(2): p. 113-24.

93. Marmarou, A., et al., *Predominance of cellular edema in traumatic brain swelling in patients with severe head injuries.* J Neurosurg, 2006. **104**(5): p. 720-30.

94. Barzó, P., et al., *Contribution of vasogenic and cellular edema to traumatic brain swelling measured by diffusion-weighted imaging.* J Neurosurg, 1997. **87**(6): p. 900-7.

95. Marmarou, A., et al., *Contribution of edema and cerebral blood volume to traumatic brain swelling in head-injured patients.* J Neurosurg, 2000. **93**(2): p. 183-93.

96. Stevens, R.D., M. Shoykhet, and R. Cadena, *Emergency Neurological Life Support: Intracranial Hypertension and Herniation.* Neurocrit Care, 2015. **23 Suppl 2**(Suppl 2): p. S76-82.

97. Greenberg, M.S., *Handbook of neurosurgery*.

98. Nordström, C.H., et al., *Assessment of the lower limit for cerebral perfusion pressure in severe head injuries by bedside monitoring of regional energy metabolism.* Anesthesiology, 2003. **98**(4): p. 809-14.

99. Lo, E.H., *A new penumbra: transitioning from injury into repair after stroke.* Nat Med, 2008. **14**(5): p. 497-500.

100. Menon, D.K., *Procrustes, the traumatic penumbra, and perfusion pressure targets in closed head injury.* Anesthesiology, 2003. **98**(4): p. 805-7.

101. Wu, H.M., et al., *Redefining the pericontusional penumbra following traumatic brain injury: evidence of deteriorating metabolic derangements based on positron emission tomography.* J Neurotrauma, 2013. **30**(5): p. 352-60.

102. Schröder, M.L., et al., *Focal ischemia due to traumatic contusions documented by stable xenon-CT and ultrastructural studies.* J Neurosurg, 1995. **82**(6): p. 966-71.

103. Plesnila, N., et al., *Relative cerebral blood flow during the secondary expansion of a cortical lesion in rats.* Neurosci Lett, 2003. **345**(2): p. 85-8.

104. Wahl, M., et al., *Vasomotor and permeability effects of bradykinin in the cerebral microcirculation.* Immunopharmacology, 1996. **33**(1-3): p. 257-63.

105. Maier-Hauff, K., et al., *The kallikrein-kinin system as mediator in vasogenic brain edema. Part 2: Studies on kinin formation in focal and perifocal brain tissue.* J Neurosurg, 1984. **61**(1): p. 97-106.

106. Unterberg, A. and A.J. Baethmann, *The kallikrein-kinin system as mediator in vasogenic brain edema. Part 1: Cerebral exposure to bradykinin and plasma.* J Neurosurg, 1984. **61**(1): p. 87-96.

107. Unterberg, A., et al., *The kallikrein-kinin system as mediator in vasogenic brain edema. Part 3: Inhibition of the kallikrein-kinin system in traumatic brain swelling.* J Neurosurg, 1986. **64**(2): p. 269-76.

108. Zhang, C., J. Chen, and H. Lu, *Expression of aquaporin-4 and pathological characteristics of brain injury in a rat model of traumatic brain injury.* Mol Med Rep, 2015. **12**(5): p. 7351-7.

109. Lopez-Rodriguez, A.B., et al., *Changes in cannabinoid receptors, aquaporin 4 and vimentin expression after traumatic brain injury in adolescent male mice. Association with edema and neurological deficit.* PLoS One, 2015. **10**(6): p. e0128782.

110. Liang, F., et al., *Deletion of aquaporin-4 is neuroprotective during the acute stage of micro traumatic brain injury in mice.* Neurosci Lett, 2015. **598**: p. 29-35.

111. Mazzini, L., et al., *Posttraumatic hydrocephalus: a clinical, neuroradiologic, and neuropsychologic assessment of long-term outcome.* Arch Phys Med Rehabil, 2003. **84**(11): p. 1637-41.

112. Pierce, J.E., et al., *Enduring cognitive, neurobehavioral and histopathological changes persist for up to one year following severe experimental brain injury in rats.* Neuroscience, 1998. **87**(2): p. 359-69.

113. Pischiutta, F., et al., *Single severe traumatic brain injury produces progressive pathology with ongoing contralateral white matter damage one year after injury.* Exp Neurol, 2018. **300**: p. 167-178.

114. Ertürk, A., et al., *Interfering with the Chronic Immune Response Rescues Chronic Degeneration After Traumatic Brain Injury.* J Neurosci, 2016. **36**(38): p. 9962-75.

115. Jeong, H.K., et al., *Brain inflammation and microglia: facts and misconceptions.* Exp Neurobiol, 2013. **22**(2): p. 59-67.

116. Bergold, P.J., *Treatment of traumatic brain injury with anti-inflammatory drugs.* Exp Neurol, 2016. **275 Pt 3**(Pt 3): p. 367-380.

117. Jassam, Y.N., et al., *Neuroimmunology of Traumatic Brain Injury: Time for a Paradigm Shift.* Neuron, 2017. **95**(6): p. 1246-1265.

118. Dinet, V., K.G. Petry, and J. Badaut, *Brain-Immune Interactions and Neuroinflammation After Traumatic Brain Injury.* Front Neurosci, 2019. **13**: p. 1178.

119. Witcher, K.G., et al., *Traumatic Brain Injury Causes Chronic Cortical Inflammation and Neuronal Dysfunction Mediated by Microglia.* J Neurosci, 2021. **41**(7): p. 1597-1616.

120. Karve, I.P., J.M. Taylor, and P.J. Crack, *The contribution of astrocytes and microglia to traumatic brain injury.* Br J Pharmacol, 2016. **173**(4): p. 692-702.

121. Simon, D.W., et al., *The far-reaching scope of neuroinflammation after traumatic brain injury.* Nat Rev Neurol, 2017. **13**(3): p. 171-191.

122. Kalra, S., et al., *Pathogenesis and management of traumatic brain injury (TBI): role of neuroinflammation and anti-inflammatory drugs.* Inflammopharmacology, 2022. **30**(4): p. 1153-1166.

123. Sulhan, S., et al., *Neuroinflammation and blood-brain barrier disruption following traumatic brain injury: Pathophysiology and potential therapeutic targets.* J Neurosci Res, 2020. **98**(1): p. 19-28.

124. Susarla, B.T., et al., *Temporal patterns of cortical proliferation of glial cell populations after traumatic brain injury in mice.* ASN Neuro, 2014. **6**(3): p. 159-70.

125. Jin, X., et al., *Temporal changes in cell marker expression and cellular infiltration in a controlled cortical impact model in adult male C57BL/6 mice.* PLoS One, 2012. **7**(7): p. e41892.

126. Komoltsev, I.G., et al., *Neuroinflammatory Cytokine Response, Neuronal Death, and Microglial Proliferation in the Hippocampus of Rats During the Early Period After Lateral Fluid Percussion-Induced Traumatic Injury of the Neocortex.* Mol Neurobiol, 2022. **59**(2): p. 1151-1167.

127. Boulton, M. and A. Al-Rubaie, *Neuroinflammation and neurodegeneration following traumatic brain injuries.* Anat Sci Int, 2024.

128. Burda, J.E., A.M. Bernstein, and M.V. Sofroniew, *Astrocyte roles in traumatic brain injury.* Exp Neurol, 2016. **275 Pt 3**(0 3): p. 305-315.

129. Fehily, B. and M. Fitzgerald, *Repeated Mild Traumatic Brain Injury: Potential Mechanisms of Damage.* Cell Transplant, 2017. **26**(7): p. 1131-1155.

130. Amlerova, Z., et al., *Reactive gliosis in traumatic brain injury: a comprehensive review.* Front Cell Neurosci, 2024. **18**: p. 1335849.

131. Loane, D.J. and A. Kumar, *Microglia in the TBI brain: The good, the bad, and the dysregulated.* Exp Neurol, 2016. **275 Pt 3**(0 3): p. 316-327.

132. Donat, C.K., et al., *Microglial Activation in Traumatic Brain Injury.* Front Aging Neurosci, 2017. **9**: p. 208.

133. Magaki, S.D., C.K. Williams, and H.V. Vinters, *Glial function (and dysfunction) in the normal & ischemic brain.* Neuropharmacology, 2018. **134**(Pt B): p. 218-225.

134. Sims, N.R. and W.P. Yew, *Reactive astrogliosis in stroke: Contributions of astrocytes to recovery of neurological function.* Neurochem Int, 2017. **107**: p. 88-103.

135. Pekny, M. and M. Nilsson, *Astrocyte activation and reactive gliosis.* Glia, 2005. **50**(4): p. 427-434.

136. Ramlackhansingh, A.F., et al., *Inflammation after trauma: microglial activation and traumatic brain injury.* Ann Neurol, 2011. **70**(3): p. 374-83.

137. Johnson, V.E., et al., *Inflammation and white matter degeneration persist for years after a single traumatic brain injury.* Brain, 2013. **136**(Pt 1): p. 28-42.

138. Sargin, D., et al., *Uncoupling of neurodegeneration and gliosis in a murine model of juvenile cortical lesion.* Glia, 2009. **57**(7): p. 693-702.

139. Villapol, S., K.R. Byrnes, and A.J. Symes, *Temporal dynamics of cerebral blood flow, cortical damage, apoptosis, astrocyte-vasculature interaction and astrogliosis in the pericontusional region after traumatic brain injury.* Front Neurol, 2014. **5**: p. 82.

140. Aloisi, F., *Immune function of microglia.* Glia, 2001. **36**(2): p. 165-79.

141. Eikelenboom, P., et al., *Neuroinflammation - an early event in both the history and pathogenesis of Alzheimer's disease.* Neurodegener Dis, 2010. **7**(1-3): p. 38-41.

142. Packer, J.M., et al., *Impaired cortical neuronal homeostasis and cognition after diffuse traumatic brain injury are dependent on microglia and type I interferon responses.* Glia, 2024. **72**(2): p. 300-321.

143. Shaw, B.C., et al., *Immunity impacts cognitive deficits across neurological disorders.* J Neurochem, 2024. **168**(10): p. 3512-3535.

144. Borst, K., A.A. Dumas, and M. Prinz, *Microglia: Immune and non-immune functions.* Immunity, 2021. **54**(10): p. 2194-2208.

145. Wolf, S.A., H.W. Boddeke, and H. Kettenmann, *Microglia in Physiology and Disease.* Annu Rev Physiol, 2017. **79**: p. 619-643.

146. Akiyama, H., et al., *Inflammation and Alzheimer's disease.* Neurobiol Aging, 2000. **21**(3): p. 383-421.

147. Praticò, D. and J.Q. Trojanowski, *Inflammatory hypotheses: novel mechanisms of Alzheimer's neurodegeneration and new therapeutic targets?* Neurobiol Aging, 2000. **21**(3): p. 441-5; discussion 451-3.

148. Qian, L., P.M. Flood, and J.S. Hong, *Neuroinflammation is a key player in Parkinson's disease and a prime target for therapy.* J Neural Transm (Vienna), 2010. **117**(8): p. 971-9.

149. Brettschneider, J., et al., *Microglial activation and TDP-43 pathology correlate with executive dysfunction in amyotrophic lateral sclerosis.* Acta Neuropathol, 2012. **123**(3): p. 395-407.

150. Crowley, M.G., M.G. Liska, and C.V. Borlongan, *Stem cell therapy for sequestering neuroinflammation in traumatic brain injury: an update on exosome-targeting to the spleen.* J Neurosurg Sci, 2017. **61**(3): p. 291-302.

151. Chen, Y. and R.A. Swanson, *Astrocytes and brain injury.* J Cereb Blood Flow Metab, 2003. **23**(2): p. 137-49.

152. Palmer, A.M., et al., *Traumatic brain injury-induced excitotoxicity assessed in a controlled cortical impact model.* J Neurochem, 1993. **61**(6): p. 2015-24.

153. Robel, S., et al., *Genetic deletion of cdc42 reveals a crucial role for astrocyte recruitment to the injury site in vitro and in vivo.* J Neurosci, 2011. **31**(35): p. 12471-82.

154. Carpentier, P.A., et al., *Differential activation of astrocytes by innate and adaptive immune stimuli.* Glia, 2005. **49**(3): p. 360-74.

155. Bush, T.G., et al., *Leukocyte infiltration, neuronal degeneration, and neurite outgrowth after ablation of scar-forming, reactive astrocytes in adult transgenic mice.* Neuron, 1999. **23**(2): p. 297-308.

156. Bardehle, S., et al., *Live imaging of astrocyte responses to acute injury reveals selective juxtavascular proliferation.* Nat Neurosci, 2013. **16**(5): p. 580-6.

157. Adams, C., et al., *Neurogliovascular dysfunction in a model of repeated traumatic brain injury.* Theranostics, 2018. **8**(17): p. 4824-4836.

158. Zhou, Y., et al., *Persistent Neurovascular Unit Dysfunction: Pathophysiological Substrate and Trigger for Late-Onset Neurodegeneration After Traumatic Brain Injury.* Front Neurosci, 2020. **14**: p. 581.

159. Muoio, V., P.B. Persson, and M.M. Sendeski, *The neurovascular unit - concept review.* Acta Physiol (Oxf), 2014. **210**(4): p. 790-8.

160. Díaz-Castro, B., S. Robel, and A. Mishra, *Astrocyte Endfeet in Brain Function and Pathology: Open Questions.* Annu Rev Neurosci, 2023. **46**: p. 101-121.

161. Salehi, A., J.H. Zhang, and A. Obenaus, *Response of the cerebral vasculature following traumatic brain injury.* J Cereb Blood Flow Metab, 2017. **37**(7): p. 2320-2339.

162. Jullienne, A., et al., *Chronic cerebrovascular dysfunction after traumatic brain injury.* J Neurosci Res, 2016. **94**(7): p. 609-22.

163. Kenney, K., et al., *Cerebral Vascular Injury in Traumatic Brain Injury.* Exp Neurol, 2016. **275 Pt 3**: p. 353-366.

164. Bouma, G.J., et al., *Cerebral circulation and metabolism after severe traumatic brain injury: the elusive role of ischemia.* J Neurosurg, 1991. **75**(5): p. 685-93.

165. Hlatky, R., et al., *Significance of a reduced cerebral blood flow during the first 12 hours after traumatic brain injury.* Neurocrit Care, 2004. **1**(1): p. 69-83.

166. Jeremitsky, E., et al., *Harbingers of poor outcome the day after severe brain injury: hypothermia, hypoxia, and hypoperfusion.* J Trauma, 2003. **54**(2): p. 312-9.

167. Inoue, Y., et al., *Changes in cerebral blood flow from the acute to the chronic phase of severe head injury.* J Neurotrauma, 2005. **22**(12): p. 1411-8.

168. Paulson, O.B., S. Strandgaard, and L. Edvinsson, *Cerebral autoregulation.* Cerebrovasc Brain Metab Rev, 1990. **2**(2): p. 161-92.

169. Rangel-Castilla, L., et al., *Cerebral hemodynamic effects of acute hyperoxia and hyperventilation after severe traumatic brain injury.* J Neurotrauma, 2010. **27**(10): p. 1853-63.

170. Rangel-Castilla, L., et al., *Cerebral pressure autoregulation in traumatic brain injury.* Neurosurg Focus, 2008. **25**(4): p. E7.

171. Enevoldsen, E.M. and F.T. Jensen, *Autoregulation and CO2 responses of cerebral blood flow in patients with acute severe head injury.* J Neurosurg, 1978. **48**(5): p. 689-703.

172. Bouma, G.J., et al., *Blood pressure and intracranial pressure-volume dynamics in severe head injury: relationship with cerebral blood flow.* J Neurosurg, 1992. **77**(1): p. 15-9.

173. Bouma, G.J. and J.P. Muizelaar, *Cerebral blood flow, cerebral blood volume, and cerebrovascular reactivity after severe head injury.* J Neurotrauma, 1992. **9 Suppl 1**: p. S333-48.

174. Bartnik-Olson, B.L., et al., *Impaired neurovascular unit function contributes to persistent symptoms after concussion: a pilot study.* J Neurotrauma, 2014. **31**(17): p. 1497-506.

175. Tomkins, O., et al., *Blood-brain barrier disruption in post-traumatic epilepsy.* J Neurol Neurosurg Psychiatry, 2008. **79**(7): p. 774-7.

176. Tomkins, O., et al., *Frequent blood-brain barrier disruption in the human cerebral cortex.* Cell Mol Neurobiol, 2001. **21**(6): p. 675-91.

177. Rodríguez-Baeza, A., et al., *Morphological features in human cortical brain microvessels after head injury: a three-dimensional and immunocytochemical study.* Anat Rec A Discov Mol Cell Evol Biol, 2003. **273**(1): p. 583-93.

178. Habgood, M.D., et al., *Changes in blood-brain barrier permeability to large and small molecules following traumatic brain injury in mice.* Eur J Neurosci, 2007. **25**(1): p. 231-8.

179. Beschorner, R., et al., *CD14 expression by activated parenchymal microglia/macrophages and infiltrating monocytes following human traumatic brain injury.* Acta Neuropathol, 2002. **103**(6): p. 541-9.

180. Risau, W. and H. Wolburg, *Development of the blood-brain barrier.* Trends Neurosci, 1990. **13**(5): p. 174-8.

181. Abbott, N.J., L. Rönnbäck, and E. Hansson, *Astrocyte-endothelial interactions at the blood-brain barrier.* Nat Rev Neurosci, 2006. **7**(1): p. 41-53.

182. Mills, W.A., 3rd, et al., *Astrocyte plasticity in mice ensures continued endfoot coverage of cerebral blood vessels following injury and declines with age.* Nat Commun, 2022. **13**(1): p. 1794.

183. Sun, M.C., et al., *Regulation of aquaporin-4 in a traumatic brain injury model in rats.* J Neurosurg, 2003. **98**(3): p. 565-9.

184. Hu, H., et al., *Increased expression of aquaporin-4 in human traumatic brain injury and brain tumors.* J Zhejiang Univ Sci B, 2005. **6**(1): p. 33-7.

185. Shapira, Y., et al., *Blood-brain barrier permeability, cerebral edema, and neurologic function after closed head injury in rats.* Anesth Analg, 1993. **77**(1): p. 141-8.

186. Başkaya, M.K., et al., *The biphasic opening of the blood-brain barrier in the cortex and hippocampus after traumatic brain injury in rats.* Neurosci Lett, 1997. **226**(1): p. 33-6.

187. Strbian, D., et al., *The blood-brain barrier is continuously open for several weeks following transient focal cerebral ischemia.* Neuroscience, 2008. **153**(1): p. 175-81.

188. Korn, A., et al., *Focal cortical dysfunction and blood-brain barrier disruption in patients with Postconcussion syndrome.* J Clin Neurophysiol, 2005. **22**(1): p. 1-9.

189. Hu, J.H., et al., *A bibliometric analysis of the relationship between traumatic brain injury and Alzheimer's disease (1993-2023).* Front Aging Neurosci, 2024. **16**: p. 1462132.

190. Faden, A.I. and D.J. Loane, *Chronic neurodegeneration after traumatic brain injury: Alzheimer disease, chronic traumatic encephalopathy, or persistent neuroinflammation?* Neurotherapeutics, 2015. **12**(1): p. 143-50.

191. Brett, B.L., et al., *Traumatic Brain Injury and Risk of Neurodegenerative Disorder.* Biol Psychiatry, 2022. **91**(5): p. 498-507.

192. Wu, Z., et al., *Traumatic brain injury triggers APP and Tau cleavage by delta-secretase, mediating Alzheimer's disease pathology.* Prog Neurobiol, 2020. **185**: p. 101730.

193. Wilbur, J., *Dementia: Dementia Types.* FP Essent, 2023. **534**: p. 7-11.

194. Zou, K., M. Abdullah, and M. Michikawa, *Current Biomarkers for Alzheimer's Disease: From CSF to Blood.* J Pers Med, 2020. **10**(3).

195. Wilson, C.A., R.W. Doms, and V.M. Lee, *Intracellular APP processing and A beta production in Alzheimer disease.* J Neuropathol Exp Neurol, 1999. **58**(8): p. 787-94.

196. Graham, N.S. and D.J. Sharp, *Understanding neurodegeneration after traumatic brain injury: from mechanisms to clinical trials in dementia.* J Neurol Neurosurg Psychiatry, 2019. **90**(11): p. 1221-1233.

197. Hicks, A.J., et al., *Associations of Enlarged Perivascular Spaces With Brain Lesions, Brain Age, and Clinical Outcomes in Chronic Traumatic Brain Injury.* Neurology, 2023. **101**(1): p. e63-e73.

198. Hicks, A.J., et al., *Traumatic Brain Injury as a Risk Factor for Dementia and Alzheimer Disease: Critical Review of Study Methodologies.* J Neurotrauma, 2019. **36**(23): p. 3191-3219.

199. Raza, Z., et al., *Dementia in military and veteran populations: a review of risk factors-traumatic brain injury, post-traumatic stress disorder, deployment, and sleep.* Mil Med Res, 2021. **8**(1): p. 55.

200. Ponsford, J., *Factors contributing to outcome following traumatic brain injury.* NeuroRehabilitation, 2013. **32**(4): p. 803-15.

201. Algattas, H. and J.H. Huang, *Traumatic Brain Injury pathophysiology and treatments: early, intermediate, and late phases post-injury.* Int J Mol Sci, 2013. **15**(1): p. 309-41.

202. Blennow, K., J. Hardy, and H. Zetterberg, *The neuropathology and neurobiology of traumatic brain injury.* Neuron, 2012. **76**(5): p. 886-99.

203. Clark, R.S., et al., *Increases in Bcl-2 and cleavage of caspase-1 and caspase-3 in human brain after head injury.* Faseb j, 1999. **13**(8): p. 813-21.

204. Yakovlev, A.G., et al., *Activation of CPP32-like caspases contributes to neuronal apoptosis and neurological dysfunction after traumatic brain injury.* J Neurosci, 1997. **17**(19): p. 7415-24.

205. Cernak, I., et al., *Role of the cell cycle in the pathobiology of central nervous system trauma.* Cell Cycle, 2005. **4**(9): p. 1286-93.

206. Reider-Groswasser, I., et al., *Late CT findings in brain trauma: relationship to cognitive and behavioral sequelae and to vocational outcome.* AJR Am J Roentgenol, 1993. **160**(1): p. 147-52.

207. MacKenzie, J.D., et al., *Brain atrophy in mild or moderate traumatic brain injury: a longitudinal quantitative analysis.* AJNR Am J Neuroradiol, 2002. **23**(9): p. 1509-15.

208. Smith, D.H., V.E. Johnson, and W. Stewart, *Chronic neuropathologies of single and repetitive TBI: substrates of dementia?* Nat Rev Neurol, 2013. **9**(4): p. 211-21.

209. Smith, D.H., et al., *Progressive atrophy and neuron death for one year following brain trauma in the rat.* J Neurotrauma, 1997. **14**(10): p. 715-27.

210. Muizelaar, J.P., et al., *Cerebral blood flow and metabolism in severely head-injured children. Part 1: Relationship with GCS score, outcome, ICP, and PVI.* J Neurosurg, 1989. **71**(1): p. 63-71.

211. Carrera, E., et al., *Spontaneous hyperventilation and brain tissue hypoxia in patients with severe brain injury.* J Neurol Neurosurg Psychiatry, 2010. **81**(7): p. 793-7.

212. Spaite, D.W., et al., *The Effect of Combined Out-of-Hospital Hypotension and Hypoxia on Mortality in Major Traumatic Brain Injury.* Ann Emerg Med, 2017. **69**(1): p. 62-72.

213. Carney, N., et al., *Guidelines for the Management of Severe Traumatic Brain Injury, Fourth Edition.* Neurosurgery, 2017. **80**(1): p. 6-15.

214. Feldman, Z., et al., *Effect of head elevation on intracranial pressure, cerebral perfusion pressure, and cerebral blood flow in head-injured patients.* J Neurosurg, 1992. **76**(2): p. 207-11.

215. Prof. Dr. Dr. B. Widder, G., Dr. Wenke Finkenzeller, Prof. Dr. H. C. Hansen, PD Dr. O. Kastrup vor DGNB, *Leitlinie zur Begutachtung nach gedecktem Schädel-Hirntrauma im Erwachsenenalter*. 2024.

216. Darby, J.M., et al., *Local "inverse steal" induced by hyperventilation in head injury.* Neurosurgery, 1988. **23**(1): p. 84-8.

217. Andrews, R.J., J.R. Bringas, and R.P. Muto, *Effects of mannitol on cerebral blood flow, blood pressure, blood viscosity, hematocrit, sodium, and potassium.* Surg Neurol, 1993. **39**(3): p. 218-22.

218. Bayir, H., et al., *Therapeutic hypothermia preserves antioxidant defenses after severe traumatic brain injury in infants and children.* Crit Care Med, 2009. **37**(2): p. 689-95.

219. Hawryluk, G.W.J., et al., *Guidelines for the Management of Severe Traumatic Brain Injury: 2020 Update of the Decompressive Craniectomy Recommendations.* Neurosurgery, 2020. **87**(3): p. 427-434.

220. Cooper, D.J., et al., *Patient Outcomes at Twelve Months after Early Decompressive Craniectomy for Diffuse Traumatic Brain Injury in the Randomized DECRA Clinical Trial.* J Neurotrauma, 2020. **37**(5): p. 810-816.

221. Cooper, D.J., et al., *Decompressive craniectomy in diffuse traumatic brain injury.* N Engl J Med, 2011. **364**(16): p. 1493-502.

222. Hutchinson, P.J., et al., *Trial of Decompressive Craniectomy for Traumatic Intracranial Hypertension.* N Engl J Med, 2016. **375**(12): p. 1119-30.

223. Mas, M.F., A. Mathews, and E. Gilbert-Baffoe, *Rehabilitation Needs of the Elder with Traumatic Brain Injury.* Phys Med Rehabil Clin N Am, 2017. **28**(4): p. 829-842.

224. Narayan, R.K., et al., *Clinical trials in head injury.* J Neurotrauma, 2002. **19**(5): p. 503-57.

225. Stein, D.G., *Embracing failure: What the Phase III progesterone studies can teach about TBI clinical trials.* Brain Inj, 2015. **29**(11): p. 1259-72.

226. Menon, D.K., *Unique challenges in clinical trials in traumatic brain injury.* Crit Care Med, 2009. **37**(1 Suppl): p. S129-35.

227. Shao, F., et al., *Microglia and Neuroinflammation: Crucial Pathological Mechanisms in Traumatic Brain Injury-Induced Neurodegeneration.* Front Aging Neurosci, 2022. **14**: p. 825086.

228. Permenter, C.M., R.J. Fernández-de Thomas, and A.L. Sherman, *Postconcussive Syndrome*, in *StatPearls*. 2024, StatPearls Publishing

Copyright © 2024, StatPearls Publishing LLC.: Treasure Island (FL) ineligible companies. Disclosure: Ricardo Fernández-de Thomas declares no relevant financial relationships with ineligible companies. Disclosure: Andrew Sherman declares no relevant financial relationships with ineligible companies.

229. Zhang, D., et al., *Frontal White Matter Hyperintensities Effect on Default Mode Network Connectivity in Acute Mild Traumatic Brain Injury.* Front Aging Neurosci, 2021. **13**: p. 793491.

230. Zanier, E.R., et al., *Shape descriptors of the "never resting" microglia in three different acute brain injury models in mice.* Intensive Care Med Exp, 2015. **3**(1): p. 39.

231. Abrahamson, E.E. and M.D. Ikonomovic, *Brain injury-induced dysfunction of the blood brain barrier as a risk for dementia.* Exp Neurol, 2020. **328**: p. 113257.

232. Dunn, C., et al., *Blood-Brain Barrier Breakdown and Astrocyte Reactivity Evident in the Absence of Behavioral Changes after Repeated Traumatic Brain Injury.* Neurotrauma Rep, 2021. **2**(1): p. 399-410.

233. Whitehead, B., et al., *Cerebral hypoperfusion exacerbates vascular dysfunction after traumatic brain injury.* Exp Neurol, 2024. **380**: p. 114907.

234. Singh, A., et al., *Social deficits mirror delayed cerebrovascular dysfunction after traumatic brain injury.* Acta Neuropathol Commun, 2024. **12**(1): p. 126.

235. Fordington, S. and M. Manford, *A review of seizures and epilepsy following traumatic brain injury.* J Neurol, 2020. **267**(10): p. 3105-3111.

236. Golub, V.M. and D.S. Reddy, *Post-Traumatic Epilepsy and Comorbidities: Advanced Models, Molecular Mechanisms, Biomarkers, and Novel Therapeutic Interventions.* Pharmacol Rev, 2022. **74**(2): p. 387-438.

237. Pease, M., et al., *Insights into epileptogenesis from post-traumatic epilepsy.* Nat Rev Neurol, 2024. **20**(5): p. 298-312.

238. Wu, Y., et al., *Blood-Brain Barrier Dysfunction in Mild Traumatic Brain Injury: Evidence From Preclinical Murine Models.* Front Physiol, 2020. **11**: p. 1030.

239. Rasmusson, D.X., et al., *Head injury as a risk factor in Alzheimer's disease.* Brain Inj, 1995. **9**(3): p. 213-9.

240. Johnson, V.E., W. Stewart, and D.H. Smith, *Traumatic brain injury and amyloid-β pathology: a link to Alzheimer's disease?* Nat Rev Neurosci, 2010. **11**(5): p. 361-70.

241. Edwards, G., 3rd, I. Moreno-Gonzalez, and C. Soto, *Amyloid-beta and tau pathology following repetitive mild traumatic brain injury.* Biochem Biophys Res Commun, 2017. **483**(4): p. 1137-1142.

242. Panayi, N., et al., *Traumatic Brain Injury in Mice Generates Early-Stage Alzheimer's Disease Related Protein Pathology that Correlates with Neurobehavioral Deficits.* Mol Neurobiol, 2024. **61**(10): p. 7567-7582.

243. McKee, A.C., et al., *Chronic traumatic encephalopathy (CTE): criteria for neuropathological diagnosis and relationship to repetitive head impacts.* Acta Neuropathol, 2023. **145**(4): p. 371-394.

244. Changa, A.R., R.A. Vietrogoski, and P.W. Carmel, *Dr Harrison Martland and the history of punch drunk syndrome.* Brain, 2018. **141**(1): p. 318-321.

245. McKee, A.C., et al., *Chronic traumatic encephalopathy in athletes: progressive tauopathy after repetitive head injury.* J Neuropathol Exp Neurol, 2009. **68**(7): p. 709-35.

246. Mez, J., et al., *Clinicopathological Evaluation of Chronic Traumatic Encephalopathy in Players of American Football.* Jama, 2017. **318**(4): p. 360-370.

247. Sayed, N., et al., *Clinical phenotype of dementia after traumatic brain injury.* J Neurotrauma, 2013. **30**(13): p. 1117-22.

248. Kaup, A.R. and K. Yaffe, *Reassuring News About Football and Cognitive Decline?: Not So Fast.* JAMA Neurol, 2017. **74**(8): p. 898-899.

249. Lighthall, J.W., *Controlled cortical impact: a new experimental brain injury model.* J Neurotrauma, 1988. **5**(1): p. 1-15.

250. Cernak, I., et al., *Involvement of the central nervous system in the general response to pulmonary blast injury.* J Trauma, 1996. **40**(3 Suppl): p. S100-4.

251. Dixon, C.E., et al., *A fluid percussion model of experimental brain injury in the rat.* J Neurosurg, 1987. **67**(1): p. 110-9.

252. Marmarou, A., et al., *A new model of diffuse brain injury in rats. Part I: Pathophysiology and biomechanics.* J Neurosurg, 1994. **80**(2): p. 291-300.

253. Foda, M.A. and A. Marmarou, *A new model of diffuse brain injury in rats. Part II: Morphological characterization.* J Neurosurg, 1994. **80**(2): p. 301-13.

254. Kundu, S. and S. Singh, *What Happens in TBI? A Wide Talk on Animal Models and Future Perspective.* Curr Neuropharmacol, 2023. **21**(5): p. 1139-1164.

255. Guillen, J., *FELASA guidelines and recommendations.* J Am Assoc Lab Anim Sci, 2012. **51**(3): p. 311-21.

256. Zweckberger, K., et al., *Effect of decompression craniotomy on increase of contusion volume and functional outcome after controlled cortical impact in mice.* J Neurotrauma, 2003. **20**(12): p. 1307-14.

257. Terpolilli, N.A., et al., *Inhaled nitric oxide reduces secondary brain damage after traumatic brain injury in mice.* J Cereb Blood Flow Metab, 2013. **33**(2): p. 311-8.

258. Trabold, R., et al., *The role of bradykinin B(1) and B(2) receptors for secondary brain damage after traumatic brain injury in mice.* J Cereb Blood Flow Metab, 2010. **30**(1): p. 130-9.

259. Shrouder, J.J., et al., *Continued dysfunction of capillary pericytes promotes no-reflow after experimental stroke in vivo.* Brain, 2024. **147**(3): p. 1057-1074.

260. Xu, X., et al., *Anti-inflammatory and immunomodulatory mechanisms of atorvastatin in a murine model of traumatic brain injury.* J Neuroinflammation, 2017. **14**(1): p. 167.

261. Fu, R., et al., *Phagocytosis of microglia in the central nervous system diseases.* Mol Neurobiol, 2014. **49**(3): p. 1422-34.

262. González Ibanez, F., et al., *Immunofluorescence Staining Using IBA1 and TMEM119 for Microglial Density, Morphology and Peripheral Myeloid Cell Infiltration Analysis in Mouse Brain.* J Vis Exp, 2019(152).

263. Stankov, A., et al., *Visualisation of Microglia with the use of Immunohistochemical Double Staining Method for CD-68 and Iba-1 of Cerebral Tissue Samples in Cases of Brain Contusions.* Pril (Makedon Akad Nauk Umet Odd Med Nauki), 2015. **36**(2): p. 141-5.

264. Brenner, M. and A. Messing, *Regulation of GFAP Expression.* ASN Neuro, 2021. **13**: p. 1759091420981206.

265. Lertkiatmongkol, P., et al., *Endothelial functions of platelet/endothelial cell adhesion molecule-1 (CD31).* Curr Opin Hematol, 2016. **23**(3): p. 253-9.

266. Xu, L., A. Nirwane, and Y. Yao, *Basement membrane and blood-brain barrier.* Stroke Vasc Neurol, 2019. **4**(2): p. 78-82.

267. Dadgostar, E., et al., *Aquaporin 4 in Traumatic Brain Injury: From Molecular Pathways to Therapeutic Target.* Neurochem Res, 2022. **47**(4): p. 860-871.

268. Huwait, E.A., et al., *Identification of amyloid antibodies for Alzheimer disease - immunotherapy.* Arch Physiol Biochem, 2022. **128**(5): p. 1275-1282.

269. Young, K. and H. Morrison, *Quantifying Microglia Morphology from Photomicrographs of Immunohistochemistry Prepared Tissue Using ImageJ.* J Vis Exp, 2018(136).

270. Colonna, M. and O. Butovsky, *Microglia Function in the Central Nervous System During Health and Neurodegeneration.* Annu Rev Immunol, 2017. **35**: p. 441-468.

271. Kim, J., P. Pavlidis, and A.V. Ciernia, *Development of a high-throughput pipeline to characterize microglia morphological states at a single-cell resolution.* eNeuro, 2024.

272. Morrison, H., et al., *Quantitative microglia analyses reveal diverse morphologic responses in the rat cortex after diffuse brain injury.* Sci Rep, 2017. **7**(1): p. 13211.

273. Liu, L. and G.P. Shi, *CD31: beyond a marker for endothelial cells.* Cardiovasc Res, 2012. **94**(1): p. 3-5.

274. Hallof-Büstrich, H. and B. Di Benedetto, *Examining the Coverage of Blood Vessels by Astrocyte Endfeet in an Animal Model of Major Depressive Disorder.* Methods Mol Biol, 2019. **1938**: p. 255-263.

275. Eriksdotter-Nilsson, M., H. Björklund, and L. Olson, *Laminin immunohistochemistry: a simple method to visualize and quantitate vascular structures in the mammalian brain.* J Neurosci Methods, 1986. **17**(4): p. 275-86.

276. Jung, S.S., S. Gauthier, and N.R. Cashman, *Beta-amyloid precursor protein is detectable on monocytes and is increased in Alzheimer's disease.* Neurobiol Aging, 1999. **20**(3): p. 249-57.

277. Bu, W., et al., *Mild Traumatic Brain Injury Produces Neuron Loss That Can Be Rescued by Modulating Microglial Activation Using a CB2 Receptor Inverse Agonist.* Front Neurosci, 2016. **10**: p. 449.

278. Slemmer, J.E., et al., *Causal role of apoptosis-inducing factor for neuronal cell death following traumatic brain injury.* Am J Pathol, 2008. **173**(6): p. 1795-805.

279. Trabold, R., et al., *Role of vasopressin V(1a) and V2 receptors for the development of secondary brain damage after traumatic brain injury in mice.* J Neurotrauma, 2008. **25**(12): p. 1459-65.

280. Schwarzmaier, S.M., et al., *In vivo temporal and spatial profile of leukocyte adhesion and migration after experimental traumatic brain injury in mice.* J Neuroinflammation, 2013. **10**: p. 32.

281. Engel, D.C., et al., *Changes of cerebral blood flow during the secondary expansion of a cortical contusion assessed by 14C-iodoantipyrine autoradiography in mice using a non-invasive protocol.* J Neurotrauma, 2008. **25**(7): p. 739-53.

282. Krieg, S.M., et al., *Decreased Secondary Lesion Growth and Attenuated Immune Response after Traumatic Brain Injury in Tlr2/4(-/-) Mice.* Front Neurol, 2017. **8**: p. 455.

283. Krieg, S.M., R. Trabold, and N. Plesnila, *Time-Dependent Effects of Arginine-Vasopressin V1 Receptor Inhibition on Secondary Brain Damage after Traumatic Brain Injury.* J Neurotrauma, 2017. **34**(7): p. 1329-1336.

284. Terpolilli, N.A., et al., *The novel nitric oxide synthase inhibitor 4-amino-tetrahydro-L-biopterine prevents brain edema formation and intracranial hypertension following traumatic brain injury in mice.* J Neurotrauma, 2009. **26**(11): p. 1963-75.

285. Schwarzmaier, S.M., et al., *The Formation of Microthrombi in Parenchymal Microvessels after Traumatic Brain Injury Is Independent of Coagulation Factor XI.* J Neurotrauma, 2016. **33**(17): p. 1634-44.

286. Meissner, L., et al., *Temporal Profile of MicroRNA Expression in Contused Cortex after Traumatic Brain Injury in Mice.* J Neurotrauma, 2016. **33**(8): p. 713-20.

287. Schwarzmaier, S.M., M. Gallozzi, and N. Plesnila, *Identification of the Vascular Source of Vasogenic Brain Edema following Traumatic Brain Injury Using In Vivo 2-Photon Microscopy in Mice.* J Neurotrauma, 2015. **32**(13): p. 990-1000.

288. Rauen, K., et al., *Arginine vasopressin V1a receptor-deficient mice have reduced brain edema and secondary brain damage following traumatic brain injury.* J Neurotrauma, 2013. **30**(16): p. 1442-8.

289. Engel, T., et al., *In vivo contributions of BH3-only proteins to neuronal death following seizures, ischemia, and traumatic brain injury.* J Cereb Blood Flow Metab, 2011. **31**(5): p. 1196-210.

290. Krieg, S.M., et al., *Effect of small molecule vasopressin V1a and V2 receptor antagonists on brain edema formation and secondary brain damage following traumatic brain injury in mice.* J Neurotrauma, 2015. **32**(4): p. 221-7.

291. Schwarzmaier, S.M., et al., *Temporal profile of thrombogenesis in the cerebral microcirculation after traumatic brain injury in mice.* J Neurotrauma, 2010. **27**(1): p. 121-30.

292. Zweckberger, K., et al., *Effect of early and delayed decompressive craniectomy on secondary brain damage after controlled cortical impact in mice.* J Neurotrauma, 2006. **23**(7): p. 1083-93.

293. McConeghy, K.W., et al., *A review of neuroprotection pharmacology and therapies in patients with acute traumatic brain injury.* CNS Drugs, 2012. **26**(7): p. 613-36.

294. Carswell, H.V., et al., *Neuroprotection by a selective estrogen receptor beta agonist in a mouse model of global ischemia.* Am J Physiol Heart Circ Physiol, 2004. **287**(4): p. H1501-4.

295. Mannix, R., et al., *Sex differences in the effect of progesterone after controlled cortical impact in adolescent mice: a preliminary study.* J Neurosurg, 2014. **121**(6): p. 1337-41.

296. Kleiber, M., *Metabolic turnover rate: a physiological meaning of the metabolic rate per unit body weight.* J Theor Biol, 1975. **53**(1): p. 199-204.

297. West, G.B. and J.H. Brown, *The origin of allometric scaling laws in biology from genomes to ecosystems: towards a quantitative unifying theory of biological structure and organization.* J Exp Biol, 2005. **208**(Pt 9): p. 1575-92.

298. Wang, H.C., et al., *Where are we in the modelling of traumatic brain injury? Models complicated by secondary brain insults.* Brain Inj, 2014. **28**(12): p. 1491-503.

299. Zhang, Y.P., et al., *Traumatic brain injury using mouse models.* Transl Stroke Res, 2014. **5**(4): p. 454-71.

300. Lighthall, J.W., C.E. Dixon, and T.E. Anderson, *Experimental models of brain injury.* J Neurotrauma, 1989. **6**(2): p. 83-97.

301. Xiong, Y., A. Mahmood, and M. Chopp, *Animal models of traumatic brain injury.* Nat Rev Neurosci, 2013. **14**(2): p. 128-42.

302. *The Brain Trauma Foundation. The American Association of Neurological Surgeons. The Joint Section on Neurotrauma and Critical Care. Computed tomography scan features.* J Neurotrauma, 2000. **17**(6-7): p. 597-627.

303. Dixon, C.E., et al., *A controlled cortical impact model of traumatic brain injury in the rat.* J Neurosci Methods, 1991. **39**(3): p. 253-62.

304. Robertson, C.L., et al., *Cerebral glucose metabolism in an immature rat model of pediatric traumatic brain injury.* J Neurotrauma, 2013. **30**(24): p. 2066-72.

305. Shear, D.A., et al., *Nicotinamide Treatment in Traumatic Brain Injury: Operation Brain Trauma Therapy.* J Neurotrauma, 2016. **33**(6): p. 523-37.

306. Fox, G.B., R.A. LeVasseur, and A.I. Faden, *Behavioral responses of C57BL/6, FVB/N, and 129/SvEMS mouse strains to traumatic brain injury: implications for gene targeting approaches to neurotrauma.* J Neurotrauma, 1999. **16**(5): p. 377-89.

307. Smith, D.H., et al., *A model of parasagittal controlled cortical impact in the mouse: cognitive and histopathologic effects.* J Neurotrauma, 1995. **12**(2): p. 169-78.

308. Lighthall, J.W., H.G. Goshgarian, and C.R. Pinderski, *Characterization of axonal injury produced by controlled cortical impact.* J Neurotrauma, 1990. **7**(2): p. 65-76.

309. Costine, B.A., et al., *Neuron-specific enolase, but not S100B or myelin basic protein, increases in peripheral blood corresponding to lesion volume after cortical impact in piglets.* J Neurotrauma, 2012. **29**(17): p. 2689-95.

310. Manley, G.T., et al., *Controlled cortical impact in swine: pathophysiology and biomechanics.* J Neurotrauma, 2006. **23**(2): p. 128-39.

311. Duhaime, A.C., et al., *Maturation-dependent response of the piglet brain to scaled cortical impact.* J Neurosurg, 2000. **93**(3): p. 455-62.

312. King, C., et al., *Brain temperature profiles during epidural cooling with the ChillerPad in a monkey model of traumatic brain injury.* J Neurotrauma, 2010. **27**(10): p. 1895-903.

313. Kotapka, M.J., et al., *Selective vulnerability of hippocampal neurons in acceleration-induced experimental head injury.* J Neurotrauma, 1991. **8**(4): p. 247-58.

314. Mychasiuk, R., A. Farran, and M.J. Esser, *Assessment of an experimental rodent model of pediatric mild traumatic brain injury.* J Neurotrauma, 2014. **31**(8): p. 749-57.

315. Viano, D.C., et al., *Evaluation of three animal models for concussion and serious brain injury.* Ann Biomed Eng, 2012. **40**(1): p. 213-26.

316. Dixon, C.E., J.W. Lighthall, and T.E. Anderson, *Physiologic, histopathologic, and cineradiographic characterization of a new fluid-percussion model of experimental brain injury in the rat.* J Neurotrauma, 1988. **5**(2): p. 91-104.

317. Thibault, L.E., et al., *Biomechanical aspects of a fluid percussion model of brain injury.* J Neurotrauma, 1992. **9**(4): p. 311-22.

318. Cernak, I., *Animal models of head trauma.* NeuroRx, 2005. **2**(3): p. 410-22.

319. Chopra, S., et al., *More highly myelinated white matter tracts are associated with faster processing speed in healthy adults.* Neuroimage, 2018. **171**: p. 332-340.

320. Alibhai, J.D., A.B. Diack, and J.C. Manson, *Unravelling the glial response in the pathogenesis of Alzheimer's disease.* Faseb j, 2018. **32**(11): p. 5766-5777.

321. Androvic, P., et al., *Decoding the Transcriptional Response to Ischemic Stroke in Young and Aged Mouse Brain.* Cell Rep, 2020. **31**(11): p. 107777.

322. Clarke, L.E., et al., *Normal aging induces A1-like astrocyte reactivity.* Proc Natl Acad Sci U S A, 2018. **115**(8): p. E1896-e1905.

323. Streit, W.J., et al., *Dystrophic microglia in the aging human brain.* Glia, 2004. **45**(2): p. 208-12.

324. Arevalo, M.A., et al., *Actions of estrogens on glial cells: Implications for neuroprotection.* Biochim Biophys Acta, 2010. **1800**(10): p. 1106-12.

325. Yee, G. and A. Jain, *Geriatric Head Injury*, in *StatPearls*. 2024, StatPearls Publishing

Copyright © 2024, StatPearls Publishing LLC.: Treasure Island (FL) ineligible companies. Disclosure: Ashika Jain declares no relevant financial relationships with ineligible companies.

326. Bodnar, C.N., et al., *A Systematic Review of Closed Head Injury Models of Mild Traumatic Brain Injury in Mice and Rats.* J Neurotrauma, 2019. **36**(11): p. 1683-1706.

327. Biegon, A., *Considering Biological Sex in Traumatic Brain Injury.* Front Neurol, 2021. **12**: p. 576366.

328. Gupte, R., et al., *Sex Differences in Traumatic Brain Injury: What We Know and What We Should Know.* J Neurotrauma, 2019. **36**(22): p. 3063-3091.

329. Bramlett, H.M. and W.D. Dietrich, *Neuropathological protection after traumatic brain injury in intact female rats versus males or ovariectomized females.* J Neurotrauma, 2001. **18**(9): p. 891-900.

330. Roof, R.L., et al., *Progesterone facilitates cognitive recovery and reduces secondary neuronal loss caused by cortical contusion injury in male rats.* Exp Neurol, 1994. **129**(1): p. 64-9.

331. Wang, J., et al., *Estrogen Attenuates Traumatic Brain Injury by Inhibiting the Activation of Microglia and Astrocyte-Mediated Neuroinflammatory Responses.* Mol Neurobiol, 2021. **58**(3): p. 1052-1061.

332. Villapol, S., D.J. Loane, and M.P. Burns, *Sexual dimorphism in the inflammatory response to traumatic brain injury.* Glia, 2017. **65**(9): p. 1423-1438.

333. Acaz-Fonseca, E., et al., *Sex differences in glia reactivity after cortical brain injury.* Glia, 2015. **63**(11): p. 1966-1981.

334. Hoffman, A.N., et al., *Sex Differences in Behavioral Sensitivities After Traumatic Brain Injury.* Front Neurol, 2020. **11**: p. 553190.

335. Wu, L., et al., *Lasting effects of general anesthetics on the brain in the young and elderly: "mixed picture" of neurotoxicity, neuroprotection and cognitive impairment.* J Anesth, 2019. **33**(2): p. 321-335.

336. Mesa Suárez, P., et al., *[Brain damage after general anesthesia].* Med Clin (Barc), 2016. **146**(9): p. 384-8.

337. Tanaka, T., et al., *General anesthetics inhibit LPS-induced IL-1β expression in glial cells.* PLoS One, 2013. **8**(12): p. e82930.

338. Brambrink, A.M., et al., *Isoflurane-induced apoptosis of oligodendrocytes in the neonatal primate brain.* Ann Neurol, 2012. **72**(4): p. 525-35.

339. Reiffurth, C., et al., *Deep Isoflurane Anesthesia Is Associated with Alterations in Ion Homeostasis and Specific Na+/K+-ATPase Impairment in the Rat Brain.* Anesthesiology, 2023. **138**(6): p. 611-623.

340. Sun, W., et al., *In vivo Two-Photon Imaging of Anesthesia-Specific Alterations in Microglial Surveillance and Photodamage-Directed Motility in Mouse Cortex.* Front Neurosci, 2019. **13**: p. 421.

341. Ma, X., et al., *Animal Models of Traumatic Brain Injury and Assessment of Injury Severity.* Mol Neurobiol, 2019. **56**(8): p. 5332-5345.

342. Cole, J.T., et al., *Craniotomy: true sham for traumatic brain injury, or a sham of a sham?* J Neurotrauma, 2011. **28**(3): p. 359-69.

343. Uryu, K., et al., *Repetitive mild brain trauma accelerates Abeta deposition, lipid peroxidation, and cognitive impairment in a transgenic mouse model of Alzheimer amyloidosis.* J Neurosci, 2002. **22**(2): p. 446-54.

344. Cherry, J.D., et al., *Microglial neuroinflammation contributes to tau accumulation in chronic traumatic encephalopathy.* Acta Neuropathol Commun, 2016. **4**(1): p. 112.

345. Bolton, A.N. and K.E. Saatman, *Regional neurodegeneration and gliosis are amplified by mild traumatic brain injury repeated at 24-hour intervals.* J Neuropathol Exp Neurol, 2014. **73**(10): p. 933-47.

346. Shitaka, Y., et al., *Repetitive closed-skull traumatic brain injury in mice causes persistent multifocal axonal injury and microglial reactivity.* J Neuropathol Exp Neurol, 2011. **70**(7): p. 551-67.

347. Escartin, C., et al., *Reactive astrocyte nomenclature, definitions, and future directions.* Nat Neurosci, 2021. **24**(3): p. 312-325.

348. Shandra, O., et al., *Repetitive Diffuse Mild Traumatic Brain Injury Causes an Atypical Astrocyte Response and Spontaneous Recurrent Seizures.* J Neurosci, 2019. **39**(10): p. 1944-1963.

349. Early, A.N., et al., *Effects of advanced age upon astrocyte-specific responses to acute traumatic brain injury in mice.* J Neuroinflammation, 2020. **17**(1): p. 115.

350. Walz, W. and M.K. Lang, *Immunocytochemical evidence for a distinct GFAP-negative subpopulation of astrocytes in the adult rat hippocampus.* Neurosci Lett, 1998. **257**(3): p. 127-30.

351. Kofler, B., et al., *Id-1 expression defines a subset of vimentin/S-100beta-positive, GFAP-negative astrocytes in the adult rat pineal gland.* Histochem J, 2002. **34**(3-4): p. 167-71.

352. Xu, J., *New Insights into GFAP Negative Astrocytes in Calbindin D28k Immunoreactive Astrocytes.* Brain Sci, 2018. **8**(8).

353. Walz, W., *Controversy surrounding the existence of discrete functional classes of astrocytes in adult gray matter.* Glia, 2000. **31**(2): p. 95-103.

354. Delcambre, G.H., et al., *Immunohistochemistry for the detection of neural and inflammatory cells in equine brain tissue.* PeerJ, 2016. **4**: p. e1601.

355. Lier, J., W.J. Streit, and I. Bechmann, *Beyond Activation: Characterizing Microglial Functional Phenotypes.* Cells, 2021. **10**(9).

356. Hoogland, I.C., et al., *Systemic inflammation and microglial activation: systematic review of animal experiments.* J Neuroinflammation, 2015. **12**: p. 114.

357. Hendrickx, D.A.E., et al., *Staining of HLA-DR, Iba1 and CD68 in human microglia reveals partially overlapping expression depending on cellular morphology and pathology.* J Neuroimmunol, 2017. **309**: p. 12-22.

358. Choudhary, M. and G. Malek, *CD68: Potential Contributor to Inflammation and RPE Cell Dystrophy.* Adv Exp Med Biol, 2023. **1415**: p. 207-213.

359. Iadecola, C., *The Neurovascular Unit Coming of Age: A Journey through Neurovascular Coupling in Health and Disease.* Neuron, 2017. **96**(1): p. 17-42.

360. Li, W., et al., *Blood-Brain Barrier Mechanisms in Stroke and Trauma.* Handb Exp Pharmacol, 2022. **273**: p. 267-293.

361. Cash, A. and M.H. Theus, *Mechanisms of Blood-Brain Barrier Dysfunction in Traumatic Brain Injury.* Int J Mol Sci, 2020. **21**(9).

362. Tooyama, I., et al., *Visualization of Amyloid Oligomers in the Brain of Patients with Alzheimer's Disease.* Acta Histochem Cytochem, 2023. **56**(6): p. 87-94.

363. Blömeke, L., et al., *Aβ oligomers peak in early stages of Alzheimer's disease preceding tau pathology.* Alzheimers Dement (Amst), 2024. **16**(2): p. e12589.

364. Jia, J., et al., *Biomarker Changes during 20 Years Preceding Alzheimer's Disease.* N Engl J Med, 2024. **390**(8): p. 712-722.

365. Scheltens, P., et al., *Alzheimer's disease.* Lancet, 2021. **397**(10284): p. 1577-1590.

366. Tiwari, S., et al., *Alzheimer's disease: pathogenesis, diagnostics, and therapeutics.* Int J Nanomedicine, 2019. **14**: p. 5541-5554.

367. Wang, J., et al., *Quantification of surviving neurons after contusion, dislocation, and distraction spinal cord injuries using automated methods.* J Exp Neurosci, 2019. **13**: p. 1179069519869617.

368. Duan, W., et al., *Novel Insights into NeuN: from Neuronal Marker to Splicing Regulator.* Mol Neurobiol, 2016. **53**(3): p. 1637-1647.

369. Armstrong, R.C., et al., *White matter damage and degeneration in traumatic brain injury.* Trends Neurosci, 2024. **47**(9): p. 677-692.

370. Anderson, M.A., et al., *Astrocyte scar formation aids central nervous system axon regeneration.* Nature, 2016. **532**(7598): p. 195-200.

371. Gentleman, S.M., et al., *Long-term intracerebral inflammatory response after traumatic brain injury.* Forensic Sci Int, 2004. **146**(2-3): p. 97-104.

372. Gottlieb, A., et al., *Time dependent analysis of rat microglial surface markers in traumatic brain injury reveals dynamics of distinct cell subpopulations.* Sci Rep, 2022. **12**(1): p. 6289.

373. Witcher, K.G., et al., *Comparison between midline and lateral fluid percussion injury in mice reveals prolonged but divergent cortical neuroinflammation.* Brain Res, 2020. **1746**: p. 146987.

374. Wu, M., et al., *VEGF regulates the blood-brain barrier through MMP-9 in a rat model of traumatic brain injury.* Exp Ther Med, 2022. **24**(6): p. 728.

375. Abdul-Muneer, P.M., N. Chandra, and J. Haorah, *Interactions of oxidative stress and neurovascular inflammation in the pathogenesis of traumatic brain injury.* Mol Neurobiol, 2015. **51**(3): p. 966-79.

376. Tang, T., et al., *TIMP1 protects against blood-brain barrier disruption after subarachnoid haemorrhage by inhibiting ubiquitination of astrocytic β1-integrin.* Stroke Vasc Neurol, 2024. **9**(6): p. 671-684.

377. Rosenberg, G.A., E.Y. Estrada, and S. Mobashery, *Effect of synthetic matrix metalloproteinase inhibitors on lipopolysaccharide-induced blood-brain barrier opening in rodents: Differences in response based on strains and solvents.* Brain Res, 2007. **1133**(1): p. 186-92.

378. Ahmadighadykolaei, H., J.A. Lambert, and M. Raeeszadeh-Sarmazdeh, *TIMP-1 Protects Tight Junctions of Brain Endothelial Cells From MMP-Mediated Degradation.* Pharm Res, 2023. **40**(9): p. 2121-2131.

379. Li, F., et al., *Neuroprotective Mechanism of MOTS-c in TBI Mice: Insights from Integrated Transcriptomic and Metabolomic Analyses.* Drug Des Devel Ther, 2024. **18**: p. 2971-2987.

380. Yap, R.S., J. Kumar, and S.L. Teoh, *Potential Neuroprotective Role of Neurotrophin in Traumatic Brain Injury.* CNS Neurol Disord Drug Targets, 2024. **23**(10): p. 1189-1202.

381. Maas, A.I., *Neuroprotective agents in traumatic brain injury.* Expert Opin Investig Drugs, 2001. **10**(4): p. 753-67.

382. Barkhoudarian, G., D.A. Hovda, and C.C. Giza, *The Molecular Pathophysiology of Concussive Brain Injury - an Update.* Phys Med Rehabil Clin N Am, 2016. **27**(2): p. 373-93.

383. Frantseva, M., et al., *Neurotrauma/neurodegeneration and mitochondrial dysfunction.* Prog Brain Res, 2002. **137**: p. 171-6.

384. Franz, C.K., et al., *Impact of traumatic brain injury on amyotrophic lateral sclerosis: from bedside to bench.* J Neurophysiol, 2019. **122**(3): p. 1174-1185.

385. Maroon, J.C., et al., *Chronic traumatic encephalopathy in contact sports: a systematic review of all reported pathological cases.* PLoS One, 2015. **10**(2): p. e0117338.

386. Park, K.W., *Anti-amyloid Antibody Therapies for Alzheimer's Disease.* Nucl Med Mol Imaging, 2024. **58**(4): p. 227-236.

387. Itoh, T., et al., *Improvement of cerebral function by anti-amyloid precursor protein antibody infusion after traumatic brain injury in rats.* Mol Cell Biochem, 2009. **324**(1-2): p. 191-9.

388. Ikonomovic, M.D., et al., *Novel therapies for combating chronic neuropathological sequelae of TBI.* Neuropharmacology, 2019. **145**(Pt B): p. 160-176.

Acknowledgements

First and foremost, I would like to thank my supervisors, Prof. Dr. med. Nikolaus Plesnila and Prof. Dr. med. Nicole Terpolilli, for providing me with the opportunity to work on this project, their guidance throughout and for creating a setting and atmosphere that made working there incredibly enjoyable.
I also especially want to thank Dr. Burcu Şeker and Dr. Joshua Shrouder for the insightful scientific conversations, their amazing support at the confocal microscope and immunohistochemistry stainings. Many thanks also to Uta Mamrak for teaching me various skills during my first months in the lab, as well as to Hedwig Pietsch for her continuous help and support in the lab.

Thank you also to my lab mates and friends, Dr. Susana Valero-Freitag, Rebecca Sienel, Bernhard Groschup, Dr. Severin Filser, Dr. Sodai Yoshimura, Carina Exner, Eva Krestel, Xianjiang Lin, Kosisochukwu Umeasalugo, Samixa Pudasaini, Antonia Clarissa Wehn, for the good time in- and outside the lab.

Finally, I want to thank my parents for their endless love and support.

Eidesstattliche Versicherung

Braun, Chiara Anina

Name, Vorname

Ich erkläre hiermit an Eides statt, dass ich die vorliegende Dissertation mit dem Titel

Acute and chronic brain damage after experimental traumatic brain injury: temporal profile of neuroinflammatory, vascular and neurodegenerative changes

selbständig verfasst, mich außer der angegebenen keiner weiteren Hilfsmittel bedient und alle Erkenntnisse, die aus dem Schrifttum ganz oder annähernd übernommen sind, als solche kenntlich gemacht und nach ihrer Herkunft unter Bezeichnung der Fundstelle einzeln nachgewiesen habe.

Ich erkläre des Weiteren, dass die hier vorgelegte Dissertation nicht in gleicher oder in ähnlicher Form bei einer anderen Stelle zur Erlangung eines akademischen Grades eingereicht wurde.

München, 03.07.2025

Ort, Datum

Chiara Anina Braun

Unterschrift Chiara Anina Braun

LMU LUDWIG-MAXIMILIANS-UNIVERSITÄT MÜNCHEN

Dekanat Medizinische Fakultät
Promotionsbüro

Erklärung zur Übereinstimmung der gebundenen Ausgabe der Dissertation mit der elektronischen Fassung

Braun, Chiara Anina

Name, Vorname

Hiermit erkläre ich, dass die elektronische Version der eingereichten Dissertation mit dem Titel:

Acute and chronic brain damage after experimental traumatic brain injury: temporal profile of neuroinflammatory, vascular and neurodegenerative changes

in Inhalt und Formatierung mit den gedruckten und gebundenen Exemplaren übereinstimmt.

München, 03.07.2025

Ort, Datum

Chiara Anina Braun

Unterschrift Chiara Anina Braun